August 2021

Theory of Ion Transport and Ion Current Rectification in Nanofluidic Diodes

Julia Ellen Proctor
Clemson University, jellenproc@gmail.com

THEORY OF ION TRANSPORT AND ION CURRENT RECTIFICATION IN NANOFLUIDIC DIODES

A Thesis
Presented to
the Graduate School of
Clemson University

In Partial Fulfillment
of the Requirements for the Degree
Master of Science
Electrical Engineering

---

by
Julia Ellen Proctor
August 2021

Accepted by:
Dr. William R. Harrell, Committee Chair
Dr. Pingshan Wang
Dr. Judson Ryckman

ABSTRACT

In this thesis, nanofluidic diodes were studied theoretically using fundamental physics as a basis. A comprehensive theory was constructed for ion current rectification (ICR) in nanofluidic systems, written from an engineering and physics perspective. The primary goal of this work was to clarify the fundamental theory of ICR through the interpretation and consideration of various literature sources on the topic, which often use contradictory definitions and simplifications. New figures were created for this research to more effectively convey and clarify vital concepts such as electric double layers (EDL), and included multiple definitions to compare different theoretical approaches. Lastly, a simulation was written to apply our developed theory by numerically modeling the electric potential profile in a nanofluidic diode of asymmetric ion concentration. The simulation results were interpreted to help visualize the formation of EDL in the system, and to conceptualize the mechanisms producing ICR.

Three main types of nanofluidic diodes were identified by their characteristic asymmetries and studied in-depth: asymmetry in fixed wall charge, asymmetry in ion concentration, and asymmetry in channel diameter. Foundational electrostatic physics equations, such as the Poisson-Boltzmann equation and Ohm's law, were derived and manipulated to produce important equations describing electric potential and ion current conductivity in nanofluidic systems. Several of these – the Debye-Hückel approximation of the Poisson-Boltzmann equation, the Debye screening length equation, and the Grahame equation – were later used in the simulation of electric potential profiles. Building

on fundamental concepts, the Poisson-Nernst-Planck (PNP) equations were shown to describe the sources of ion movement in nanofluidics in the form of a self-consistent set of coupled mean-field equations. Utilizing these equations and employing electric potential and ion current conductivity relationships, the three main types of nanofluidic diodes were analyzed to examine their sources of ICR, and each was explained through molecular-level behavioral considerations at different applied voltages.

Based on the theory developed to explain ICR, a theoretical causal chain for ICR was identified. To visualize asymmetrical electrostatic impact, which is the foundational requirement for ICR to be present in a nanofluidic system, electric potential profiles were simulated for a nanofluidic diode of asymmetric ion concentration. Using the Grahame equation and the Debye length equation to substitute values into the Debye-Hückel approximation, the electric potential was numerically calculated for the example system in equilibrium, forward bias and reverse bias. The simulation results qualitatively agreed with similar models from the literature which were obtained through PNP and analytical methods.

Analysis of our simulation results using the theory we developed revealed the importance of an electric potential well which forms near one opening of the nanochannel. This “trench” causes ion accumulation, which increases that ion’s conductivity. Applying forward voltage bias results in this high conductivity at the ions’ entrance, while reverse bias results in the high conductivity at the ions’ exit. Thus, forward bias is characterized by greater ion flux into the channel than out of it, increasing overall ion concentration in

the channel and promoting higher ion current through the system. Reverse bias is characterized by greater ion flux out of the channel than into it, decreasing overall ion concentration in the channel and suppressing ion current through the system. Asymmetry in electrostatic impact is therefore sufficient to explain ion current rectification in nanofluidic diodes, and the simulation results were used to illustrate this theoretical discussion.

ACKNOWLEDGMENTS

I would like to thank my advisor Dr. William R. Harrell for his guidance, advice, and encouragement. Our discussions of nanofluidics, his experience with technical research, and his feedback on my work were invaluable to my success in completing this thesis. I tremendously appreciate all of his help throughout the research process.

I am also very thankful for Dr. Pingshan Wang and Dr. Judson Ryckman, who were the other members of my committee, for their engagement and input during my thesis defense, asking questions that expanded my perspective of this research. I am grateful, too, for Dr. Wang's invitations to his research group's meetings, where I learned many valuable lessons about collaborative research and technical communication.

Finally, I would like to thank my family, whose unwavering support and unconditional love gave me the strength and resolve to pursue my endeavors, from undergraduate Physics to graduate Electrical Engineering and beyond.

TABLE OF CONTENTS

Page

Table of Contents (Continued) Page

LIST OF FIGURES

List of Figures (Continued)

Figure Page

List of Figures (Continued)

Figure Page

CHAPTER 1

Introduction

A nanofluidic diode is a system filled with an electrolyte solution which features a nano-scale channel with charged inner walls that connects two micro-scale reservoirs containing electrodes. One polarity of applied voltage across the electrodes produces a conductive path for ion current, while the opposite voltage polarity restricts ion current. This ion current rectification shares behavioral characteristics with semiconductor diodes, and is of interest to engineers and scientists, due to its ability to control the flow of ions.

Nature is a major source of inspiration for nanofluidics, because all cell membranes contain channels that pass biologically important ions and molecules. Controlling the transport of ions and other types of matter in the methods observed in biological systems has wide-reaching applications in not only biology, but chemistry, medicine, and more. From an engineering standpoint, it would be valuable to understand how nanofluidic mechanisms operate so that new technology can be developed. There is active research being conducted all around the globe, including the synthesis of biological nanochannels in artificial environments and the design and testing of fabricated nanofluidic systems, but there are still many ion transport mechanisms not yet fully understood.

The field of nanofluidics is immensely complicated and multidisciplinary, making it difficult to navigate the literature at times. There is limitless detail into the biological inspiration, chemistry, and physics of nanofluidics, and therefore it is a challenge to narrow the topics down to their fundamental basics. The purpose of this thesis research is to

build a well-structured, physics-based theory that explains nanofluidic diodes for engineering purposes. Also, through our discussion of ion transport theory in nanofluidics, we will uncover and identify the causal chain for ion current rectification, as well as model the electric potential profile in one type of nanofluidic diode. The organization of this thesis will now be summarized so that the reader can understand and anticipate the arrangement of topics which construct our theoretical research.

Chapter 2 presents background information about the biological inspiration for nanofluidics and nanofluidic diodes. This chapter also examines some examples of biological nanochannels and how their structures are theorized to enable such highly specific functionalities.

Chapter 3 discusses main motivating factors that drive research in the field of nanofluidics. Biological and synthetic nanochannels are compared, and then the concept of mass transport through these nanochannels is introduced. The chapter ends with a summary of some prominent applications of mass transport using nanofluidics for the development of future technology.

Chapter 4 sets the stage for our theoretical investigation by introducing three primary types of nanofluidic diodes. Diagrams of example systems which each exhibit a different structural source of ion current rectification are presented. These illustrations give context to the descriptions of nanofluidic diodes, and also provide useful references around which to consistently frame the theory in future chapters. Lastly, the meanings of

diode-like current-voltage behavior, ion current rectification (ICR), and the rectification factors used to quantify ICR are defined.

Chapter 5 focuses on fundamental nanofluidic theory that applies to any nanofluidic system, not just nanofluidic diodes. It begins by presenting the conceptual descriptions of charge screening, electric double layers (EDL) and the Debye length before delving into the quantitative models of these topics. Electrokinetic transport mechanisms are introduced next, which describe electrophoresis, electroosmosis, and diffusion. Lastly, this chapter presents the mean-field approximation models for ion transport in nanofluidics, with a particular focus on the Poisson-Nernst-Planck model, building their equations from fundamental concepts and explaining their relevance.

Chapter 6 embarks on developing the theory specific to ion current rectification in nanofluidic diodes. Important topics include charge selectivity, ionic conduction, and system dependences are explained, applying fundamental nanofluidics theory from chapter 5. This chapter then analyzes, in detail, the three types of nanofluidic diodes using the example systems presented in chapter 4, and takes a molecular-level approach to understanding the “off” and “on” modes of each diode. Finally, it draws parallels between nanofluidic diodes and semiconductor diodes to supplement the theory of operation. Descriptions of how these nanofluidic and semiconductor systems are analogous and how they contrast give insight into their possible applications.

Chapter 7 focuses on the numerical simulation aspect of theoretical modeling, now that mathematical models have been constructed. Common approaches to simulating

nanofluidic systems are summarized. Lastly, a novel application of fundamental theory is simulated, presented, and analyzed, to evaluate the accuracy of the causal chain for ion current rectification that we developed.

Chapter 8 provides an overview of the conclusions we can draw from the theory which we developed and tested in this research. Since the intent behind this thesis was to foster an intuitive understanding of nanofluidic diodes for engineering purposes, there are numerous research paths that can apply this work. Therefore, this chapter ends with some possible future research directions which would expand upon the material we have compiled.

CHAPTER 2

Biological Relevance

To preface this study of ion rectification in nanochannels, and to give perspective to the field of nanofluidics, we will begin with a discussion of the biological inspiration behind nanofluidics. This section will start by introducing biological examples of nanochannels to demonstrate mechanisms we could one day harness, and will continue on to show some of the motivations and applications for research of nanofluidic devices. Understanding the broader field will contextualize the specific phenomenon of ion recti fication, building a strong foundation for the study of these complex systems.

Although the nanofluidic systems we will focus on are complicated, their biological counterparts are far more intricate, thanks to their highly specific purposes. Organisms are compartmentalized in many ways, and membranes enclose such sections to distinguish separate environments. Membranes are found around organelles within single cells, around cells themselves, and even around organs in the body [1]. But life cannot function when completely sealed off from the world, and some substances are vital to pass in and out to maintain the processes necessary to life. So membranes feature special proteins that form pores or channels which allow only specific ions, molecules, or other mass to pass through. These channels serve as gateways between one side to the other side of the membrane.

A quick note about terminology in this paper should be made before launching into discussion. There is technically a difference between a nanochannel and a nanopore

for structures with nano-scale critical dimensions that connect two sides of a membrane or barrier, distinguished by the ratio between the length and diameter of the open tube. If the length and diameter are commensurate in size, the opening is referred to as a nanopore. If the length is much larger than the diameter, the opening is known as a nanochannel or nano-capillary. However, there is no official universal definition for where the cutoff is for this dimensional ratio, and many sources in the field of nanofluidics use these terms somewhat interchangeably. For simplicity, in this work we will refer to all of these structures, regardless of their dimensional ratios, as nanochannels.

In figure 2.1, we depict three examples of biological nanochannels. These nanochannels are each shown from the side view and the top view, to better show the structures formed by the proteins. Structural dimensions are labeled in nanometers to convey the tiny scale of these biological nanochannels. The complex protein structure that forms each channel has sections with different types of amino acids, which help to finely tune the nanochannel's mass transport capability and allow it to precisely perform its needed function. The following colors distinguish between some such types in figure 2.1: the acidic amino acids, which can be neutral or negatively charged, are colored red; the basic amino acids, which can be neutral or positively charged, are colored blue; and all other (non-acidic and non-basic) amino acids are colored white.

The biological nanochannels in figure 2.1 are most commonly studied for DNA translocation and sensing purposes. Figure 2.1 (A) depicts α-hemolysin, which is a toxin released by *Staphylococcus aureus* (a bacterium in the family of staph infections) that

binds to a susceptible cell and creates a channel in its outer membrane. The channel it creates allows rapid uncontrolled permeation of water, ions, and small organic molecules, damaging the cell and possibly leading to its death [2]. Yet, α-hemolysin has emerged as a very useful protein-formed nanochannel for research purposes, due to its small, selective size and resistance to pH and temperature fluctuations. It is commonly studied to assist DNA sequencing and other biotechnological purposes [3].

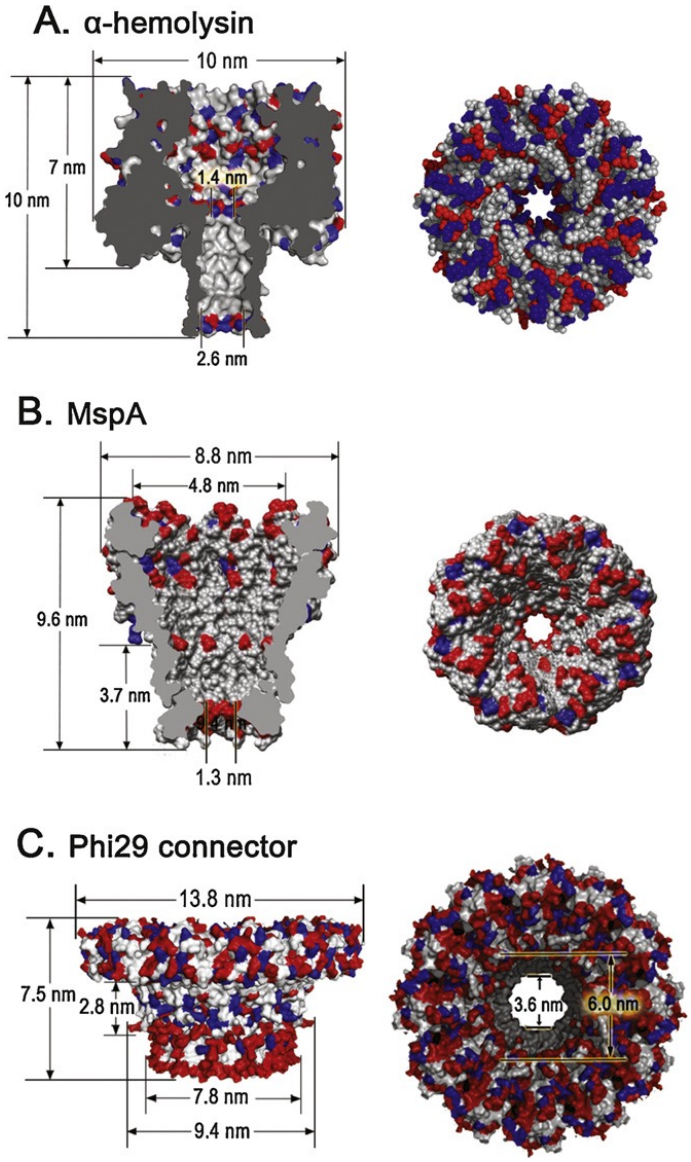

Figure 2.1: Structure of three biological nanochannels (nanopores). Side and top views of (A) heptameric α-hemolysin toxin from *Staphylococcus aureus*; (B) octameric MspA porin from *Mycobacterium smegmatis*; (C) dodecameric connector channel from bacteriophage phi29 DNA packaging motor. In the figures, acidic (red), basic (blue), and other (white) amino acids are shown [4]. Image credit: [4]. In their neutral forms, acidic amino acids can donate protons and become negatively charged, while neutral basic amino acids can accept protons and become positively charged [5].

Figure 2.1 (B) depicts MspA, which is a major pathway for diffusion in a species of bacteria known as *Mycobacterium smegmatis*. Like α-hemolysin, MspA is very robust, and its structure remains stable when the solution's pH or temperature changes. MspA is also of interest to researchers for DNA sequencing, and it offers a higher signal-to-noise ratio of current fluctuations than α-hemolysin, indicating that it is well-suited to be used as a sensor [6].

Figure 2.1 (C) depicts a phi29 connector, which functions as a DNA translocation channel in the phi29 bacteriophage [7]. All linear double-stranded DNA or RNA viruses, phi29 included, package their genomes using a DNA-packaging motor, and each motor contains a central nanochannel known as a connector. This connector's morphological structure is seen in many different viruses, though the individual protein sequences vary greatly between species [7]. Just like the previous two biological nanochannels, the phi29 connector is being researched for DNA sequencing and other sensing purposes, as it is efficient and robust, and can be artificially synthesized in the lab.

This discussion of biological nanochannels was intended to demonstrate some of the many different functions carried out by biological nanochannels, and how they are being repurposed for humanity's use. Among the many varieties and purposes of biological nanochannels are channels specifically structured to translocate ions of biological significance, and they are known as ion channels. Ion channels are structured to meticulously allow only certain ions to permeate. There have been hundreds of types of natural ionic nanochannels discovered, and each type has a precise job to carry out. Evolution has fine-

ly tuned the structure of each type, granting them excellent abilities to regulate ion flow, which is important for many basic biological processes, such as excitation, gene regulation, secretion, absorption, and signaling [8]. Mechanisms for controlling ion flow include conditional "open/closed" states, high selectivity, and preferential direction of ion flow (known as ion current rectification).

Some ion channels are voltage-gated or chemical-gated channels, which allow or prevent permeation depending on the external voltage applied or the bonding of certain chemicals, respectively. Gated nanochannels usually have distinct open and closed states that they can exist in, triggered by some form of external stimulation. An ion pump is a type of gated biological nanochannel that actively transports certain ions into and/or out of the cell, and can pump against the concentration gradient by altering its structure when activated and deactivated. Other nanochannels remain in a single state, maintaining a static structure that passively carries out its function.

One of the most common features of all biological ion channels is selectivity, which is when a channel demonstrates strong preference towards the chemical identity of the translocating ion [1]. The biological nanochannel often gets its selective ability from certain types of ions that attach to bonding sites on proteins within the channel [9]. The location of these binding sites and the type of ions that can bind to them are dependent on the protein structure, and since there are a near-infinite amount of ways to fold proteins of different sizes and sequences, evolution has developed countless structures to carry out various specific tasks.

In this study, we are most interested in nanochannels that exhibit ion current rectification, so we will briefly look at one biological nanochannel which is highly selective towards potassium ions (K^+), and permits the flow of those ions only in one direction of flow – into the cell. This protein-formed channel is known as the inward-rectifier potassium channel, or K_{IR} for short, and is found in many types of cells' membranes [1]. K_{IR} channels can be 3 or 4 orders of magnitude more selective towards K^+ ions than Ca^+ ions, which is impressive, considering those ion species have the same valence charge. For this precise selectivity to work, the channel's smallest diameter must be similar to the ion's diameter so that each ion that passes through is strongly affected by the makeup of the channel walls. In K_{IR} channels, this selective ability is attributed to carbonyl oxygen atoms in the channel's selectivity filter [1]. The mechanisms enabling preferential flow direction in K_{IR} channels, like most nanobiological functions, are still not fully understood, but research points to the adsorption of ions and polyamines, which cause an asymmetrical chemical profile across the length of the channel, as a likely cause. Additionally, the solutions inside and outside the cell are highly asymmetric, as the contents of the cytoplasmic environment differ greatly from that of the extracellular matrix [1]. As we will discuss in later sections, asymmetry with respect to the plane of the membrane is required to produce ion rectification, so these sources of asymmetry mentioned for the K_{IR} channel are likely sources for its rectification ability.

The asymmetric ionic concentrations inside and outside of the cell sets up a potential difference across the cell's membrane, known as the membrane potential [5]. It is

the task of the membrane's protein-formed nanochannels, including K_{IR} channels, to maintain the resting membrane potential at a constant value by controlled flux of particular ions through the cell's membrane.

This membrane potential is especially important for cells that transmit signals, such as neurons, to be triggered at the correct potential difference. Once the potential difference reaches a specific threshold value, known as the action potential, which is high enough to indicate a meaningful signal must be passed, voltage-gated channels open up and allow ions to rapidly diffuse into the cell, in turn triggering the biological response for transmitting the signal [5]. After the signal is passed to the next neuron, the cell must return to its resting membrane potential to be ready for the next signal. Ion pumps are the primary method used for returning the ion concentration inside the cell to values lower than outside, creating the potential difference required.

Unlike gated channels which open or close depending on external stimuli (external voltage value or chemical bonding and unbonding), and unlike ion pumps which actively push ions against the potential gradient (and are fascinating and complicated in their own right), K_{IR} channels are always open [5]. They continue to passively screen ions and only allow a steady, albeit slow, diffusive flux of potassium ions into the cell to compensate for the ion pumps' activity and maintain the resting membrane potential [5]. Without K_{IR} channels, the solution within the cell, known as the cytoplasmic environment, would become too depleted of potassium ions for the cell to function properly.

K_{IR} channels conduct K^+ ions better in the inward direction because they possess ion-binding sites along their pore structure that are both conductive and inhibitory. At internal negative membrane voltages (the potential difference across the membrane is more negative inside the cell compared to outside), K^+ ions are transported into the cell. When the internal membrane voltage becomes more positive than on the outside, K^+ ions are blocked by intracellular multivalent ions [5]. This preferential flow is achieved without the nanochannel changing shape, and is therefore one of the primary inspirations for fabricating nanofluidic diodes.

Through these examples and brief discussion, we can better appreciate how highly specialized biological nanochannels are, and can more easily extend our conceptual understanding to the immensely vast range of applications within even just a single organism. Knowing that cells feature nanochannels in their membranes, and understanding that cells themselves are highly specialized (and can be classified into broad categories such as muscular, structural, protection, and communication), it is clear that biological nanochannels have needed to evolve efficient ways to fulfill their small yet vital roles in the functions of the cell. The cell, in turn, serves its own small role in the functions of the organism itself. The most efficient and effective methods often result in incredibly intricate structures of precise protein makeup and folding, since they have been refined through natural selection over hundreds of millions of years. As such, humanity's pursuit of uncovering them and the mechanics they utilize for our own understanding is only just beginning.

CHAPTER 3

Technology Applications

Now that we have glimpsed some of the many natural functions of biological nanochannels, let us explore the applications that humanity would benefit from if we were able to replicate those abilities. There are hundreds of published articles and research papers which present ideas for applications across the fields of medicine, biology, chemistry, electrical engineering, and more. In this section, we will review some of the main themes of these applications, to provide motivation for the study of nanofluidic channels. But first, the distinction between biological nanochannels and synthetic nanochannels should be clarified to provide a sense of how technology utilizing human-made nanochannels will be inherently different than naturally-occurring biological nanochannels.

3.1: Comparing Biological and Synthetic Nanochannels

As discussed in the previous section, biological nanopores and nanochannels are composed of proteins, with specific composition and geometry that allow for immaculate precision. Even though the capabilities to create human-made nanochannels have expanded in recent decades, synthetic nanochannels created in the lab today are very simple in comparison to their natural counterparts.

The most significant differences are in the typical dimensions and charge profiles: ionic nanochannels in biology are 1-2 orders of magnitude smaller than most synthetic

nanochannels. Typical diameters for synthetic nanochannels are around 5-50 nm, with lengths commonly in the tens of micrometers. For biological ion channels, the most constricted parts of the channel are usually on the order of 0.1-1 nm in diameter, and 1-2 nm in length [5, 10]. The positions of charges are more controlled in biological ion channels than the methods researchers currently use to produce surface charge in the walls of synthetic channels.

Since this study of nanofluidic ion channels aims to focus on the physics of operation and methods of theoretical modeling, we will not cover the details of fabrication methods. Instead, we will briefly mention the most prevalent ones that appear in published works for how nanochannels are created and how fixed charge is embedded in the walls.

The most promising methods we know of to minimize the differences in size and precise structure between biological and fabricated nanochannels are through the use of carbon nanotubes and graphene pores [1], but methods using thicker, more solid substrates are more prevalent in the experimental research field of nanofluidics. One such common method of fabricating both microchannels and nanochannels is etching the length of channels into a substrate, such as a polymer or glass, to form 3 sides of a nanoscale rectangular cross-section, then affixing a flat sheet of substrate over it to form the 4th side [1, 11]. Lithographic methods, similar to those used to fabricate semiconductor devices, are also commonly used [12]. Another method is irradiating a substrate with large ions such as bismuth, producing a conical nanopore from the impact of each ion [1].

Methods of affixing desired surface charge profiles rely heavily on chemistry topics which fall outside the scope of this research, but the main takeaway is that it is possible to create nearly-uniform fixed surface charges on fabricated nanochannel walls, and some methods allow the formation of areas of different polarity or density of applied surface charge. Among these methods is diffusion-limited patterning and other modifications of surface chemistry. Surface chemical modifications become less ideal as the system dimensions shrink due to the finite sizes of the applied molecules [13]. An alternative method, which interferes less with channel geometry and can provide more ideal and abrupt transitions in charge density, is through the use of different oxide materials joined together, connecting nanochannels of inherently different surface charge characteristics [13].

Creating nanochannels by these methods produces much smoother channel walls, as their atomic structures are more compact and rigid than proteins. Proteins are composed of chains of atoms forming coils, helixes, or sheets, which are then folded or coiled upon themselves [5]. Larger sizes and smoother, more solid substrates make modeling synthetic nanochannels easier than modeling biological ion channels. There are many more complex effects introduced by the scale and nonuniformity of protein channel structures, including more pronounced quantum effects, complex chemical interactions, and irregular charge profiles. With so many quantities involved in the function of biological systems, and the fact that they are nonlinearly linked, biological systems are exceedingly difficult to model [5].

In practice, fabrication methods for creating nanofluidic systems are not perfect and the level of precision is nowhere close to that of biological nanochannels, but the relative uniformity of the resulting geometry and surface charge simplifies the system greatly for modeling. Therefore, the approach we will take is to model simple systems that have characteristics commonly found in fabricated nanofluidics.

3.2: Mass Transport Using Nanofluidics

A common theme in nanofluidic applications is the utilization of mass transport, so a cursory understanding of the major effects and variations is important to establish before launching into examples of specific nanofluidic applications. Mass transport facilitated by nanofluidics is a very important and applicable function of nanochannels, and it is also the most similar function to biological examples of nanofluidics. Types of transportable mass includes ions, molecules, proteins, and more; virtually anything that is small enough to occupy the channel can be transported [14].

There are 3 major mechanisms of mass transport: the volume exclusion effect, hydrophobic interactions, and electrostatic interactions [15]. In the field of biochemistry, the excluded volume effect is also known as “hard interactions”. It describes the effect that one ion, molecule, protein, or any type of mass in an aqueous solution has on other mass due to the volume it occupies, effectively displacing solution and excluding any other matter from existing in that volume [16]. When suspended in water, mass with a nonzero charge attracts water molecules, which are polar due to the bent shape of H_2O.

Positive matter suspended in an aqueous solution will attract the oxygen side of water molecules, which is slightly negative, while negative matter will attract the hydrogen side of water molecules, which is slightly positive. This describes the "hydration" of mass, and will increase its effective volume, thus increasing the exclusion effect.

Hydrophobic interactions occur between nonpolar matter in aqueous solution. Nonpolar matter, which has no net charge, will not attract water molecules, but will tend to adhere to other nonpolar molecules in aqueous solution. The "hydrophobic bonds" that cause the interactions are not actually chemical bonds, but they describe the spontaneous tendency of nonpolar groups to cluster together in water to minimize contact with the water molecules [17].

While the volume exclusion effect and hydrophobic interactions are very important to the stability of proteins and have important effects in biochemical applications and other sub-nanometer scale structures, the third and final major mechanism for mass transport is much more familiar to physicists and engineers. This mechanism is known as electrostatics, and as it is relevant to electronics technology, it is more relevant to this study. Electrostatic interactions are the interactions of fixed surface charges in the nanochannel with charged matter suspended in the solution. This is another important effect for biochemical systems because proteins usually have sections of embedded charge, but it stands out as the most important effect for the systems we will focus on. In our research, electrostatic effects are the forces that the permanent surface charges exert on ions

in the electrolyte solution flowing through the nanochannel [15], and are the primary mechanisms enabling charge selectivity and ion rectification.

3.3: Future Technology Under Development

Now that we are cognizant of the main differences between fabricated and biological nanochannels, and the main mechanisms for mass transport through nanochannels have been introduced (with emphasis on electrostatic interactions), we will explore some of the most promising applications of synthetic nanochannels from a device perspective. These applications represent some of the main nanofluidic research areas being investigated around the world, showing the diversity of fields which could make use of nanofluidic technology.

A broad category of applications is nanofluidic sensors, giving hope to the future of nanofluidic devices. Biosensing, especially DNA sequencing, is a huge area of interest for researchers, due to the demand for a fast, accurate, cheap method to record DNA chains and to analyze other biological material. Recall figure 2.1, which contains diagrams of three biological nanochannels that are often used in DNA sequencing applications. These biological protein-formed channels are one type of confinement that ensures the DNA strand is not tangled or overlapped as it moves through the sensing system, but synthetic substrate-formed nanochannels could be used as well. Whether the nanochannels are biological or fabricated from a substrate, the hypothesis for nanofluidic application is that DNA sequences can be recorded by measuring the current modulations

as a DNA strand passes through the channel [18]. Small fluctuations in the current can be attributed to the different bases in the sequence, since these bases have characteristic charges that would interact with the nanochannel's surface charge differently and therefore affect the flow.

Extending this concept, many types of matter passing through a nanochannel could be detected through various methods. A popular device goal which integrates ion transport technology with microfluidics and nanofluidics is known as lab-on-a-chip (LOC) systems. The devices currently in active development will ideally be portable and powerful sensors which can analyze samples more conveniently than in a traditional lab setting. LOC systems are anticipated to be very useful in biomedical and biochemical fields, and in any application that would benefit from the fast analysis of a small quantity of sample, such as polluted substances, to obtain characteristics of its composition [19].

Another category of device applications is energy conversion. There are a large variety of applications in this category, and they can be grouped by the main force that drives their mass transport. Driving forces include concentration/diffusion, pressure, light, and temperature [20]. An example of how concentration-driven energy harvesting is conducted is by setting up a salinity gradient across nanochannels between two reservoirs, forming a system that can harvest Gibbs free energy of mixing as the concentrations diffuse [20]. Nanofluidic channels have also been shown to allow for electrochemomechanical energy conversion, which uses applied pressure gradients to move ions of only one polarity through the channel between two reservoirs. This migration

triggers chemical reactions in the solutions contained in the reservoirs, which then move electrons through an electrical load from one reservoir to the other in response to the migration of one polarity of ions through the nanochannel [21].

While the previous application's function utilized chemical reactions in the reservoirs, there are applications that benefit from containing the reactions within the nanochannels themselves. The nano-scale confinements inherent to nanochannels are useful for manipulating chemical reactions, so chemical reaction modification is another motivation for developing nanofluidic technology. It provides a tool for confining chemical species and controlling what interacts with it and how much, effectively enhancing the catalytic activities [20]. By immobilizing and encapsulating the catalysts, the nanofluidic channels confine chemical reactions much like a reactor does, and so they are well-suited for chemistry applications.

Because nanochannels can, under certain setups, selectively pass desired mass types while preventing others from traveling through, nanofluidics shows promise for separation purposes, such as water desalination, drug delivery, and gas filtration [20]. Research is being conducted into designing membranes which contain nanochannels that regulate what substances can permeate through, and this nanofiltration technology would be useful in many different fields.

Understanding channel diffusion can lead us to control the transfer of ions for purposes such as the delivery of medications. Chemical delivery nanochannels placed between two ionic solutions of different concentration exhibit easier flow from high to

low concentration than from low to high [11]. Researching the mechanics of ion transport would lead to more sophisticated methods of medicine delivery that apply to more situations than just concentration diffusion. Control of flow rate is vital for medicine, and advancing nanofluidic technology would be ideal for rapid, targeted, easily adjustable delivery of drug doses [20]. There is also evidence that ions can be pumped against a concentration gradient by applying a periodic, time-dependent potential difference across a nanochannel, which expands the situations nanofluidic mass transport can be applied to in the medical field and beyond [22].

A specific category of ion transport in nanofluidics is rectified ion transport. Ion current rectification is the focus of this research, and such control over the direction of ion flow finds applications not only to the medical field, but it is also analogous to the electrical concept of rectified current – a vital phenomenon for all kinds of electronic devices. Instead of electron current being rectified, however, rectifying nanochannels do so with ion current, by allowing ion flow in one direction and suppressing ion flow in the opposite direction.

Due to this functional similarity to semiconductor diodes, there is interest in developing other electronic components that normally use semiconductor diode technology, such as transistors. A nanofluidic triode which functions as a switch was constructed by Cheng and Guo [13], and inspires the possibility of a nanofluidic bipolar junction transistor. Voltage-gated nanochannels that resemble MOSFETs have been demonstrated by Guan, Li, and Reed [12], and logic gates constructed out of nanofluidic diodes have been

demonstrated by Gomez, Ramirez, et al. [23]. In particular, AND, OR and NOR logic functions were demonstrated through nanofluidic diodes, using electrical input and output signals [23].

This translation of signal between “wet” and “dry” electronics shows fascinating potential for applications of controlling ion current with the more familiar electron current, or vice versa. Clearly, there is value in understanding how nanofluidic diodes can be engineered to rectify ion current, and this intriguing analogous behavior to semiconductor electronics begs the question of how far the similarities go.

CHAPTER 4

Introduction of Systems to be Studied

Now that we have introduced nanofluidic diodes and the broader perspective of nanofluidics research, we will direct our attention to the systems at the focus of this research before we begin our investigation of the theory. This section will also review ion current rectification (ICR), which will come up very often in this research as it is what nanofluidic diodes are supposed to exhibit.

4.1: General System Explanation

As we develop the theory, we will see that an asymmetry in electrostatic impact, achieved through a physical asymmetry in the nanofluidic system, is required to produce ion current rectification. In this research, we chose three of the most highly-studied types of asymmetries to focus on, and to isolate and clarify these types, we will present each using an example system with its own diagram. In figure 4.1, we will present a general system with no asymmetries that will not rectify current, as a way to define a “default”, symmetric system. Then, we will use figures 4.2, 4.3 and 4.4 to introduce each type of asymmetry individually, essentially modifying the default system from figure 4.1 in three different ways.

Figure 4.1 shows a 2-dimensional length-wise cross-section of a general system for the purpose of labeling the main components and establishing the default system. This

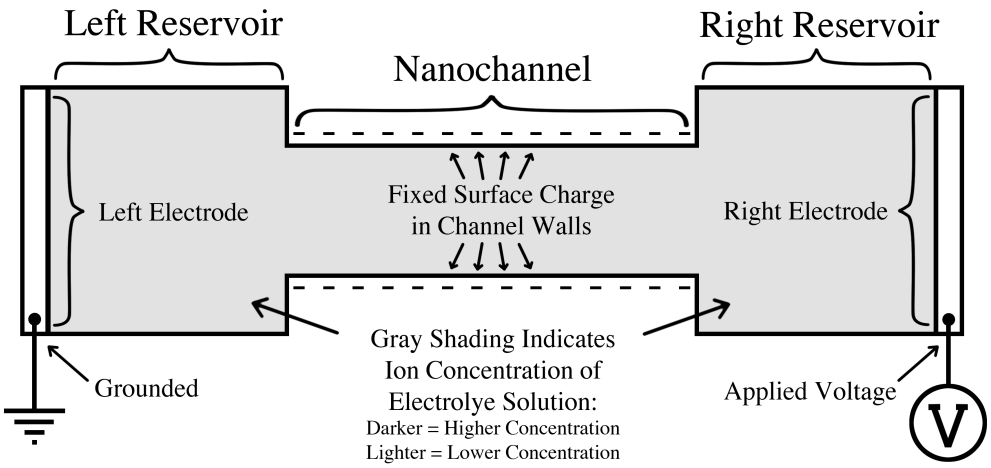

Figure 4.1: A symmetric nanofluidic system (not to scale), with main components labeled.

figure and the ones to follow are not to scale; the channel is vertically enlarged to better show the characteristics of and behaviors within the nanofluidic structure.

As seen in figure 4.1, the nanochannel connects two square reservoirs, sometimes called baths, which are usually micrometers in scale, and so the reservoir widths are usually 2-3 orders of magnitude larger than the diameter of the channel connecting them. The purpose of the two reservoirs is to contain the bulk of the ion solutions of known concentrations, which can flow between them by traversing the nanochannel. In figure 4.1, the concentrations are uniform, so the gray shading is also uniform to convey this.

The electrolyte solution used for these systems is potassium chloride, which is a 1:1 electrolyte because each ion is singly-charged, one species being positive and the other negative. The molar concentration of the solution quantifies the number of moles of KCl per unit volume, while the ionic concentration quantifies the number of ions per unit volume. This is important to clarify because each mole of KCl contains two moles of

ions: one mole of K^+ ions and one mole of Cl^- ions. There are an equal number overall of both ion types, and a property called electroneutrality holds in equilibrium so that the ions are uniformly distributed. So unless specified by species, ion concentration here refers to the concentrations of both types of ions, since their distributions within a single unit volume is approximately equivalent. Low ion concentration means there are fewer K^+ and Cl^- ions per unit volume, while high ion concentration means there are more K^+ and Cl^- ions per unit volume.

Throughout this research, we will regularly refer to the concentrations of either ion species, to paint the picture of how they differ from each other in nanofluidic diodes, as well as to quantify relationships. To maintain consistency, we will use units of number density, as opposed to molar density, in the equations presented. The relationship between number density (symbol: n, units: number/m^3) and molar density (symbol: c, units: mol/m^3) is simply expressed using Avogadro's number, N_A, as $n = N_A c$ [24]. Molarity (M) is also a commonly-used unit, and quantifies the number of moles per liter (equivalently, moles per cm^3). If c is in units of M, then the conversion to number density is simply $n = 1000 \cdot N_A c$.

The nanochannel's walls hold a fixed surface charge, which in the symmetric case is uniform in density along the length of the channel. This charge density is embedded within the substrate itself when the nanochannel is fabricated and, in the systems presented here, cannot change. It is important to distinguish the fixed surface charge from the ions in the electrolyte solution; the ions only exist in the fluid and the the fixed

surface charge only exists in the solid wall. Often, we will refer to the surface charge as the “wall charge”, as it is not to be confused with the ions that are electrostatically held to the surface, against the solid-liquid interface.

Lastly, there is one electrode in each reservoir, to apply the external electric field across the channel and drive the ion current through the nanochannel. The left electrode is grounded, and the right electrode is given an applied voltage, which can vary in magnitude and polarity, allowing for control of the electric field magnitude and direction across the system.

4.2: Three Main Types of Asymmetry

The three diagrams below present the three main types of asymmetry that can cause ion current rectification. These are the modifications to the general system from figure 4.1 that we will study in our research on nanofluidic diodes, and so it is important to lay them out clearly. Doing so will give context to later chapters, where we will cover the fundamental theory behind mechanisms at play within these nanofluidic systems.

Each of the three cases features one type of asymmetry: figure 4.2 has fixed surface charge asymmetry, but symmetric ion concentration and geometry; figure 4.3 has ion concentration asymmetry, but symmetric fixed surface charge and geometry; figure 4.4 has geometry asymmetry, but symmetric fixed surface charge and ion concentration. These three cases are separate device designs, they are not able to transform from one to another. For the cases of surface charge asymmetry and geometrical asymmetry, the

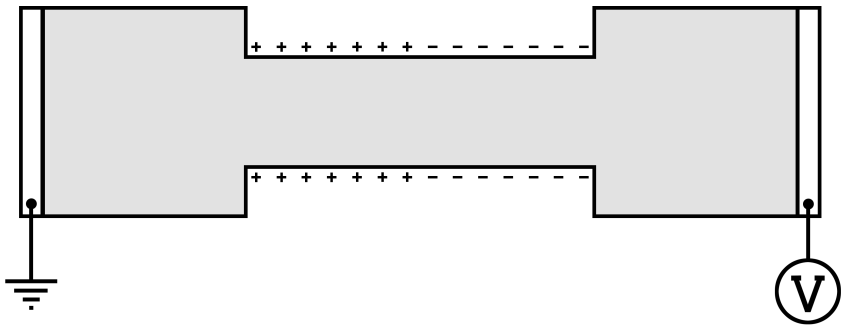

Figure 4.2: Asymmetry in fixed surface charge. The left half of the nanochannel has a uniform positive surface charge density, while the right half has a uniform negative surface charge density.

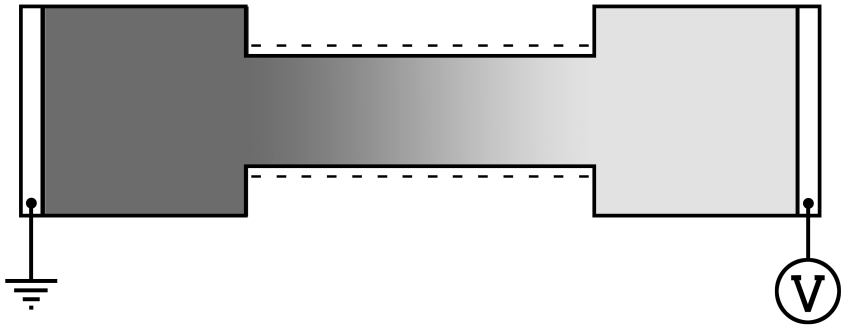

Figure 4.3: Asymmetry in ion concentration. The left reservoir holds a high ion concentration, while the right holds a low ion concentration. The shade gradient across the channel corresponds to the resulting concentration gradient between the two reservoirs.

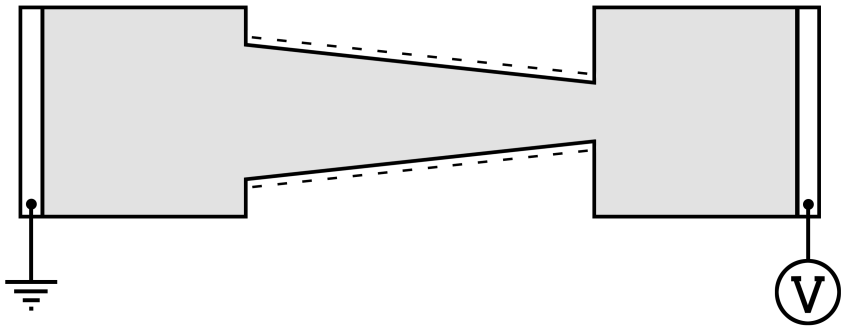

Figure 4.4: Asymmetry in geometry. The channel diameter is at a minimum on the right opening, and at a maximum on the left opening, with a smooth slope along the channel between them. The result is a conical nanochannel.

structure is locked in during device fabrication. Asymmetry in bulk ion concentration is enacted by filling the reservoirs with the same electrolyte solution of different concentrations.

4.3: Ion Current Rectification (ICR) and Diode-Like Behavior

It is prudent to review the meaning of "ion current" and "rectification" so that it is clear what we are referring to when we build the theory behind nanofluidic diodes. Ion current is simply the measure of charge movement, with the charge carriers taking the form of cations (positive ions) and anions (negative ions) that flow in a solution. Current points in the direction that cations flow, since they are positive. Anions also contribute their transport of charge to the total current, but anion current is in the opposite direction of its movement. So, cations and anions flowing in opposite directions will both contribute current in the same direction.

Rectification occurs in a system when one direction of current is preferred over the other, and devices that exhibit this behavior are known as diodes. When the applied voltage that induces current is in "reverse bias", denoting the direction of the electric field it produces, the system experiences repressed current flow. Increasing the voltage difference farther into the reverse bias mode will not produce significant increases in charge transport. When the applied voltage is in "forward bias", the system strongly conducts current flow. Increasing the voltage farther into forward bias produces a rapid, usually nonlinear, increase in current. We show a basic plot for a current-voltage

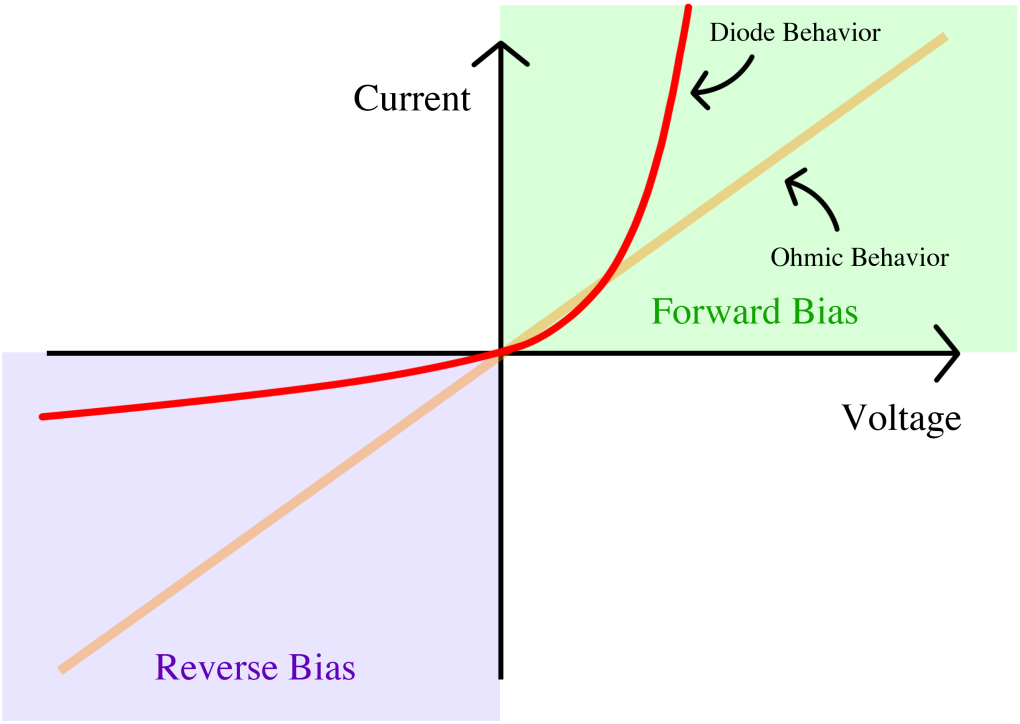

Figure 4.5: Comparison of general current vs. voltage trends for linear ohmic behavior and nonlinear diode-like behavior.

relationship that exhibits current rectification, also known as diode-like behavior, to emphasize the distinction between forward bias and reverse bias.

Figure 4.5 features the two regions of operation for diodes: reverse bias and forward bias, separated by the point where applied voltage equals zero. We compare the diode-like behavior (red line) to linear, ohmic behavior (orange line), which follows Ohm's law: $I = \Delta V/R$ [25]. It is common knowledge that Ohm's law describes how current, I (A), through a wire of resistance, R (Ω), depends directly on the electric potential difference applied across the wire, ΔV (V). In ohmic behavior, the current-voltage trend is linear, with a constant slope of 1/R. This raises an interesting implication

about diode behavior for our study of nanofluidic diodes: resistance must vary with applied voltage. As we will uncover throughout this research, conductivity (the inverse of resistivity) must be asymmetrical across a nanochannel in order for ion current to show rectification. This asymmetrical conductivity is obtained through asymmetrical electrostatic impact, induced by a physical asymmetry in the system, as mentioned previously.

The rectifying factor, or degree of rectification, appears commonly in the literature and defines the ratio of the magnitude of forward-bias current to the magnitude of reverse-bias current [26]. This factor is a useful way to quantify the rectification ability of a system. The acronym ICR can also refer to this ratio for ion current. Since nanofluidic diodes are created to rectify ion current, we usually want this degree of rectification to be as high as possible.

Now that we have familiarized ourselves with the systems targeted for this research and the general concept of ion current rectification, we will be able to better frame our theory around them. Figures 4.2, 4.3, and 4.4 serve as central diagrams for this research, and they will be referred to commonly in our discussion of nanofluidic diodes in order to visualize the main physical asymmetries which enable ion current rectification.

CHAPTER 5

Fundamental Nanofluidics Theory

Nanofluidics and microfluidics are becoming extensively-researched fields, with mechanisms that have been well-documented, experimentally tested and measured in abundance, as well as modeled using a variety of methods. This is not to say that everything has been discovered and explained, however, as many mechanics and characteristics of nanofluidic systems lack complete quantitative models. Only in the most recent few decades have we developed methods to reliably fabricate nano-scale devices, as well as the computational capacity to handle the complex numerical simulations for modeling them. However, as nanofluidics is a highly multidisciplinary field, researchers have a wide variety of approaches to document their work from. This makes for a rather esoteric and diverse collection of literature, and it is filled with multiple different definitions and simplifications that can appear contradictory and confusing. Therefore, a strong motivation for this chapter is to bring clarity to the field for the engineering of nanofluidic diodes. We will do this by considering many sources in our discussion, and by creating new diagrams to better communicate these complex topics.

The focus for this chapter is on the fundamental concepts most important to the field of nanofluidics and ionic transport, with the broader understanding of how these concepts appear in and are often derived from microfluidics. The concepts covered here are in one way or another directly relevant to the understanding or modeling of the systems under investigation and will therefore be addressed in depth. Other details which are

not specifically relevant to ion current rectification in nanofluidics, but nonetheless are noteworthy, are included for the sake of completeness, as well as to give context to the modeling decisions, especially simplifications made later on.

The fundamentals of microfluidics and nanofluidics share plenty of overlap, but the smaller scale of nanofluidics means that certain mechanisms influence system behavior more than they do in microfluidics, such as the effect of surface charge. As the diameter of the channel shrinks, the surface to volume ratio rises dramatically, leading to behavior unique to nanofluidics that are not observable in microfluidics [15]. The nanoscale dimensions are necessary for ion current rectification (ICR) – the key mechanism in a nanofluidic diode. For this research project, the systems being studied have functional features with nanometer-scale dimensions. Because of this and the fact that the ions being transported are freely suspended in a fluid, ionic nanochannels exhibiting electrokinetic (movement of charge) phenomena constitute nanofluidic systems.

A foundational concept for how nanofluidic diodes operate is that of the Debye length, which will be covered in great detail in this chapter because it is so important to ICR. The internal diameter of nanochannels is usually comparable to the Debye length of the ionic solution, which can range from about 1-100 nm [27]. Microfluidic devices are exclusively larger than the Debye length, rendering its effect almost negligible, while in nanofluidic devices, the Debye length plays a primary role in functionality. The ionic distributions inside nanochannels are a direct consequence of the relationship between surface charge density in the walls, the diameter of the channel, and the ion concentrations in

the bulk [15]. The proof will develop as we build on these concepts, and we will see how deeply fundamental they are to the function of nanofluidic diodes.

5.1: Charge Screening, the Electric Double Layer, and the Debye Length

In the context of ion channels, the key difference between microfluidics and nanofluidics is the influence of the fixed surface charge on the ions in the channel. To elaborate, we must first discuss the phenomenon of ion screening, characterized by the Debye length. Through investigation of the Debye length, it will become clear how ion screening plays a stronger role in nanofluidics as compared to microfluidics, and more importantly, pave the way for understanding the important phenomenon of the electric double layer.

Ions suspended in an aqueous solution are subject to movement due to any external electric fields present, since by definition ions are atoms or molecules that carry a nonzero charge. To summarize the widely-known fundamentals, the charge is zero if the number of electrons and the number of protons are the same, negative if the ion has one or more electrons than what can be counterbalanced by its nucleic protons ("extra" electrons), and positive if the ion has one or more protons in its nucleus that are not balanced out by orbiting electrons ("missing" electrons). Due to this net charge, ions themselves are sources of electric fields and therefore interact with one another, experiencing forces due to the electric fields generated by the charge of other ions.

The electrostatic force that induces this movement is the Coulomb force, which has been discovered and verified through experimentation and is given by

$$\mathbf{F}_1 = \frac{q_1 Q}{4\pi\varepsilon \left|\mathbf{r}\right|^2}\hat{\mathbf{r}} \,. \tag{5.1}$$

The Coulomb force F_1 (kg·m/s^2, or equivalently, N) that acts on a charge Q due to a separate charge q_1, in a fluid of absolute permittivity ε, is dependent on the polarity and magnitude of charges q_1 and Q (in coulombs, C). F_1 is inversely related to the square of the distance of separation between them, **r** (in meters, m), represented as a vector that points from q_1 to Q. The notation $\hat{\mathbf{r}}$ denotes the unit vector form of **r** [28]. From equation 5.1, we can see that like-polarity charges produce a repulsive force, and opposite-polarity charges produce an attractive force between the two charges.

Note that the absolute permittivity, ε, is characteristic of the medium, and quantifies the factor of decrease that the electric field experiences in that medium. The symbol ε is shorthand for the product $\varepsilon_0\varepsilon_r$, with ε_0 being the permittivity of free space and ε_r being the dielectric permittivity (or relative permittivity) of the specific medium.

The net, or total, force exerted on each ion is the combination of Coulomb forces exerted by each ion surrounding it, obtained through simple vector addition of the forces. As previously stated, these forces are the result of electric fields. The relationship between the net Coulomb force, **F** (N), exerted on a charge Q (C) and the net electric field present, **E** (N/C, or equivalently, V/m), is given by

$$\mathbf{F} = Q\mathbf{E} \,. \tag{5.2}$$

Combining equations 5.1 and 5.2, we can express the net electric field at any point due to the positions of all charges present as a summation of the electric fields generated by each of the n charges as

$$\mathbf{E} = \frac{1}{4\pi\varepsilon} \sum_{i=1}^{n} \frac{q_i}{\left|\mathbf{r}_i\right|^2} \hat{\mathbf{r}}_i \,. \tag{5.3}$$

As seen in equation 5.3, the electric field at a given point is a vector quantity, and is a function of the relative separation vectors between the given point and each charge.

Physics defines the direction of the electric field to be coming out of positive charge and going into negative charge, so electric fields are vectors because they have both magnitude and direction. It is common knowledge that opposite charges attract and like charges repel (also apparent in equation 5.1), but logically it makes sense when conceptualizing the electric fields around the charges as vectors. Oppositely-charged particles will attract because the electric fields between them agree in direction and combine constructively, while particles with the same charge polarity will repel because the electric fields' directions are discontinuous between them, and they combine destructively.

Keep in mind that although we will mostly consider ions to act as one-dimensional point charges, this is merely a convenient simplification. This simplification works best when the diameter of the channel is very large compared to the true physical size of ions in the solution. For example, a nanofluidic channel with a diameter of 20 nm is about 40 times wider than the effective diameter of a single K^+ ion (the largest ion species in the systems we study, using KCl electrolyte in aqueous solution), which is approximately 0.5

nm [29]. This ratio becomes even larger as the channel diameter increases, but as the diameter decreases, the finite ion volume becomes more important and neglecting it leads to larger error. There are ways to improve upon a point-charge model to compensate for finite volume later on if desired (such as through imposing a radius of closest approach), but since the point-charge-based model is qualitatively accurate and simpler than accounting for the ions' finite volume from the beginning, it is the model of choice for this research.

The phenomenon of charge screening is a straightforward result of how charges interact with one another, and can be illustrated through a simple example. Let us conceptualize an electrolyte solution composed of negative ions, all carrying the same magnitude of charge. Each ion will feel a repulsive force from every other ion, resulting in a volume around each ion which is depleted of other ions. The radius of this volume of exclusion will depend on the concentration of the ion solution: the more ions that are present per unit volume, the less distance they can maintain from each other, and conversely, the lower the ion concentration, the greater the distance from one another they can sustain. The field generated by each ion remains the same, but the "effectiveness" it has on repelling other ions is dependent upon the total ion concentration. In other words, the electric field around an ion is dampened by the increased presence of other like-charged ions. This is essentially the concept behind charge screening, also known as electric-field screening, which is important for understanding our next topic – the electric double layer.

5.2: Electric Double Layer Qualitative Model

For nanofluidic ion channels, the most important consequence of ion charge screening is the formation of an electric double layer on any charged surface. Whatever polarity of fixed charge is embedded in the surface of the channel walls, ions of the opposite polarity, known as counter-ions, will be strongly attracted and adhere to the surface, a process called adsorption. Ions of the same charge polarity as the embedded wall charge are known as co-ions, and are depleted close to the charged walls. With enough counter-ions adsorbed to and accumulated at the charged surface, ions farther away from the surface will be less affected by the surface charge, an effect of charge screening. The layer of counter-ions essentially cancels out the surface charge from the point of view of ions more distant from the wall. This adsorbed layer of counter-ions held closely to the charged wall, together with a more diffuse layer of counter-ions (and some co-ions) in the adjacent solution, is what we refer to as the electric double layer, or EDL [30].

A brief note on terminology should be made regarding “EDL”. In this paper, we arbitrarily chose to represent both singular (electric double layer) and plural (electric double layers) versions of the term with the same acronym, EDL. The plural term would apply to the case of multiple separate charged surfaces, as each will form its own EDL when in contact with an electrolyte solution. Although it would not be incorrect to refer to multiple electric double layers as “EDLs”, we made the stylistic choice to exclusively use “EDL” in this paper.

Our understanding of the basic structure of the EDL comes from experiments conducted over the years, but the experimental methods cannot yet completely quantify the structure and distributions of the ions in aqueous solutions near surfaces [24]. This gives computational simulations more importance to model the physics believed to be at play. The simulations and models we use to understand the EDL were developed and improved upon over time, but the layers they describe are conceptual, not rigid physical boundaries. There are regions and planes in the models which serve as frameworks to explain real-world data, but they are only frameworks. One thing that all theories agree on is that the EDL, electric field, and electric potential follow a decreasing exponential function of distance from the wall [30].

A complete qualitative model of the electric double layer which forms at the interface between a solid surface with fixed charge and a symmetric electrolyte solution has several main components, characterized by changes in the makeup and the electric potential at certain distances away from the boundary between substrate (the solid makeup of the channel wall) and solution. The Guoy-Chapman-Stern model is the most widely used model to describe an EDL [31], and it is the model we will use to guide our discussion of the EDL qualitative structure. However, there are numerous variations of EDL models in use, at times creating some seemingly conflicting definitions. For the purposes of this research, we will take these variations into consideration and adapt a qualitative model that agrees with as many models as possible, to get the clearest and most complete understanding of the basic EDL structure.

In figure 5.1, we illustrate a simplified, conceptual EDL with an electric potential vs. distance relationship overlay in purple. For this example, the substrate has a net negative fixed uniform surface charge (like the channel walls in most of our systems to be studied), so the counter-ions that make up the EDL are positive. The vertical line serves as both the electric potential (Φ) axis and the boundary between the solid surface and the electrolyte solution. The horizontal line serves as the distance (x) axis and represents the

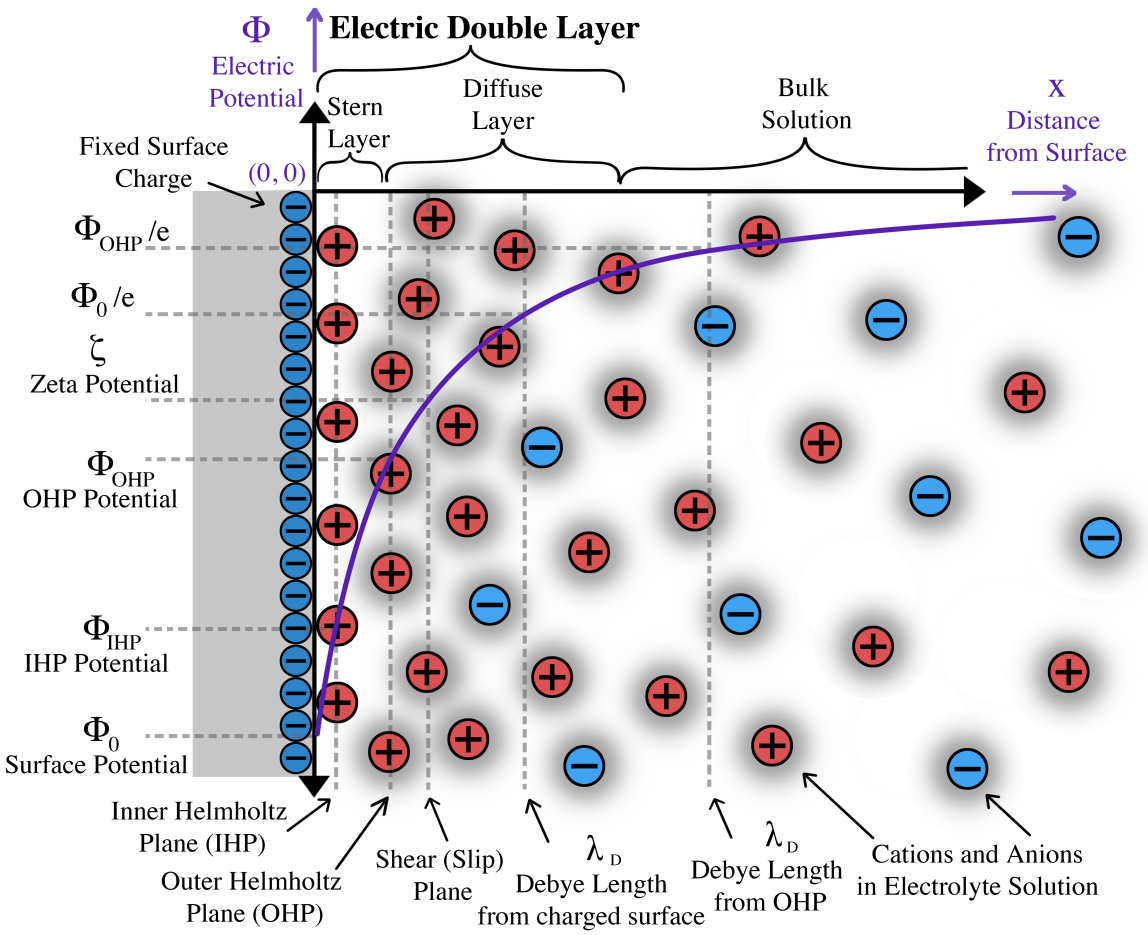

Figure 5.1: Conceptual diagram of a simplified electric double layer (EDL) that forms at the boundary between a charged solid surface and an electrolyte solution. Hydrated ions are denoted by a gray shadow.

perpendicular length away from the surface. The circles represent positive and negative charges, denoted by the sign inside them. The fixed charge is depicted as negative charges lined up to the left of the vertical axis, and the ions in the electrolyte solution are represented by charges to the right of the vertical axis.

The diagram is not to scale, it is just a basic representation to serve the purpose of illustrating the EDL model. The ions are treated as idealized rigid spheres, and the solvation of the ions (or more specifically, hydration, if in aqueous solution) has been simplified to be represented by a drop shadow. A more accurate, but more complex, diagram would show water molecules clustered around all of the ions in the electrolyte solution except for the ions adsorbed to the surface.

Now that the basic layout and simplifications of the diagram have been conveyed, we can focus on the qualitative EDL structure that we show with figure 5.1, which is based on the Guoy-Chapman-Stern model. We will begin with general descriptions of the two layers this model describes, and then elaborate on the electric potentials defined to quantify them.

The first layer, known as the Stern layer, is closest to the surface and encompasses the ions that are strongly held with attractive Coulombic forces by the fixed surface charge. The Stern layer is populated exclusively with counter-ions that are electrostatically adhered to the surface, so its ions are considered immobile with respect to the surface. The most firmly adhered ions are electrostatically held so close to the surface that no water molecules come between ion and substrate, so they are not considered hydrated, and

are “specifically adsorbed” to the surface. Immobile, adsorbed ions are what the Stern layer accounts for as an improvement to the Guoy-Chapman model, which only considers the diffuse layer [24].

Hydrated ions are distinct from the specifically adsorbed non-hydrated ions in the Stern layer. Their closest approach marks the end of the Stern layer and the beginning of the diffuse layer. There are two planes defined for the Stern layer: the Inner Helmholtz Plane (IHP) and the Outer Helmholtz Plane (OHP). The IHP passes through the centers of non-hydrated ions that are specifically adsorbed to the surface, while the OHP passes through the centers of the hydrated ions at their closest approach to the surface [31]. The most important concept to grasp for the Stern layer is that it can be considered completely immobile in most cases. The short-range Coulomb forces on ions in the Stern layer over-power most reasonable externally applied electric fields, and frictional forces oppose shear (along the plane of the surface) movement of ions in contact with the surface [32].

Moving perpendicularly away from the charged surface, the electric field from the negative surface charge is screened out by the counter-ions in the EDL, and the distribution of cations and anions in the solution exponentially approaches its bulk value. Electro-neutrality can be assumed in the bulk solution, meaning the positive and negative ions are evenly distributed and there is no net electric field. While the bulk solution is electrically neutral, this is not true near the charged walls. When moving from the bulk towards the charged wall, there is increasing depletion of co-ions and increasing accumulation of

counter-ions. Understandably, this is due to electrostatic repulsion and attraction acting on the ions from the fixed surface charge [24].

The volume between the Stern layer and the bulk solution is known as the Guoy-Chapman diffuse layer, or simply the diffuse layer, due to the less rigid distribution of the ions that populate it. The diffuse layer has a higher concentration of counter-ions than co-ions, but unlike the Stern layer, there exist some co-ions present in the diffuse layer. Also unlike the immobile Stern layer, the ions in the diffuse layer can move with respect to the substrate due to externally applied electric fields–an important distinguishing characteristic. Note that all of the ions in the diffuse layer are hydrated, while all of the ions in the Stern layer are non-hydrated and are specifically adsorbed to the wall.

Considered together, the Stern layer and the diffuse layer are the two regions that comprise the electric double layer. Their boundaries are not rigid physical separations, rather, their thicknesses can be defined by the distance where the electric potential reaches certain values.

There exist some conflicting definitions of what the “double” in electric double layer stands for. Some sources will distinguish the “triple-layer model”, where consideration of the adsorbed ions (the Stern layer) constitutes a third layer [31]. Then, “double” is implied to refer to the diffuse layer and the layer of embedded surface charge. This distinction is overly confusing for our purposes, and in many other literature sources, EDL refers to just the two ion layers in the solution (Stern and diffuse), which is what we will

adopt for this research. We mention this alternate definition simply to acknowledge its existence and to clarify our choice of terms.

For the systems we are studying, electric potential is quantified with respect to the value in the bulk electrolyte solution, and serves as a convenient scalar measure of net electric field. In general, the electric potential is related to the electric field by

$$\mathbf{E} = -\nabla\Phi\,, \tag{5.4}$$

where the electric field represented as a vector, **E** (V/m), is the negative of the gradient of the electric potential, Φ (V) [28]. Equation 5.4 also helps conceptually connect the electric field to the electric potential: the slope of the electric potential is the electric field vector with opposite direction. Referring back to figure 5.1, we can see this aligns with our understanding in two dimensions. The slope of the electric potential vs. distance trend is positive when moving in the +x-direction, indicating the electric field points in the –x-direction. Since the largest component of the net electric field is from the negative surface charge, it makes sense that the electric field points toward those charges.

The potential at the wall is known as the surface potential and appears in figure 5.1 as Φ_0. It is negative due to the polarity of the surface charge, and its magnitude is the largest in the system. Keep in mind that there can be different definitions of the "surface potential", depending on the context. We will use Φ_0 to specifically reference the electric potential at the charged substrate surface (the boundary between solid wall and electrolyte solution). We will use Φ_s to reference the potential at a surface with a more flexible definition, such as situations that treat the OHP as the boundary between fixed charge

and mobile charge (see the Guoy-Chapman-Stern model, discussed later). The potentials at the IHP and the OHP are sometimes named; here we will use Φ_{IHP} for the potential at the IHP and Φ_{OHP} for the potential at the OHP. The OHP is also known as the onset of the diffuse layer [31], which brings us to the third plane from the surface, the shear or slip plane.

The shear plane is oriented through the centers of the first hydrated ions that are mobile, hence the name. It indicates the electric potential at the location of the first ions that can shear (move in the direction parallel to the surface) from the rigidly held ions in the Stern layer and the closest hydrated ions which are also essentially immobile. The electric potential at this shear plane is commonly defined as the zeta (ζ) potential.

The final distinguishing plane of the EDL structure separates the diffuse layer from the bulk solution. This plane is located at the Debye length (which will be discussed in-depth later). For most purposes it marks the "end" of the EDL, but the specific position depends on the model being used. Some sources define the Debye plane as being located one Debye length away from the charged solid surface, where the potential has decayed to the Φ_0/e point (see reference [24]). Other sources, specifically the ones that follow the Guoy-Chapman-Stern model, define it as being located one Debye length away from the OHP, so its potential would be Φ_{OHP}/e (see reference [31]). In figure 5.1, both are presented, and the brackets distinguishing the bulk solution from the diffuse layer take the midpoint between the two definitions.

Most disagreements among different models stem from a simplification that can be made about the Stern layer. One of the more mild simplifications involves assuming the potential at the OHP is equivalent to the zeta potential, since the OHP is only a maximum of a few molecular diameters away from the shear plane [24]. A more significant simplification would be taking the surface potential to be the same as the zeta potential [24]. The logic for such a simplification applies mostly for microfluidic systems, or nanofluidic systems where the thickness of the Stern layer is very small compared to the diameter of the channel. In this simplification, the Stern layer is considered to be part of the wall's surface charge as it is immobile and doesn't contribute significantly to ion current. The concept of the wall is shifted to be the interface between the Stern layer and the diffuse layer, with the total surface charge density being the charge in the substrate plus the charge of the ions that populate the Stern layer [27]. This simplification works best for high surface charge density, since in that case the majority of the counter-ions that balance the substrate's surface charge are located within the first few angstroms from the surface [27].

It is also especially useful for cases of high surface charge density in the substrate, because some models (see the Guoy-Chapman model, discussed later) may overestimate the concentration of counter-ion accumulation at the interface. To account for the adsorbed counter-ions' finite volumes, a linear drop in potential can be described across the Stern layer, and the notions of the "wall" and its potential are given to the OHP (see the Guoy-Chapman-Stern model, discussed later).

For the purposes of this research, the difference between the Debye length from the charged surface and the Debye length from the OHP is fairly negligible, but more importantly, neither one *actually* marks the finite "end" of the EDL. The electric potential magnitude decreases exponentially as distance increases from the charged surface, but even in what we define as the bulk solution, there is still a nonzero potential contributed by the charged surface. The takeaway is that the EDL does not have a firm "edge", but the Debye length provides a convenient way to characterize its distance of influence.

5.3: Foundational Physics Models

So far, our theory has mainly been qualitative in nature, with a few simple physics relationships to review the basics of electrostatics. This has worked well for introducing the reader to such important topics as the electric double layer and the concept of the Debye length. But in order to get a deeper understanding of these models and work towards numerically modeling the behavior of nanofluidic diodes, we must have an efficient way to quantify these concepts. The purpose of this section is to review the remaining foundational physics models which are important to nanofluidic diode systems.

We will start with Gauss's law, which quantifies the fundamental relationship between the electric flux (electric field density passing through per unit area) through a hypothetical closed three-dimensional surface and the charge enclosed by that surface. Gauss's law is given as

$$\oint \mathbf{E} \cdot d\mathbf{a} = \frac{1}{\varepsilon} Q_{enc}\,, \tag{5.5}$$

where the lefthand side of the equation represents the electric flux (the electric field **E** (V/m) passing through each infinitesimal unit area $d\mathbf{a}$ (m^2), integrated over the whole closed surface), and the righthand side relating the flux to the enclosed charge, Q_{enc} (C), and the absolute permittivity of the medium, ε [28].

The enclosed charge, Q_{enc}, can be written as the volume integral of the charge density that is within the closed surface:

$$Q_{enc} = \int_V \rho \, dv\,. \tag{5.6}$$

Here, ρ is used to denote volumetric charge density (C/m^3), and dv denotes infinitesimal volume contributions to be integrated over the total volume, V (m^3). Substituting equation 5.6 into equation 5.5, and substituting equation 5.4 into equation 5.5 to write electric field in terms of electric potential, equation 5.5 simplifies to

$$\nabla^2 \Phi = -\frac{\rho}{\varepsilon}\,, \tag{5.7}$$

where Φ (V) is the resulting electric potential due to the volumetric charge density ρ in a medium with absolute permittivity ε [28]. Equation 5.7 is a very significant equation in all applied fields of electrostatics, and is known as Poisson's equation or the Poisson equation. For the nanofluidic systems we are studying, ρ is the charge density of the mobile ions in an aqueous KCl electrolyte solution, and ε is the absolute permittivity of water.

5.4: Electric Double Layer Mathematical Model

Let us return to the electric double layer now that we understand the roots of the Poisson equation, so that we can build a quantitative model. For this research, we will study the first mathematical model that was developed for EDL around 1910-1913 by Guoy and Chapman, and later improved upon by Stern [24].

The Guoy-Chapman model provides a fairly good (though simplified) approximation of the electric potential profile in an electrolyte solution near a plane of uniform fixed charge [24]. However, it is built from classical models of the EDL, which struggle to closely predict quantitative experimental values due to simplifications. These include neglecting ion-ion correlations, finite ion sizes, nonbonding interactions between ions known as steric effects, and electrostatic image interactions [33]. Despite this, the model's strength lies in the fact that it accurately describes the fundamental behavior of the ions in a compact manner.

5.4.1: The Poisson-Boltzmann Equation and the Debye Length Equation

In our EDL model, the ions populating the diffuse layer follow a typical organization described by the Boltzmann distribution. Thermodynamics defines a Boltzmann distribution as the most probable distribution of a set of indistinguishable particles at a given thermodynamic state [24]. Consider an ionic species *i* that has a bulk concentration $n_{i,\infty}$ at a very far distance away from the charged surface (when distance goes to infinity), and satisfies the electroneutrality condition given by

$$\sum_{i=1}^{N} z_i n_{i,\infty} = 0 \,. \tag{5.8}$$

Then the local concentration n_i (number of ions/m^3) of this ion species is given by the Boltzmann distribution:

$$n_i = n_{i,\infty} e^{\frac{-z_i q_e \Phi}{k_B T}} \,. \tag{5.9}$$

The valence of the ion species i is z_i, q_e is the elementary charge (the charge of an electron in Coulombs), Φ (V) is the electric potential, k_B is the Boltzmann constant, and T (K) is the absolute temperature of the system [24].

To represent the volumetric ion charge density, we must sum all N ionic species that are present in the solution,

$$\rho = \sum_{i=1}^{N} q_e z_i n_i \,. \tag{5.10}$$

Note that this ρ denotes the same thing as it does in equations 5.6 and 5.7. Now, by substituting equations 5.9 and 5.10 into the Poisson equation (equation 5.7), we obtain the Poisson-Boltzmann (P–B) equation, which describes the electric potential distribution in the diffuse layer of the EDL, and can be written as

$$\nabla^2 \Phi = -\frac{1}{\varepsilon} \sum_{i=1}^{N} q_e z_i n_{i,\infty} e^{\frac{-z_i q_e \Phi}{k_B T}} \,. \tag{5.11}$$

Clearly, there is no straightforward way to solve equation 5.11 for Φ, as it is both the subject of a del-squared operator and in an exponential term. Because of this, the Debye-Hückel theory was developed to approximate an analytical solution for the Poisson-Boltzmann equation by linearizing equation 5.11 [12].

For the Debye-Hückel approximation to hold, the potential in the diffuse layer (which is what the P-B equation describes) must be very small; e.g. $z_i q_e \Phi / k_B T \ll 1$. Then, by performing the series expansion for the exponential term and only using the first two terms, e.g. $e^{-a} = 1 - a$ for small a, the P-B equation takes the form

$$\nabla^2 \Phi = \kappa^2 \Phi \tag{5.12}$$

where

$$\kappa^2 = \frac{\sum_i^N q_e^2 z_i^2 n_{i,\infty}}{\varepsilon k_B T}. \tag{5.13}$$

Finally, applying the boundary conditions of $\lim_{x\to\infty} \Phi = 0$, $\lim_{x\to\infty} \nabla\Phi = 0$, and $\Phi(x = 0) = \Phi_s$ gives the Debye-Hückel approximation as a solution to the P-B equation:

$$\Phi(x) = \Phi_s e^{-\kappa x}, \tag{5.14}$$

where Φ_s is the surface potential and x is the perpendicular distance from the surface [12].

In the Guoy-Chapman model, the surface potential is the potential at the charged substrate, Φ_s. We will later explore a variation of equation 5.14 for the Guoy-Chapman-Stern model that considers the surface potential to be represented by Φ_{OHP}.

The decay coefficient, κ, is important because its inverse is known as the Debye length, which we identified in our qualitative description of the EDL structure as an essential concept. The Debye length characterizes the range over which the EDL imposes a perturbation in the solution [30]. It is also known as the screening length, referring to how it defines the distance over which the mobile counter-ions screen out the electric field generated by the fixed surface charge [15]. In quantitative terms, the Debye length is

the distance from the charged surface where the potential has decayed to 1/e, or 36.7%, of the surface potential value. For a symmetric, *z:z* electrolyte, the Debye length λ_D (m) is given by

$$\lambda_D = \kappa^{-1} = \sqrt{\frac{\varepsilon k_B T}{2q_e^2 z^2 n_\infty}}\,. \tag{5.15}$$

Since the bulk solution satisfies electroneutrality, the two ion species' bulk concentrations are equal and are denoted simply as n_∞. As we can see in equation 5.15, the Debye length inversely scales with the square root of the ion's bulk concentration. This aligns with our previous qualitative discussion, since higher concentration means the electric field can be screened over shorter distances due to a higher presence of counter-ions canceling out the surface charge.

The Debye length decay has been confirmed through many experimental studies for monovalent ($z = 1$) electrolyte systems at low to moderate concentrations [30]. The nanofluidic diodes at the focus of this research use a monovalent solution, KCl, in low to moderate concentrations, so the Debye length models the diffuse layer well for our purposes. For multivalent electrolyte systems however, theoretical and experimental studies suggest that the Debye length does not describe the decay length as accurately [30].

To illustrate how the screening length changes with electrolyte concentration, in figure 5.2 we set up a simple ion concentration gradient that spans 60 μm, and plotted the Debye length across the gradient. This system also models how the EDL thickness would vary in a simple representation of a uniformly charged nanochannel connecting two

reservoirs of different concentrations (see figure 4.3). The uniform slope of the gradient is a simplifying assumption made about the electrolyte's transition between high and low concentrations. It neglects areas of depletion and accumulation that will form in the system at steady-state, which are most prominent at the openings of the channel. Also, in reality, the concentration profiles for cations and anions will diverge and reach different steady-state trends due to opposite electrostatic forces, but in figure 5.2, the general trend given to the concentration profiles is the same.

From equation 5.15, we can immediately see how rapidly the Debye length grows as the ion concentration drops. At the left opening of the nanochannel (x = 0 μm), where

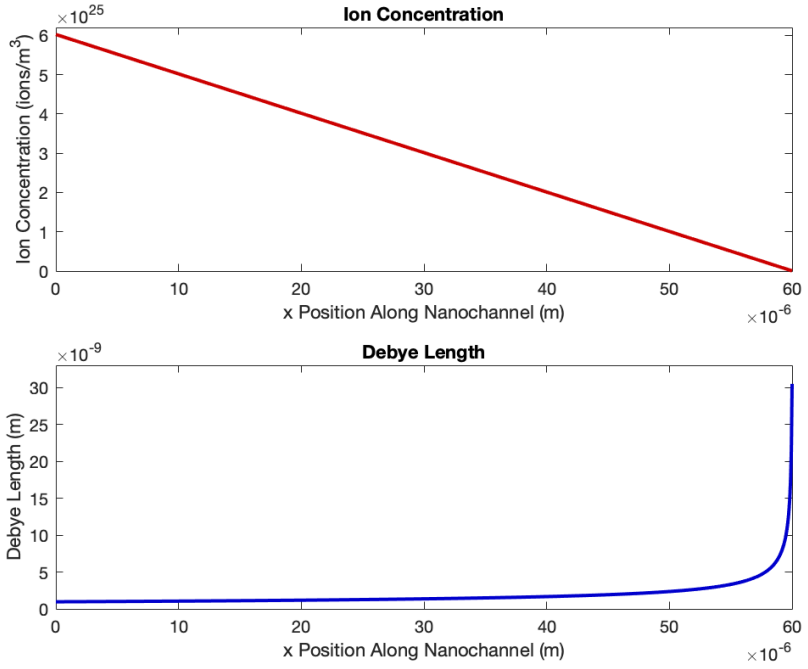

Figure 5.2: (Top) Simplified representation of electrolyte concentration vs. position along nanochannel. (Bottom) Corresponding Debye screening length along nanochannel. The nanofluidic channel is 60 μm long, the left reservoir has an ion concentration of 0.1 M (~6×10^{25} ions/m^3), and the right reservoir has an ion concentration of 0.1 mM (~ 6×10^{22} ions/m^3).

the bulk ion concentration is about 6×10^{25} ions/m^3, the Debye length is only about 1 nm thick. At the right opening (x = 60 μm), where bulk ion concentration is 3 orders of magnitude lower at about 6×10^{22} ions/m^3, the Debye length reaches a thickness of about 30 nm. This would mean that a channel diameter of 60 nm or less would be sufficient for this system to experience good EDL overlap at one channel opening. The significance of this asymmetrical overlap will become more clear when we investigate the sources of ion current rectification in-depth.

5.4.2: The Grahame Equation

The electric field produced by fixed wall charge is strongest at the wall's surface, so the corresponding electric potential magnitude is at a maximum at the surface as well. A relationship can be drawn between the strength of the electric potential at the surface and the surface charge density which produces it. The Grahame equation, named after the person who developed it, provides a simple quantitative way of expressing this relationship. The Grahame equation can be obtained from the one-dimensional Poisson equation (1D form of equation 5.7) when applying the boundary condition that the gradient of the electric potential is zero as distance goes to infinity, and assuming an electro-neutrality condition [12]. More directly, the Grahame equation can be obtained by analytically integrating the nonlinear Poisson-Boltzmann equation (5.11) and again applying appropriate boundary conditions.

The surface potential (in volts) is related to the surface charge density, σ_s (C m^{-2}), and is described by the Grahame equation, given by [12, 27]

$$\sigma_{\mathbf{s}} = \sqrt{8\varepsilon n_\infty k_B T}\sinh\left(\frac{q\Phi_{\mathbf{s}}}{2k_B T}\right) \text{ or } \sigma_{\mathbf{s}} = \frac{2\varepsilon_r\varepsilon_0\kappa k_b T}{q}\sinh\left(\frac{q\Phi_{\mathbf{s}}}{2k_B T}\right). \qquad \textbf{(5.16)}$$

Equation 5.16 applies for a symmetric (cations an anions have same charge magnitude) electrolyte solution of permittivity ε, with ions of charge q (C), bulk number density n_∞ (m^{-3}), Boltzmann's constant k_B, and temperature T [12]. The Grahame equation is often used to approximate the surface charge density affixed to the substrate, as it is easier to measure electric surface potential than to directly measure σ_s. For this research, we use the Grahame equation to find the surface potential for a given fixed charge density, so that we can plot the Guoy-Chapman model for decaying electric potential (equation 5.14).

Before we continue, note the distinction between σ and ρ, with the former denoting charge per unit area and the latter denoting charge per unit volume. In nanofluidics, ρ is commonly used for charge density in the electrolyte and σ for surface charge density. The surface charge density is usually represented by a subscript s, as in σ_s, and this also helps distinguish it from conductivity, which is inconveniently also represented by σ. These notations are extremely prevalent in published literature, so we will use them in accordance with existing work, despite the potentially confusing overlap.

5.4.3: *The Guoy-Chapman-Stern Model*

Our quantitative understanding so far covers the Guoy-Chapman model, which assumes that the ions form a diffuse layer, but neglects the Stern layer [24]. Considering the existence of the immobile Stern layer improves upon the Guoy-Chapman prediction of electric potential in EDL because it accounts for the finite size of ions in the Stern layer. Though it still treats ions as free-moving point charges in the Guoy-Chapman diffuse layer, by considering the finite volume occupied by ions in the Stern layer, the model avoids the erroneous result of predicting impossibly high ion concentrations accumulated at the walls. All together, the qualitative success of the Guoy-Chapman-Stern model has led to it being the most widely used quantitative model for EDL [31].

Consider the basic electric double layer structure presented in figure 5.3. The Guoy-Chapman-Stern model utilizes the electric potential values at three planes: $\Phi_0 = \Phi(0)$ at the boundary between solid and liquid at $x = 0$ (let us call it the 0-plane), $\Phi_{IHP} = \Phi(\text{IHP})$ at the inner Helmholtz plane at $x = \text{IHP}$, and $\Phi_{OHP} = \Phi(\text{OHP})$ at the outer Helmholtz plane at $x = \text{OHP}$. Permittivity is not constant throughout EDL, and the Guoy-Chapman-Stern model uses three relative permittivity values for the three regions between planes: ε_1 for $0 < x < \text{IHP}$, ε_2 for $\text{IHP} < x < \text{OHP}$, and ε_r for $x > \text{OHP}$. Lastly, we denote charge density with σ_0 for the density of fixed charges per unit area in the substrate on the 0-plane (located at $x = 0$) and σ_{Stern} for the density of specifically adsorbed ions (in the Stern layer) on the IHP ($x = \text{IHP}$). Taken together, the total fixed charge density can

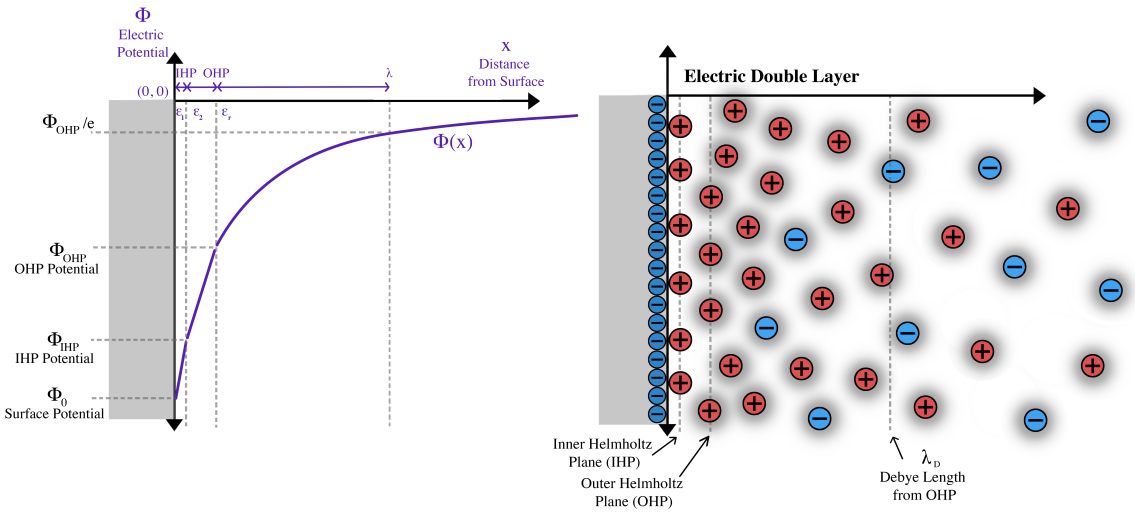

Figure 5.3: Guoy-Chapman-Stern model for an electric double layer. (Left) Electric potential as a function of distance from surface. (Right) Simplified EDL structure.

be written as $\sigma_{immobile} = \sigma_0 + \sigma_{Stern}$ [31]. $\sigma_{immobile}$ accounts for both the fixed charge embedded in the wall and the static charges adsorbed just outside the wall.

The Guoy-Chapman-Stern model assumes that the electric potential distribution $\Phi(x)$ obeys the Laplace equation in the region between the 0-plane and the OHP (the Stern layer: $0 < x <$ OHP), and the Poisson equation beyond the OHP (the diffuse layer: $x >$ OHP) [31]. Formally written in one-dimension form (only x-dependent), the potentials for these regions are

$$\frac{d^2\Phi}{dx^2} = 0, \quad 0 < x < OHP \tag{5.17}$$

and

$$\frac{d^2\Phi}{dx^2} = -\frac{\rho_{ions}(x)}{\varepsilon_r \varepsilon_0}, \quad x > OHP \tag{5.18}$$

where ε_0 is vacuum permittivity and $\rho_{ions}(x)$ is the space charge density resulting from the ions in the solution [31], obtained using equation 5.10.

We know that the diffuse layer is described by the Poisson-Boltzmann equation (equation 5.11), with an approximate solution in the Debye-Hückel form (equation 5.14). In the Guoy-Chapman model, $\Phi_s = \Phi_0$ because the entire EDL is considered to be a diffuse layer. In the Guoy-Chapman-Stern model, the beginning of the diffuse layer is at the outer Helmholtz plane (OHP), so the Debye-Hückel approximation uses $\Phi_s = \Phi_{OHP}$, and the distance is taken to be from the OHP instead of $x = 0$. So, equation 5.18 can be solved in the same manner as equation 5.7, with a few additional conditions.

The boundary conditions that apply for equations 5.17 and 5.18 are [31]

$$\Phi(IHP^-) = \Phi(IHP^+) = \Phi(IHP) \tag{5.19}$$

$$\Phi(OHP^-) = \Phi(OHP^+) = \Phi(OHP) \tag{5.20}$$

$$\left.\frac{d\Phi}{dx}\right|_{x=0^+} = -\frac{\sigma_0}{\varepsilon_1\varepsilon_0} \tag{5.21}$$

$$\varepsilon_1 \left.\frac{d\Phi}{dx}\right|_{x=IHP^-} - \varepsilon_2 \left.\frac{d\Phi}{dx}\right|_{x=IHP^+} = \frac{\sigma_{IHP}}{\varepsilon_0} \tag{5.22}$$

$$\varepsilon_2 \left.\frac{d\Phi}{dx}\right|_{x=OHP^-} - \varepsilon_r \left.\frac{d\Phi}{dx}\right|_{x=OHP^+} = 0 \tag{5.23}$$

$$\left.\frac{d\Phi}{dx}\right|_{x=OHP^+} = -\frac{\sigma_{immobile}}{\varepsilon_r\varepsilon_0} \tag{5.24}$$

in addition to the boundary conditions we used before,

$$\Phi(x) \to 0 \ \textbf{and} \ \frac{d\Phi}{dx} \to 0 \ \textbf{as} \ x \to \infty. \tag{5.25}$$

The superscript + and – that appear in equations 5.19-5.23 denote the side being approached from to evaluate at the plane. The + means the side of the plane facing the positive x-direction and the – means the side facing the negative x-direction.

Equations 5.19 and 5.20 account for continuity in electric potential across the IHP and OHP, respectively. Equation 5.21 applies for the assumption that there is no electric field within the solid wall [31]. Equations 5.22 and 5.23 ensure slope continuity for the electric potential across the IHP and OHP, respectively, and account for the effects of the different permittivities in the three regions, as well as the potential contributions from the specifically adsorbed ions in the IHP.

Solving equation 5.18 in the same way as we solved for equation 5.7, with the boundary conditions given in equations 5.20, 5.23, and 5.25, the Debye-Hückel linearization approximation for the diffuse layer in the Guoy-Chapman-Stern model is found to be

$$\Phi(x) = \Phi_{OHP} e^{-\kappa(x-OHP)}, \quad x > OHP, \tag{5.26}$$

with the decay coefficient, κ, being the inverse of the Debye length, and equivalent to how it was defined in equation 5.13. Since the P-B equation is only valid for ions in the diffuse layer, we consider our "surface" to be the outer Helmholtz plane (OHP), as it is considered the onset of the diffuse layer. The surface potential is then taken to be Φ_{OHP} or, in some cases, ζ potential (when ζ potential and Φ_{OHP} are approximated to be equivalent).

Returning to the Stern layer, we solve equation 5.17 for the region between the surface and IHP as well as the region between the IHP and OHP. Applying boundary con-

ditions given by equations 5.19 and 5.20 to equation 5.17, the potential distributions in these regions are linear (since the potential distribution is considered to follow the Laplace equation within the Stern layer), and are given by [31]

$$\Phi(x) = \Phi_0 + \frac{\Phi_{IHP} - \Phi_0}{IHP} x, \;\; 0 < x < IHP \tag{5.27}$$

and

$$\Phi(x) = \Phi_{IHP} + \frac{\Phi_{OHP} - \Phi_{IHP}}{OHP - IHP} x, \;\; IHP < x < OHP. \tag{5.28}$$

To obtain relationships between Φ_0, Φ_{IHP}, and Φ_{OHP}, we substitute equations 5.27 and 5.28 into equations 5.21 and 5.22, respectively, resulting in [31]

$$\Phi_0 - \Phi_{IHP} = \frac{\sigma_0 IHP}{\varepsilon_1 \varepsilon_0} \tag{5.29}$$

and

$$\Phi_{IHP} - \Phi_{OHP} = \frac{(\sigma_0 + \sigma_{IHP})(OHP - IHP)}{\varepsilon_2 \varepsilon_0}. \tag{5.30}$$

Equations 5.27 and 5.28 describe the potential distribution in the Stern layer, while equations 5.29 and 5.30 relate the potentials at each of the planes to the charge density (per unit area) on the planes themselves, and to each other.

Now, we have mentioned before how some models treat Φ_s in the Debye-Hückel approximation as the potential at the solid wall, and others treat it as the potential at the outer Helmholtz plane. In the Guoy-Chapman-Stern model, the Debye-Hückel approximation only applies in the diffuse layer, so Φ_s is treated as the potential at the onset of the diffuse layer and can be written as equation 5.26, repeated below for convenience:

$$\Phi(x) = \Phi_{OHP} e^{-\kappa(x - OHP)}, \;\; x > OHP.$$

The logic for treating the OHP as the boundary between the diffuse layer and a solid wall with total fixed charge per unit area, $\sigma_{Wall} = \sigma_0 + \sigma_{diffuse}$, is supported by the model's fulfillment of the electroneutrality condition of the whole system. The amount of charge in the entire diffuse layer per unit area can be calculated by integration of the volume charge density of diffuse ions as

$$\sigma_{diffuse} = \int_{OHP}^{\infty} \rho_{ions}(x) dx. \tag{5.31}$$

If we substitute equation 5.18 into equation 5.31 and apply the boundary condition of potential going to zero as x goes to infinity, we can express total diffuse layer charge density per unit area as

$$\sigma_{diffuse} = -\varepsilon_r \varepsilon_0 \int_{OHP}^{\infty} \frac{d^2\Phi}{dx^2} dx = \varepsilon_r \varepsilon_0 \left. \frac{d\Phi}{dx} \right|_{x=OHP^+}. \tag{5.32}$$

Then, we can apply boundary conditions given by equations 5.21, 5.22, and 5.23, along with equations 5.29, 5.30, and 5.32, to ultimately determine that

$$\sigma_0 + \sigma_{Stern} + \sigma_{diffuse} = \sigma_{immobile} + \sigma_{diffuse} = 0. \tag{5.33}$$

The immobile charge (the fixed substrate charge plus the adsorbed ions in the Stern layer) and the diffuse charge balance out, satisfying electroneutrality [31]. Since equation 5.33 shows $\sigma_{immobile} = -\sigma_{diffuse}$, equation 5.32 can be written as

$$\left. \frac{d\Phi}{dx} \right|_{x=OHP^+} = -\frac{\sigma_{immobile}}{\varepsilon_r \varepsilon_0}, \tag{5.34}$$

which is one of the boundary conditions (equation 5.24) applied to constrain Φ_{OHP} in equation 5.26.

The relationship between the total immobile charge density $\sigma_{immobile}$ and the potential at the onset of the diffuse layer Φ_{OHP} can be expressed by the Grahame equation for the Guoy-Chapman-Stern model as [13, 31]

$$\sigma_{immobile} = \frac{2\varepsilon_r \varepsilon_0 \kappa k_b T}{q} \sinh\left(\frac{q\Phi_{OHP}}{2k_B T}\right). \quad \textbf{(5.35)}$$

This is valid because equation 5.34 is equivalent to the hypothetical case of a wall located at x = OHP carrying the charge density $\sigma_{immobile} = \sigma_0 + \sigma_{Stern}$ in contact with an electrolyte solution. If taking the approximation that the OHP potential is equal to the zeta potential (the electric potential of first mobile ions), then the effective charge density of the "wall" would be calculated by equation 5.35 with Φ_{OHP} replaced by ζ [13].

The main conclusion to draw about the the Guoy-Chapman-Stern model is its strength in improving the Guoy-Chapman model in a simple way. By shifting the reference frame, the Guoy-Chapman-Stern model accounts for the finite stationary charge that accumulates at the nanochannel wall by treating it as part of the wall. The purpose of this analysis of the quantitative Guoy-Chapman-Stern model is not only to introduce its equations to the reader and compare it to the Guoy-Chapman model. It also serves to motivate the simplification that can be made by considering the OHP as the boundary between solid and liquid, as doing so helps account for the finite charge accumulation in the Stern layer. Still, the Guoy-Chapman-Stern model has similar limitations as the Guoy-Chapman model in its neglecting of the ion-ion interactions and the finite ion volume in the diffuse layer. Accounting for these factors requires a far more complicated model, however, so

the Guoy-Chapman-Stern model retains the advantage of being a simple and efficient way to predict the electric potential trends in EDL.

5.5: Electrokinetic Transport Mechanisms in Nanofluidics

The major electric mechanisms in nanofluidics can be divided into three main categories: electrostatic, electrokinetic, and electroviscous, and all three contribute to ion transport [34]. These terms refer to the electrical interaction involved with stationary charges, moving charges, and charge effect on solution viscosity, respectively. In nanofluidic diodes, electrostatic effects take the form of electric potentials produced by stationary fixed surface charge in the channel walls. We covered the important electrostatic concepts in our discussion of electric potential from fixed wall charge in EDL. Our research scope will not include electroviscous effects more than in passing, since nonuniform viscosity is not widely included in simple models. Electrokinetic effects, because they deal with moving charges, will be the focus of this subsection because we ultimately want to understand the fundamental model of ion transport characteristics in nanofluidic diodes.

5.5.1: Quantifying Ion Current

The most useful way to quantify ion transport for nanofluidic device engineering is by defining a vector called the ion current flux, represented by **J** (A/m^2). In physics, **J** is used to denote current flux (equivalent to current density) [28]:

$$\mathbf{J} = \frac{d\mathbf{I}}{da_{\perp}} = \frac{\mathbf{I}}{A}, \tag{5.36}$$

where $da_{\perp}$ is an infinitesimal cross-sectional area whose normal is in the same direction as $d\mathbf{I}$, a measurement of the charge flowing past a point over an infinitesimal amount of time. A is total cross-sectional area (m^2), and $\mathbf{I}$ is total electric current, measured in coulombs-per-second or amperes (A), where 1 C/s = 1 A [28]. Here, we use units A/m^2 for $\mathbf{J}$, to work consistently with meters as units for length. However, in the device physics field, current density units are most commonly A/cm^2. This difference in notation is not an issue, as the conversion from A/m^2 to A/cm^2 is simply multiplying by a factor of 10^4.

Current can be written in terms of charges by considering the velocity, $\mathbf{v}$ (m/s), of a uniform linear charge density, $dQ/d\boldsymbol{\ell}$ (C/m), to obtain charge flowing past a point per unit time as

$$\mathbf{I} = \frac{dQ}{d\boldsymbol{\ell}}\mathbf{v}. \tag{5.37}$$

Note that velocity can also be written as $d\boldsymbol{\ell}/dt$, and that $d\boldsymbol{\ell}$ (m) is a loosely-defined variable for infinitesimal length traveled by the infinitesimal charge dQ. The purpose of $\boldsymbol{\ell}$ is not to represent a numerical quantity, but rather to convey the other parameters' relationships with physical space.

For nanofluidic diodes, we want to express the ion current density to quantify ion transport, so we will use equation 5.10 in conjunction with equations 5.36 and 5.37. Equation 5.10 represents the ion charge density, and is repeated below for convenience:

$$\rho = \sum_{i=1}^{N} q_e z_i n_i \, .$$

Since **J** is the current per unit area, it can be expressed as the volume charge density times its velocity, or

$$\mathbf{J} = \left(\sum_{i=1}^{N} q_e z_i n_i \right) \mathbf{v} \, . \tag{5.38}$$

Equation 5.38 relates the physical flow of ions to the current density they create by transporting charge.

5.5.2: Quantifying Conductivity

Equations 5.36, 5.37, and 5.38 all define how to quantify the concept of charge flow in various forms, but none of them involve the driving source of charge motion– electric fields. The Coulomb force (equation 5.2) describes the force exerted on a charge in the presence of an electric field. When traveling through a real material, charges (electrons, ions, etc.) encounter resistance as they are pulled by an electric field due to collisions with other matter. We know that larger fields induce larger currents since the Coulomb force increases with field strength, and exerting a greater force on a charge increases its acceleration. But the greater the resistance, the lower the velocity that the charges can maintain as they flow in the material. In most substances under ordinary conditions, the current density is proportional to the electromagnetic force per unit charge, so the relationship is given as [28]

$$\mathbf{J} = \sigma(\mathbf{E} + \mathbf{v} \times \mathbf{B}), \tag{5.39}$$

where **J** (A/m^2) is current density, **E** (V/m) is electric field, **v** (m/s) is the velocity of the charges, **B** (N·s·C^{-1}·m^{-1}, or equivalently, T) is magnetic field, and σ (kg^{-1}·m^{-3}·s^3·A^2, or equivalently, Ω^{-1}·m^{-1}) is conductivity. Conductivity is the inverse of resistivity, and appears as a proportionality factor. It is an empirical constant that is characteristic to the type of material. Normally, the charge velocity **v** is small enough to be negligible, so the second term is often dropped, giving [28]

$$\mathbf{J} = \sigma\mathbf{E}. \tag{5.40}$$

Equation 5.40 is the current density form of Ohm's law, and is familiar in the field of electronics in its one-dimensional form, I = V/R.

Now, having defined how the flow of charge is expressed, and how it depends on electric field and conductivity, we will be able to build more complex quantitative relationships going forward, greatly assisting the derivation of our models.

5.6: Electrophoresis and Electroosmosis

In nanofluidic diodes, a vital characteristic for optimal function is the presence of depletion and accumulation/enrichment zones, which impact the ability of the ions to translocate across the channel. Depletion zones are where the concentration of ions is less than in the bulk, while enrichment zones are areas of ion concentration higher than bulk concentration. Recall that bulk solution concentration refers to the inherent ion concentration of the electrolyte solution in areas where outside influences are negligible, such as in

the large reservoirs on either side of the nanochannel in our nanofluidic diode devices. In areas influenced by nonuniform fields, ions can be manipulated to migrate to certain areas, causing ion accumulation, or migrate away from other areas, resulting in ion depletion. These zones can be formed by two major electrokinetic phenomena: electrophoresis and electroosmosis [15].

Electrophoresis and electroosmosis are strongly impacted by the electric double layers that form on the charged nanochannel walls. In nanofluidic diodes, the EDL interact with applied electric fields and low-Reynolds number hydrodynamic flows to create desirable effects on ion transport [35]. The Reynolds number is defined as the ratio of the inertial force to the viscous force, and appears as the most common dimensionless number in fluid dynamics [36]. In short, low-Reynolds number flows occur when pressure experienced by the fluid is effectively balanced out by the viscous force. So pressure-induced fluid movement terms can be neglected [18], because the Reynolds number is low in the systems we are studying.

In the nanofluidic diode systems we are studying, the externally applied electric field exerts a force on the ions in the EDL as well as those outside the EDL. The Stern layer is composed of rigidly-held ions, so only the ions in the diffuse layer of the EDL can significantly move under the influence of the external electric field. As the mobile ions in the diffuse layer and the bulk are pulled by the field, they collide with solute molecules (H_2O in aqueous solution). For an electric double layer on a fixed planar surface – in this case, the charged nanochannel walls – this type of induced fluid flow is called

electroosmosis. By definition, electroosmosis is defined as “the movement of liquid relative to a stationary charged surface” [24]. These ion-solution collisions drag the molecules of the solution along the same path as the ions, inducing fluid flow that reaches a peak near where the diffuse layer ends and the bulk region begins, with a speed that exponentially approaches what is known as the Smoluchowski ‘slip velocity’ or ‘shear velocity’ [35]. The slip velocity is simply a name given to the maximum fluid flow induced by electroosmosis as a way of quantifying the fluid’s momentum, and was originally described by Smoluchowski.

To understand the relevance of the term ‘slip’, one must understand the slip boundary condition and the no-slip boundary condition, by which fluid flow is constrained in microfluidics and nanofluidics [37]. In the no-slip boundary condition, there is no relative velocity between the boundary and the fluid it touches. The velocity of the fluid layer in contact with the boundary is equivalent to that of the boundary, thus there is no “slip”. When the velocity of the boundary and that of the fluid in contact with it are offset, the slip boundary condition applies, constituting a discontinuity of flow velocity at the fluid-boundary interface. The slip boundary condition rarely applies in microfluidics, but in nanofluidic diodes, the boundary between immobile ions and mobile ions can usually be characterized by a slip boundary condition to account for their offset in velocity [37].

We can now understand that electroosmosis can occur within the nanochannel, starting at the slip plane (where the mobile ions come closest to the wall, and where the ζ

potential is defined). For example, in a nanofluidic channel with uniform, negatively-charged walls, the electric double layer will consist primarily of positive counter-ions, which will move in the same direction as any externally applied electric field, pulling the fluid with it. So the electroosmotic component of flow will be in the same direction as the external electric field for nanochannels with negative fixed wall charge. The opposite is true for positively-charged walls; the EDL consists of negative counter-ions, which migrate against the direction of the applied electric field, generating electroosmotic flow that is also opposite the direction of the electric field [19]. In microfluidics, electroosmotic flow is a useful source of fluid flow for pumping and biomolecular separation. In nanofluidics, electroosmosis can also control the ionic current if the nanochannel is charged and the dimensions are less than the Debye length (so that the EDL overlap) [27].

In contrast to electroosmosis, electrophoresis is defined as "the movement of a charged surface, typically charged particles, relative to a stationary fluid" [24]. In the context of microfluidics and nanofluidics, electrophoresis is the movement of mobile ions relative to the molecules of the solute under the influence of the externally applied electric field. The electrophoretic component of flow is strongest for ions not held in the EDL, but in the bulk. These unfixed ions do not experience other significant forces besides those exerted by the externally applied electric field, and the direction of force is determined by the ion's polarity. There exist significant electrophoretic current contributions from ions in the diffuse layer as well, even though they experience stronger potential from the charged walls compared to ions in the bulk. This must be true, because when

the nanochannel's height is less than the Debye length, there is still strong electrophoretic flow, even though the EDL are overlapping and there are no regions of bulk solution concentration within the channel itself.

To give a comprehensive summary of the distinction between electrophoresis and electroosmosis, we can consider electrophoresis as the cause of electroosmosis (in the absence of pressure and temperature gradient considerations). Electrophoresis is the movement of ions (due to the applied electric field) relative to solute molecules, and electroosmosis is the movement of solute molecules resulting from those moving ions bumping into and pulling them along. The reason electroosmosis is only considered in the EDL is because ion movement dominates in one direction, since one polarity is enriched. In the bulk solution where electroneutrality applies, ion movement occurs in both directions equally since cations and anions are present in equal numbers. Therefore, outside the EDL, electroosmotic components cancel out, resulting in zero flow due to electroosmosis.

Experimentally and theoretically, electrophoresis contributes to the ionic current much more in microfluidics and nanofluidics than electroosmosis does, and therefore electroosmosis can be neglected in some conditions [15, 27, 38, 39]. Multiple studies agree that the number of ions that pass through the channel due to electrophoretic flow greatly exceeds those that do so from electroosmotic flow, especially when the fixed surface charge in the walls is low (on the order of 10^{-3} C/m^2 at most). This means that the fluid dynamics-induced ion flow (a result of electroosmosis) is usually negligible for low fixed wall charge density [38].

Daiguji, Yang, and Majumdar [27] neglect electroosmotic current contributions in their modeling of nanofluidic diode ion transport; they consider only electrophoresis. They neglected electoosmosis after finding that with low fixed wall charge density, electrophoresis dominates when the channel height is smaller than the Debye length. However, when the fixed surface charge density in the walls increases, the electroosmotic ion current becomes more significant and cannot be neglected. Daiguji, Yang and Majumdar further showed how the ratio of ionic current between electroosmotic flow and electrophoretic flow contributions is dependent upon the fixed surface charge density. This ratio increases as the surface charge density increases, but the ratio is less than about 10 percent as long as the surface charge density is less than 2×10^{-3} C/m^2 [27]. Many nanofluidic diodes feature fixed wall charge densities in this range, so electroosmosis contributions are often negligible. This is not always the case, however, as higher charge densities result in better ion current rectification (as we will later find), and so when maximizing a nanofluidic diode's rectification ability, electroosmosis can play an important role in predicting quantitative values.

Based on our understanding of EDL electric potential, these findings agree with conceptual theory, because increasing the fixed wall charge density increases the surface potential (see equation 5.16 – the Grahame equation), but does not alter the Debye length. The characteristic decay length can remain the same with an increase in surface potential, with the main consequence being that the potential at the Debye length will be higher. Higher potential at the same distance from the walls means the exclusion-enrichment ef-

fect is stronger, so electroosmosis contributes more to flow momentum. So it makes sense that higher fixed wall charge density increases the impact of electroosmosis on ion current.

5.7: Other Electrokinetic Phenomena

It is worth mentioning a couple other major electrokinetic phenomena for the sake of completeness, even though most models of nanofluidic diodes neglect them. Streaming potential and sedimentation potential can induce their own components of electrolyte flow, and so they can affect the current-voltage behavior slightly.

Streaming potential is defined as "the induced electric field when ionic solutions (e.g., aqueous electrolytes) are made to flow by external forces such as pressure along a stationary charged surface" [24]. Streaming potential is regarded as the opposite of electroosmosis, as it is an external pressure gradient that generates a streaming current, producing a potential, instead of an external electric potential gradient pulling the ions to create a pressure gradient on the solution [21].

Sedimentation potential is defined as "the induced electric field when charged surfaces or particles move with respect to stationary fluid" [24]. Since the electric field described by this phenomenon is created by the ions' movement, it is the opposite of electrophoresis, which describes the ions' movement induced by an electric field.

5.8: Fick's Laws of Diffusion

Diffusion accounts for the remaining major category of ion transport mechanisms in nanofluidic diodes, and differs from the previous effects in that it does not depend on charge interactions or electric fields. Instead, it is the gradient of the particles' concentration that induces movement. The way we will approach this discussion of diffusion is through a quick review of Fick's laws, as they succinctly explain the phenomenological relationships. Fick's laws can be derived from kinetic gas theory, because diffusion is the relation between a particle's kinetic energy (inertia) and friction forces exerted by the surrounding fluid [37]. The full derivation is beyond the scope of this research (see [37] for the full derivation, and [40] for the behavioral observation-based derivation), but we will include the main points of interest for the context of nanofluidics.

Fick's first law of diffusion describes the flux of a particle species (in our case, ions) in a steady-state system at very low Reynolds numbers [37]. The particle flux, J, is induced by gradients in chemical potential energy (a measure of energy transferrable to the particles and which depends on the local particle concentration) and damped by drag forces (friction) [37]. Combining these effects, particle flux due to diffusion can be expressed as

$$J = -D\nabla n, \tag{5.41}$$

where J ($1/m^2s$) measures the number of particles passing through a plane per unit area per second, n ($1/m^3$) is the particles' concentration, and D (m^2/s) is the diffusion coefficient [40]. The purpose of the negative sign in equation 5.41 is to indicate that the direc-

tion of diffusion is opposite that of increasing particle concentration. So, particles will diffuse (have a net flow) in the direction from higher concentration to lower concentration. The diffusion coefficient is a function of temperature, fluid viscosity, and particle radius, given as [37]

$$D = \frac{k_B T}{6\pi \eta r}, \tag{5.42}$$

where k_B is the Boltzmann constant, T is temperature, η is the fluid viscosity, and r is the particle radius. Liakopoulos, Sofos and Karakasidis found through molecular dynamics simulations that the number 6 in the denominator was most appropriate for channel widths less than five nanometers, while the number 4 (instead of 6 in equation 5.42) applied better for channels wider than five nanometers [32]. This concept would be worth examining in more detail for projects that utilize equation 5.42. However, many projects opt for using experimentally known diffusion coefficients, such as 1.96×10^{-9} m^2/s and 2.03×10^{-9} m^2/s for K^+ ions and Cl^- ions, respectively [26, 38].

Fick's second law accounts for mass conservation, and can handle changing distributions of the particles as a result. That is, it can be used for non-steady-state diffusion processes [40]. For a three-dimensional system, Fick's second law is given by

$$\frac{\partial n}{\partial t} = D \nabla^2 n . \tag{5.43}$$

Equation 5.43 can be interpreted as stating that the change in particle concentration over time is equal to the negative divergence of the particle flux J. Basically, the spatial change

in the concentration gradient corresponds to how the concentration profile will change over time.

Conceptually, these laws make sense when you think about diffusion on the particle-collision level. Thermal energy in the system manifests as kinetic energy (movement) of the particles, causing them to move in the fluid, only changing direction when colliding with a wall or another particle. Clearly, a particle in an area of higher concentration will bump into more particles than in an area of lower concentration. It follows, then, that the particle will change direction more frequently when moving toward higher concentration, but will face fewer obstacles when moving toward lower concentration. Averaging over the whole system of many particles, we see an average trend of particles moving from higher to lower concentrations (the particle flux is opposite the concentration gradient). This helps explain Fick's first law, but Fick's second law is a little more abstract. The best way to think about change in concentration gradient is to conceptualize a system where particle flux is higher in one place compared to another. The region with higher particle flux will correspond with a faster change in concentration since more particles are passing through the region per unit time, while the lower particle flux corresponds to slower concentration change, as fewer particles pass by in that same time frame.

Equations 5.41 and 5.43 should help to convey what diffusion phenomena are based on, and how diffusion is separate from electrokinetics. The main diffusive processes in nanofluidic systems are known as diffusioosmosis and diffusiophoresis, which we will briefly define.

Diffusioosmotic flow is a type of flow that is induced by the concentration differences between the EDL and the bulk solution [18]. The concentration gradient between the regions creates an osmotic pressure. As we saw with Fick's laws, the particle concentrations naturally want to balance out and become more uniformly distributed. The flux that this type of diffusion contributes is known as diffusioosmosis.

Diffusiophoretic migration refers to the flow induced by concentration gradients across the channel's length, such as asymmetry in reservoir ion concentration [18]. When one reservoir has a higher bulk concentration and the opposite reservoir has a lower bulk concentration, a gradient is set up across the channel that connects them, and the diffusive flux this contributes to the flow is known as diffusiophoresis.

5.9: Mean-Field Approximation Models for Ion Transport in Nanofluidics

A recurring theme for our theory discussion has been the notion that the systems we aim to model are far too complex to model without simplifications. As we found with the electric double layer qualitative and mathematical models, there are many added layers of complexity that can be neglected in a model that still agrees with the real behavioral trends. Although simplified models can struggle to replicate experimental measurements precisely, they can be valuable for understanding the core phenomenological causes.

Ion transport in nanofluidic systems is contributed to by many separate phenomena – not only EDL effects and electrostatic forces but also including fluid mechanics,

chemical interactions, thermodynamics, and even quantum mechanics and entropy considerations. Clearly, the most accurate models of our targeted nanofluidic diodes would take all of these factors into account, but this is rarely feasible. The vast majority of nanofluidic research efforts around the world focus on a few of the most important mechanisms to develop their models. For this conceptual and theoretical research into nanofluidic diodes, we want to determine what influences are vital to predicting ionic current in nanofluidic diode devices. If we know which effects can be neglected without significantly impacting the predicted current-voltage trends, our models will be both efficient and insightful.

Published research papers on nanofluidics can have a wide variety of goals and origins, but there is common agreement that mean-field approximations are a great tool for modeling these systems to find ion transport profiles. In fact, most simplified models are derived from one such mean-field model known as the Poisson-Nernst-Planck (PNP) equations [26]. Though originally developed for nanofluidic systems and biological systems, the PNP model can be adapted for use in semiconductor devices as well [8]. For our purposes, it is useful for modeling the ionic current in nanofluidic diodes, since the continuum hypothesis works well for nanochannel diameters as small as 2.2 nm [39].

The PNP model describes the profiles of ion concentration and electric potentials as being continuous, as opposed to the summation of discrete contributions from individual charges. Since it takes the average of the fields and concentrations in a continuum description, it is able to efficiently handle the ion charge interactions and the electrostatic

effects that factor into ion transport. These contributions are regarded as the essential ionic transport phenomena, so the PNP model is an effective yet relatively simple model [8]. At its core, it can be derived from detailed molecular models, so its physical description is firmly based in reality, not just observed data correlations [41]. Ultimately, the PNP model serves as an effective approximation that conserves computational power for low-cost simulation while modeling the system's real, underlying physics [42]. Clearly, the Poisson-Nernst-Planck equations are worth understanding in detail, so we will present a review of their functional forms and how they model the systems we want to analyze.

The PNP model is self-consistent, and is created by coupling the Nernst-Planck equation with the Poisson equation. These equations model the diffusion and drift of ions under the influence of an applied electric field, and this electric field itself is contributed to by those same ions [43]. This self-dependence is why the equations are coupled, and how the model remains self-consistent.

There is one Nernst-Planck equation and one concentration profile for each ion species involved. Since our systems utilize a KCl electrolyte solution, there are two ion species: K^+ cations (positive ions) and Cl^- anions (negative ions). This means that PNP models of our systems must have two Nernst-Planck equations, one corresponding to each ion species, as well as a concentration profile for each ion species. The Poisson equation combines the effects of both ion species, as well as fixed surface charge contributions (through the use of boundary conditions), into one equation in order to calculate the net electric potential profile throughout the system. From a controls theory perspec-

tive, the PNP system of equations treat the electrostatic potential and the charge densities of the ion species as the system's state variables [41].

5.10: The Poisson-Nernst-Planck (PNP) Model

5.10.1: The Poisson Equation

We used the Poisson equation in an earlier section to help model the EDL, but it also plays a vital role in the PNP model of ion transport. To review, the Poisson equation relates charge density to electric field (in terms of the electrostatic potential). Through equations 5.2 and 5.4, the divergence of the gradient of the potential corresponds to the electrostatic force that drives ion motion. The Poisson equation is expressed for the purposes of the generalized PNP model as [27]

$$\nabla^2 \Phi = -\frac{1}{\varepsilon_0 \varepsilon_r} \sum_{i=1}^{N} q_e z_i n_i \,, \tag{5.44}$$

where ε_0 and ε_r are the vacuum permittivity and the relative permittivity, respectively, Φ is the electric potential, q_e is the elementary charge, z_i is the valence of ion species i, and n_i is the local number concentration of ion species i. For simplified systems, the relative permittivity, ε_r, is considered uniform, but in reality it can vary, depending on nonuniform factors such as electrolyte concentration and chemical makeup.

5.10.2: The Nernst-Planck Equations and Ion Conductivity

While the Poisson equation links charge concentration with electric potential, the Nernst-Planck equation describes the electro-diffusion of ions, in terms of their concentrations, under the influence of the electric potential. The ionic flux of species i, $\mathbf{J}_i$, is given by the Nernst-Planck equation [27]:

$$\mathbf{J}_i = -D_i(\nabla n_i + \frac{q_e z_i n_i}{k_B T}\nabla\Phi) \tag{5.45}$$

where D_i is the diffusivity of the ion species, Φ is the electrostatic potential, n_i and $q_e z_i$ are the concentration and charge of ion species i, respectively, k_B is the Boltzmann constant, and T is temperature. The simplified model considers the diffusion coefficient to be uniform, but the accuracy can be improved by using a position-dependent D_i [8].

Notice that the diffusive component of ion flux is accounted for within the Nernst-Planck equation, as Fick's first law of diffusion (equation 5.41) appears as the first term to the right of the equal sign. This quantifies the flow induced by the concentration gradient, serving as a component of the overall ion flux.

The second term quantifies the electrostatically-induced component of ion current. Recall that current depends on conductivity and electric field strength through Ohm's law, equation 5.40:

$$\mathbf{J} = \sigma\mathbf{E},$$

and electric potential relates to electric field through equation 5.4:

$$\mathbf{E} = -\nabla\Phi.$$

By substituting equation 5.4 into equation 5.40, we obtain

$$\mathbf{J} = -\sigma \nabla \Phi. \tag{5.46}$$

$\mathbf{J}_i$ in equation 5.45 represents ionic flux, while $\mathbf{J}$ in equation 5.46 is current flux, so to compare them we must convert ionic flux to ion current flux. This is done by simply multiplying the Nernst-Planck equation by the charge of ion species i (q_e for monovalent electrolytes), and then Equation 5.46 appears as the second term in the current flux version of the Nernst-Planck equation. The conductivity ($\Omega^{-1}\cdot m^{-1}$) of ion species i in the electrolyte solution is therefore expressed as [12]

$$\sigma_i = D_i \frac{q_e^2 z_i n_i}{k_B T}. \tag{5.47}$$

Equation 5.47 is very useful for understanding how these parameters alter the ability for ions to flow, such as how a high concentration of an ion species increases conductivity for ions of that species. We can obtain even more insight by substituting equation 5.42 into equation 5.47, to express the diffusion coefficient as a function of fluid viscosity, η, and radius of ion species i, r_i:

$$\sigma_i = \frac{q_e^2 z_i n_i}{6\pi \eta r_i}. \tag{5.48}$$

Increasing fluid viscosity understandably decreases the ions' ability to flow, and increasing the radius also reduces conductivity because the amount of particle collisions will increase.

In summary, as its terms suggest, the Nernst-Planck equation accounts for two different types of ion flux. The first is diffusion current that is induced by concentration gradients, and the second is drift current that is caused by electric potential gradients [26].

5.10.3: The Continuity Equation and Boundary Conditions

The target functioning for a nanofluidic diode is when its behavior has stabilized and it is in steady-state. We want to find the steady-state solution, which must satisfy the continuity equation that can be written as [27]

$$\nabla \cdot \mathbf{J}_i = \nabla \cdot \left(\nabla n_i + \frac{q_e z_i n_i}{k_B T} \nabla \Phi \right) = 0 \,. \tag{5.49}$$

Equation 5.49 is the time-independent continuity equation, and using it along with appropriate boundary conditions, the PNP equations (equations 5.44 and 5.45) can be solved in order to obtain profiles for the electric potential and the ion concentrations in the system. A similar continuity equation exists in semiconductor physics, but includes a recombination term to account for electrons and holes recombining. There is no corresponding term in nanofluidics' continuity equation because cations and anions cannot recombine. Equation 5.49 ensures that the nanofluidic system is in a steady-state condition because spatial differences in flux (nonzero flux divergence) would indicate that the concentration profiles are still changing, and the flow is not yet stabilized.

The results of the PNP equations are strongly dependent on the boundary conditions used, and the behavior is very sensitive to minor changes in those conditions [43].

From a logical standpoint, it makes sense that we need to know how the system behaves at the boundary to accurately predict trends. In mathematical reasoning, most models express the underlying physics with a system of equations to solve, which requires integration constants provided by the boundary conditions [37]. Without boundary information, the model cannot be solved to obtain a unique solution, so a discussion of mean-field continuum models is incomplete without considering boundary conditions.

Boundary conditions that apply to the Poisson equation at the nanochannel walls take the same form as equations 5.21 and 5.24 [21, 27]:

$$\nabla_{\perp}\Phi = -\frac{\sigma_s}{\varepsilon_r \varepsilon_0}, \tag{5.50}$$

where σ_s is the surface charge density (charge per unit area), and the subscript $\perp$ indicates the wall-normal component. If we make the simplification that the OHP marks the "surface" of the solid-liquid boundary instead of the substrate, then $\sigma_s = \sigma_{\text{immobile}} = \sigma_0 + \sigma_{\text{Stern}}$. Otherwise, $\sigma_s = \sigma_0$, which means the surface charge density is just the density of embedded charge in the substrate. Note that σ_{immobile} denotes the area charge density of all immobile charges: the embedded charge in the substrate σ_0 and the stationary ions in the Stern layer σ_{Stern}.

It is also important to constrain the ion flux inside the nanochannel and reservoirs, thus boundary conditions at the walls must hold so that [21]

$$\mathbf{J}_{i\perp} = 0. \tag{5.51}$$

Otherwise, ion current could be flowing into or out of the solid wall, which does not happen in reality. At the reservoir walls,

$$\nabla \Phi = 0 \tag{5.52}$$

and at the electrodes,

$$n_i = n_{i,\infty} \tag{5.53}$$

$$\Phi = 0 \text{ (at the grounded electrode)} \tag{5.54}$$

$$\Phi = V_a \text{ (at the electrode where voltage is applied),} \tag{5.55}$$

where $n_{i,\infty}$ is the bulk ion concentration of ion species i [44].

Modeling the PNP equations for a nanofluidic system is no simple feat; equations 5.44 and 5.45 must be solved simultaneously, and with many meticulous boundary conditions. In addition to the boundary conditions that apply to the nanochannel walls, there are conditions that describe the interfaces at the openings of the nanochannel that connect to the reservoirs, where nano-scale meets micro-scale. These are known as Donnan equilibrium conditions.

5.10.4: Donnan Equilibrium Condition

The ion concentrations and potentials at the two entrances of the nanochannel can be determined from relationships obtained through what is known as the Donnan equilibrium [45]. The electrolyte solution inside the nanochannel meets the solution in the reservoir at the openings of the nanochannel, forming an interface. When the system is in

steady-state, there is a stable difference in ion concentration across these interfaces, where the charge concentration is compensated by an electrical potential difference [12]. Another interface between electrolyte solutions of different ion concentrations is formed at any discontinuities in the nanochannel wall's fixed charge. So, for a bipolar nanofluidic diode, a Donnan equilibrium condition applies at the cross-sectional plane where opposite fixed wall charge polarities are in contact.

The Donnan equilibrium condition for a 1:1 (symmetric and monovalent) electrolyte solution is applied when the system at the boundary is in steady-state, and is given as

$$\frac{n_{\pm A}}{n_{\pm B}} = e^{\pm \frac{q_e}{k_B T}(\Phi_B - \Phi_A)}, \tag{5.56}$$

where subscripts A and B refer to points on either side of the discontinuity [46], and ± indicates the polarity of the ion concentration, n. One Donnan equilibrium condition applies for each of the two ion polarities, and the only difference is the sign of the exponential. As stated before, equation 5.51 describes the correlation between ion concentration discontinuity and electric potential discontinuity that must apply for equilibrium and steady-state to be achieved and maintained.

5.10.5: Types of Boundary Conditions: Dirichlet and Neumann

Boundary conditions can be categorized into common basic forms for modeling purposes with discrete, sampled grids, with the two most prominent being known as the

Dirichlet boundary and the Neumann boundary [47]. The Dirichlet boundary is the simplest boundary condition, as it ascribes a known set of values to the parameter it constrains at the grid-points along the boundary. An example would be a sheet of metal, which is equipotential across its surface plane and so can be modeled by a grid of points with some fixed voltage [47].

Unlike a Dirichlet boundary condition which forces a solution at points on the boundary, a Neumann boundary condition expresses each point in terms of the surrounding points. This is because the Neumann boundary describes the known derivatives of the function at the boundary. Typically, the derivative is defined with respect to the outward unit normal vector, so the known derivative value is in the direction pointing perpendicularly out from the plane of the boundary [47]. Since the grid-points on the boundary are not given direct values in a Neumann boundary condition, methods that approximate derivatives using the difference between neighboring grid points, such as a central-difference method, are used to relate their values to the surrounding points to satisfy the derivative condition. Central-difference methods relate a central point to its four cardinal neighbors through the slope between its values. There are many variations of discretizing systems to approximate derivatives, and they usually do so by quantifying the ratio of change from point to point.

5.10.6: PNP Model Weaknesses

The Poisson-Nernst-Planck model's strength rests on its effective predictions of general nanofluidic behavior while using relatively simple equations. For nanofluidic diode systems, PNP-based simulations effectively model qualitative behaviors [44]. However, the PNP model by itself is known to struggle when predicting quantitative values, especially for systems with very small nano-scale dimensions. There are drawbacks to considering ion concentrations as continuous distributions, as taking the averages of the ions' discrete profiles is less accurate on smaller scales [42]. This section will consider some of the most prominent shortcomings of the PNP model, and suggest corrections that can help mitigate its errors.

One common simplification when using the PNP model is treating the diffusion coefficient, D_i, as a constant value for each ion species in the Nernst-Planck equation (equation 5.45). Usually, the values used are measured from the bulk electrolyte solution. The actual diffusion coefficient within the nanochannel is extremely difficult to obtain, but it is known to vary with ion concentration [8]. A more accurate treatment would be to use a spatially-dependent diffusion coefficient as a way of accounting for the true variation in diffusive ability. Another useful modification of the Nernst-Planck equation would be to add more force contributions that affect the ion flux, which can help account for other neglected factors that cause diffusive differences within the system (such as electrochemical potential).

The next weakness in the PNP model is one that also appeared in our EDL models: neglecting the finite volume of ion particles. Ion correlation effects (also known as self-energy) are also not accounted for [8], and together, these missing factors mean that the PNP model cannot account for non-electrostatic interactions between ions [42]. These factors become more significant the more confined the channel is since the true ion sizes become more comparable to those dimensions. So, smaller diameter nanochannels are more difficult to model using the PNP equations than larger ones. As mentioned in our EDL model discussion, one method to compensate for this issue is to impose a radius of closest approach for the ions, which would place restrictions on maximum ion concentrations and avoid overestimations of ion populations. Other methods have been researched as well, such as the work of J.J López-García, J. Horno and C. Grosse, who used a modified electrokinetic model to consider the finite volume and the hydration of the ions (water molecules clustering around the ions) [48]. By treating the hydrated ions as charged dielectric spheres instead of point charges, the researchers were able to model the electrolyte solution as a nonhomogeneous fluid that featured concentration-dependent coefficients of permittivity and viscosity [48]. Models that add considerations for ion size, permittivity and viscosity always improve upon the predictions by the standard electrokinetic model that consider ions as point charges.

The PNP model faces even more difficulty in modeling biological nanochannels, as there are additional complexities it does not inherently account for. The first is that the PNP equations are lacking in descriptions of ionic dielectric boundary effects. In nanobi-

ology, these are the boundaries that exist between ion flow and the protein/lipid domain [42]. It is more complex to model because protein channels have much more irregular geometry than synthetic, solid substrate-based nanochannels. So, while there exist some approximate analytic solutions to the PNP equations for regular geometries, they are unfeasible for biological channels due to their immense complexity [42]. Numerical methods are therefore invaluable for solving most PNP models of complex nanofluidic systems, and computer simulation has emerged as the strongest tool in obtaining meaningful solutions [42].

Lastly, while the PNP equations do a good job of modeling electrokinetic phenomena and basic diffusion effects that contribute to ion flux, they leave out any consideration of fluid dynamics. As a result, effects such as electroosmosis cannot be modeled using the basic PNP equations, and additional relationships should be included when the fluid dynamics of the system are known to play significant roles in operation. The most common and effective way to include fluid dynamics is by using the Navier-Stokes equation in combination with the Poisson-Nernst-Planck equations.

5.11: The Poisson-Nernst-Planck Navier-Stokes (PNP-NS) Model

5.11.1: The Navier-Stokes Equation

The PNP model does not include fluid dynamics, so microfluidic and nanofluidic systems that are significantly affected by fluid mechanics must be modeled by adding to the PNP equations. The most commonly used addition is known as the Navier-Stokes

(NS) equation, and is paired along with another continuity equation to ensure the conservation of fluid. This modified model is known as the Poisson-Nernst-Planck Navier-Stokes model, or PNP-NS. The Navier-Stokes equation is essentially a conservation of momentum equation, accounting for kinetic energy held by the fluid in which the ions are suspended [24, 37]. It describes fundamental inertia so directly that the Navier-Stokes equation can actually be derived from Newton's second law of motion, $F = ma$, but a more direct approach quantifies momentum as the product of mass times velocity [37].

We will not spend as much time analyzing the Navier-Stokes equation as we did with the PNP equations, because models that neglect fluid dynamics can still yield accurate predictions in many cases. The PNP-NS model is also significantly more complex to solve numerically compared to the PNP model (due to the greater number of equations, parameters, and necessary boundary conditions), but because this added complexity does often entail more accurate results, it is worth discussing for this review. The most important accuracy improvement with the PNP-NS model compared to the PNP model is the inclusion of electroosmosis – something the original PNP equations alone cannot model because they do not consider fluid velocity [44, 49].

To describe fluid behavior in a system, some physical properties of the fluid are required, including pressure, fluid density, and viscosity. These scalar variables, along with fluid velocity as a vector variable, account for the major properties that affect fluid dynamics [37]. In many systems, we can assume that the solution is incompressible (density is constant), and its viscosity and temperature are also constant throughout. These

assumptions can apply in most nanofluidic diode systems, and also help simplify the model. Using $\mathbf{v}$ for velocity, p for pressure, ρ for fluid mass density (not to be confused with volume charge density), and η for viscosity, the Navier-Stokes equation with electrostatic force contribution can be expressed as [37, 38, 44]:

$$\frac{\partial \mathbf{v}}{\partial t} + \mathbf{v} \cdot \nabla \mathbf{v} = \frac{1}{\rho} \left\{ -\nabla p + \eta \nabla^2 \mathbf{v} - (\sum_{i=1}^{N} q_e z_i n_i) \nabla \Phi \right\}, \tag{5.57}$$

but in steady state, the partial time derivative of velocity vanishes, giving [21]

$$\mathbf{v} \cdot \nabla \mathbf{v} = \frac{1}{\rho} \left\{ -\nabla p + \eta \nabla^2 \mathbf{v} - (\sum_{i=1}^{N} q_e z_i n_i) \nabla \Phi \right\}. \tag{5.58}$$

As before, Φ is the electrostatic potential, n_i and $q_e z_i$ are the concentration and charge of ion species i (of N total ion species), respectively.

To understand the mechanisms being described by the Navier-Stokes equation, we will start on the lefthand side and move to the right, briefly interpreting the significance of each term in equation 5.58. The expression $\mathbf{v} \cdot \nabla \mathbf{v}$ describes the convection (pattern/profile of flow) experienced by the fluid. On the righthand side of the equation, the term $-\nabla p$ denotes the influence a pressure gradient has on flow, the term $\eta \nabla^2 \mathbf{v}$ is a vector Laplacian and describes the friction within the moving fluid itself due to viscosity, η, and the term

$$-(\sum_{i=1}^{N} q_e z_i n_i) \nabla \Phi$$

describes the impact to fluid flow from the volume force due to the electric potential gradient [37]. This term is a familiar form if we recall equation 5.2: $\mathbf{F} = Q\mathbf{E}$, and equation

5.4: $\mathbf{E} = -\nabla\Phi$, with total charge expressed by the charge summation and the factor of $1/\rho$, which is multiplied by every term on the righthand side to scale the terms inversely with density.

5.11.2: The PNP-NS Continuity Equation and Boundary Conditions

Introducing new parameters such as pressure and velocity means that additional boundary conditions must also be applied. The continuity equation that conserves fluid is given as

$$\nabla\mathbf{v} = 0\,. \tag{5.59}$$

Equation 5.59 ensures that there are no sources or sinks of fluid in the system, and since the fluid is incompressible, the flow rate (velocity) coming in must equal that going out of any point. Lastly, to complete our modification of the PNP equations into the PNP-NS equations, the Poisson equation (equation 5.44) and the ion flux described by the Nernst-Planck equation (equation 5.45) remain the same, but the steady-state continuity equation (equation 5.49) is given an additional term to account for fluid velocity [21]:

$$\nabla(n_i\mathbf{v} + \mathbf{J}_i) = 0\,. \tag{5.60}$$

Boundary conditions given by equations 5.50-5.55 still apply in the PNP-NS model at the channel walls,

$$\nabla_\perp\Phi = -\frac{\sigma_s}{\varepsilon_r\varepsilon_0}$$

$$\mathbf{J}_{i\perp} = 0$$

at the reservoir walls,

$$\nabla \Phi = 0$$

and at the electrodes,

$$n_i = n_{i,\infty}$$

$$\Phi = 0 \text{ (at the grounded electrode)}$$

$$\Phi = V_a \text{ (at the electrode where voltage is applied),}$$

but the Navier-Stokes equation needs to be constrained as well, with boundary conditions at the channel walls given by [21]

$$\nabla_\perp p = \mu \nabla_\perp^2 \mathbf{v} - \left(\sum_{i=1}^{N} q_e z_i n_i \right) \nabla_\perp \Phi \tag{5.61}$$

and

$$\mathbf{v}_\perp = 0. \tag{5.62}$$

At the reservoir walls, boundary conditions are given by [44]

$$\nabla p = 0 \tag{5.63}$$

and

$$\mathbf{v} = 0. \tag{5.64}$$

Finally, at the electrodes, we have [44]

$$p = 0 \tag{5.65}$$

and

$$\nabla \mathbf{v} = 0. \tag{5.66}$$

Like the PNP model, the PNP-NS model is highly sensitive to the boundary conditions applied. The boundary conditions listed above apply in the majority of nanofluidic sys-

tems, but depending on the situation, some additional simplifications can be made, such as the slip or no-slip boundary condition, to be discussed later on in this research.

In conclusion, the Navier-Stokes equation incorporates fluid dynamics into the PNP model, which is a mean-field continuum approximation for ion transport. Although this PNP-NS model improves upon the PNP model, especially when electroosmosis is a major contributor to ion transport, it adds another layer of complexity when solving to obtain profiles for ion transport, while still suffering from some of the same limitations. These limitations include neglected interaction contributions such as ion-ion interactions and finite ion volume considerations, which become more important for smaller scale nanochannels [42].

CHAPTER 6

Ion Rectification in Nanochannels

6.1: Charge Selectivity

Nanofluidic channels, like their biological inspiration, can be highly selective to the types of particles that pass through them. In the case of nanofluidic diodes, the embedded wall charge induces charge selectivity behavior in its channel. This means it allows only particles of a certain charge to move past, and prevents others due to electrostatic effects. The electric double layer that forms when a charged surface comes in contact with an electrolyte solution, which we studied in-depth in the previous chapter, is populated primarily by counter-ions. So, in nanochannels whose dimensions are comparable to the Debye screening length, the EDL occupy most of the channel's volume, causing the channel to be enriched with counter-ions and depleted of co-ions [11]. This phenomenon is known by many names, here we will call it the exclusion-enrichment effect (EEE) which describes the result of charge selectivity.

A charge density can be embedded into the walls of fabricated nanochannels through a variety of methods developed by researchers over the years, but it is difficult to create a specific desired nonuniformity in the wall charge. By comparison, biological nanochannels have much more control, as charged amino acid residues that are present in the protein walls are the primary source of the EEE [50]. The innate intricacy and possible variety of amino acid patterning grants biological nanochannels remarkable control over what they able to pass through them.

To quantify the strength of charge selectivity for comparison of the EEE in different nanochannels, there are a few values we could define. One option is to define a ratio of the concentration of an ion species in the nanochannel in the presence of electrostatic forces to the concentration without electrostatic forces present [50]. This would be equivalent to taking the ratio of the averaged ion concentration in the nanofluidic diode versus the bulk ion concentration, and is often known as the exclusion-enrichment coefficient [12]. Selectivity could also be measured by taking the fraction of the total ionic current that is carried by counter-ions [49]. For our purposes, it is sufficient to review these definitions in order to conceptualize what makes a "good" nanofluidic diode. A high selectivity filter is usually preferred because it indicates that the charge in the walls strongly influences ion transport. This is a desirable feature for nanofluidic diodes because ion rectification is made possible by the asymmetric electrostatic profiles induced by the wall charge.

Since channels function as a pathway between two reservoirs or across a membrane barrier, the matter that passes through is said to permeate the barrier or membrane. From this perspective, the ability to control what passes through and what is prevented from permeating is referred to as permselectivity. For our purposes in working with nanofluidic diodes, permselectivity and charge selectivity are essentially the same, because the systems from chapter 4 only discriminate based on particle charge polarity. In biological nanochannels, however, the precision of permselectivity can go farther than charge preferences. For example, the inward-rectifying potassium channel that helps

maintain the potential difference across a cell's membrane has a highly effective selectivity filter. It allows potassium ions to flow through while strongly preventing ions such as sodium from entering, even though potassium and sodium ions have the same valence charge [1]. Nanofluidic diodes do not need to filter ion species so carefully in order to achieve ion current rectification, but selectivity based on charge polarity is a necessary requirement.

The EDL that form in the nanofluidic diode systems serve as the charge selectivity filter, as they are populated with counter-ions (and co-ions are depleted). Since we want the EDL present in most of the nanochannel to maximize the selectivity, the bulk ion concentration should not be too high. As equation 5.15 shows, the Debye length is inversely proportional to the square root of the bulk ion concentration, so electrolyte solutions of low ionic strength (low charge concentration) are ideal to form thicker EDL. The surface potential also has an effect on the EDL, as higher surface potentials (due to higher embedded surface charge densities, see the Grahame equation: equation 5.16) cause electrostatic potential profiles to extend farther from the wall. The resulting exclusion-enrichment effect causes the local ion concentration to be inhomogeneous in the cross-section of the nanochannel [12]. Logically, since the valence of the ions in the solution affects the Debye length, the EDL extension will depend on the electrolyte species as well. Since we are considering systems with KCl solutions (symmetrical with 1:1 valence for cations and anions), we will not elaborate on the complicated effects of asymmetric or higher valence species in this research.

With an established EDL presence in the nanochannel, so there is enrichment of counter-ions within its volume, an applied electric field from one reservoir to the other (achieved by applying a voltage difference between the electrodes submerged in each reservoir) has an interesting effect. The applied electric field, which points along the length of the channel, can cause ion depletion at one end and ion enrichment at the other end of the channel for the sake of producing the asymmetric conductivity required for nanofluidic diodes. A bulk concentration gradient is therefore formed across the nanochannel, known as concentration polarization [18]. Note that a nonuniform concentration profile develops in all three types of nanofluidic diodes we are studying, not only the one with asymmetrical reservoir concentrations.

The concentration polarization modifies the ionic current, with a stronger impact in narrower nanochannels and lower ionic strength solutions. We will explore this concept deeper when we look at how different system asymmetries cause ion current rectification, and how the applied electric field inducing regions of enrichment and depletion across the channel changes the effect on ion current when the field's direction is reversed.

The applied electric field along the length of the channel is not the only applied field that can manipulate ionic current; a field applied to the channel wall can alter the surface potential and the zeta potential, which in turn can change the exclusion-enrichment coefficient [12]. This so-called field-effect control of permselectivity is analogous to how the applied gate voltage is used in MOSFETs to control the electron/hole populations of the conducive inversion channel in the semiconductor body [12]. Although our

targeted nanofluidic diode systems do not implement this principle, there are numerous research groups that have modeled and tested field-effect nanochannels. They have demonstrated the ability to regulate the cation and anion populations in nanochannels, and by extension, the ion current is controllable. This functionality can be implemented as a conductive switch for ionic current, like a MOSFET or BJT does with electron current [13, 23, 27].

6.2: Ionic Conduction

Ionic current is not possible if there is zero ionic conductance, as the charge must be able to move for current to exist. Quantifying ionic conduction is thus necessary to understand the influences at play which permit or prevent ion flow in the on/off modes of the nanofluidic diode. Recall equations 5.47 and 5.48, which relate the conductivity for an ion species (the ability for charge to travel) to factors such as that ion species' concentration and radius, as well as the viscosity of the fluid:

$$\sigma_i = D_i \frac{q_e^2 z_i n_i}{k_B T} = \frac{q_e^2 z_i n_i}{6\pi \eta r_i}.$$

Our electrolyte solution, KCl, has two ion species: K^+ ions which have an atomic radius of 0.138 nm, and Cl^- ions whose radius is 0.181 nm [51]. When hydrated, K^+ has an effective radius of 0.25 nm and Cl^- has an effective radius of 0.2 nm [29]. According to equation 5.48 (rightmost term above), this difference in hydrated radius, with all other

factors being identical, constitutes a slightly higher conductivity for Cl^- ions than for K^+ ions.

We also observe in the conductivity equations that ion conductivity scales proportionally with that ion species' concentration. Logically, this direct relationship between conductivity and concentration makes sense. Instead of charge carriers each needing to physically move from one end to the other, they are able to "push" those in front of their path forward (through coulombic repulsion), which in turn push those in front of them forward farther down the length, and so on. This domino-like effect, by essentially transporting a wave of kinetic energy, allows charge to flow more efficiently in higher concentrations compared to lower concentrations. The relationship between conductivity and concentration is essential to understanding the mechanisms of ion rectification, which is why we emphasize its origin and logic here.

The overall conductance in a nanofluidic channel is the superposition of the bulk conductance and the EDL conductance, which are different mostly due to variation in apparent viscosity [12]. We will discuss what alters apparent viscosity when we describe slip conditions later in this chapter.

When the EDL are thinner than the diameter of the channel, the solution occupying the remaining volume has similar properties to the bulk solution. In such a region, ions effectively do not experience electric fields from the charged walls due to the EDL, so the only significant electric force that drives their movement is from the applied voltage difference between reservoirs – electrophoresis.

While ions in the bulk have one set of diffusion and mobility coefficients, ions in the EDL experience a different environment, as the wall charge adds a significant electric field component the closer the ion is to the wall. So, different coefficients characterize the ions' freedom of movement in the EDL. The counter-ion enrichment in EDL contributes to the high conductance for counter-ions in the same way that higher electron density increases conductivity in a wire.

Aside from the consequential increase in conductivity from increased counter-ion enrichment, electroosmotic transport also affects ion conductance. While the bulk solution experiences just electrophoresis, in the diffuse layer, electroosmosis serves as an additional source of ion transportation and should be considered [12].

6.3: Surface Charge Dependence for Ion Current Rectification

Combining some of the ideas we have mentioned thus far, we are able to conclude that when EDL overlap, ion current depends on the wall charge density. Stronger charge density leads to thicker EDL, and when they overlap, the EEE causes the solution in the channel to become unipolar. The fixed surface charge in the channel walls has a greater influence on the ionic current as its EEE alters the ion concentrations from their original bulk values [39]. Counter-ions dominate as they are attracted to the fixed wall charge, with that same fixed wall charge repelling co-ions and depleting them from the channel [27]. Through this causal chain, the fixed wall charge density, instead of the bulk concentration in the reservoirs, governs the ion conductance through the channel [11].

Increasing the bulk ion concentration decreases the EDL thickness, modeled by the Debye length (equation 5.15), so less volume in the channel is occupied by the unipolar EDL and more volume is occupied by ion concentrations at values similar to that of the bulk. Thus, increasing the bulk ion concentration lowers the ionic current's dependence on the fixed wall charge [27]. Interestingly, the regime of operation where ion transport is governed by the wall charge happens mostly in hydrophilic nanochannels made of a substrate with negative surface charge, such as silicon or glass [20].

6.4: Threshold Voltage for Ion Transport

When the ionic current is dependent on the embedded surface charge instead of the bulk concentration, the current-voltage characteristics feature a turning point that strikingly resembles a semiconductor diode's threshold voltage.

In bipolar nanofluidic diodes (such as the example system in figure 4.2), there is a "built-in" potential difference across the boundary between opposite fixed wall charge polarities [52]. The applied potential must overcome this potential before ions are able to conduct across the junction. However, there is a different type of "threshold voltage" that occurs in all nanofluidic diodes, where the applied electric potential changes the boundary conditions of the fluid at the walls [20].

When the applied voltage between one reservoir and the other is very low, the ions in the channel, especially the ones closest to the wall, feel a stronger electrostatic attraction to the charged walls than from the applied field, and so their transport through

the channel is slow. However, as the applied voltage bias is increased (in the nanofluidic diode's "on" voltage polarity), it reaches a threshold value where the applied electric field overcomes the fixed wall charge's electrostatic field. Beyond that threshold voltage, in terms of current-voltage characteristics, the system experiences a dramatic, nonlinear increase in ion transport and ion current [20]. Below the threshold voltage, the ion current-voltage relationship is much more linear and repressed (smaller slope magnitude).

On a more technical level, the threshold voltage denotes the point at which the zero-slip boundary condition breaks down [20]. When the applied field is strong enough for the ions closest to the fixed surface to become mobile, they drag solute molecules with them, and so the fluid's velocity relative to the surface at the boundary becomes nonzero. This is a type of electroosmosis, and it enhances ion transport properties, contributing to the sharp increase in ion current as applied voltage bias continues past the threshold voltage.

6.5: Slip Conditions

The criteria for the slip boundary condition to apply instead of the no-slip (or zero-slip) boundary condition is not only affected by externally applied voltage, but can be linked to surface charge density as well. It has been found that increasing the density of the fixed wall charge decreases the slip length. The slip length defines the distance from the boundary (into the solid) where the linear approximation of the fluid velocity profile goes to zero [20, 53, 54].

The reason that slip length shrinks with increasing surface charge density can be rationalized by considering the static structure factor of liquid water, which defines the rigidity of clustering water molecules [53]. Since water molecules are highly polar, they are electrostatically attracted to the fixed charges in the wall. Accumulating water molecules take on a structure with unique properties due to their shape and the fact that they are polar [53]. It follows logically that a higher fixed charge density would lead to more rigid structuring, and less freedom of movement for the molecules closest to the surface, causing an apparent increase in viscosity and a consequential decrease in the diffusion coefficient (according to equation 5.42).

We depict the concept of slip length in figure 6.1, to visualize how the fluid velocity vector profile (shear; parallel to the plane of the wall) is given a linear approximation, and the distance from the boundary where the linear trend reaches zero marks the slip length. Molecular dynamics simulations confirm that the slip length decreases as the surface charge density increases, caused by the presence of the surface charge increasing the ordering structure of liquid water [53]. If the slip length is zero, then the no-slip boundary condition would apply, and fluid velocity would be zero (relative to the immobile region) at the boundary between mobile and immobile regions. A positive slip length indicates that the fluid in contact with the interface is mobile relative to the surface. If the slip length is negative, it refers to a layer of stationary fluid (with a thickness equal to the slip length) between the stationary solid wall and the non-stationary fluid.

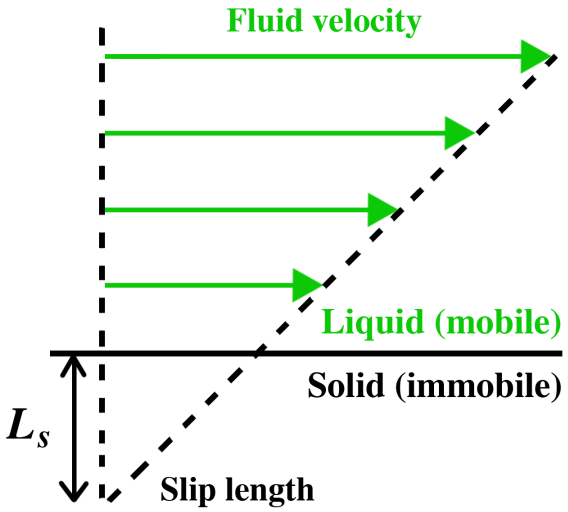

Figure 6.1: Simple depiction of the slip length definition, adapted from [54]. L_s is the slip length, and defines where the linearized velocity profile (green vector arrows) goes to zero. The horizontal black line denotes the wall surface, i.e. the boundary/interface between liquid and solid.

The concept of slip at the boundaries of a nanochannel is important for nanofluidic diode models, since the diffusion of water molecules through a nanochannel can be much different than in the bulk. This difference is often attributed to the status of fluid flow at the channel walls [20], so slip boundary conditions can have a sizable effect on predicted ion transport profiles, especially for systems with lower fixed wall charge densities.

Slip conditions are important to consider when designing nanofluidic diodes, because different materials interact with solutions in different ways. When the solution is aqueous, these interactions can be either hydrophobic or hydrophilic in nature, corresponding to weak affinity and strong affinity, respectively, between water and surface [20, 32]. The friction factor (a measure of frictional force strength, which opposes

movement) is found to usually decrease as channel walls become more hydrophobic, and increase for more hydrophilic walls [32]. This means that water molecules can slip on hydrophobic walls, and consequentially require a slip boundary condition to describe fluid transport behavior [20], and the slip length as defined in figure 6.1 would be a positive nonzero value.

In this research, we will not pursue the complex quantitative relationships that model these concepts, but it is worth emphasizing that better liquid/wall wetting (terminology used to describe stronger liquid/wall interactions) is just one factor contributing to friction between fluid and wall. It is electrostatic interactions that contribute most to the friction factor [20], though wettability does affect slippage, and is therefore a prominent concept in nanofluidics.

6.6: Sources of Ion Current Rectification

A nanofluidic diode gets its name from the diode-like behavior of its current-voltage characteristics. As we reviewed in chapter 4 when the systems were first introduced, diodes rectify current, meaning that at one applied voltage polarity, current flows across the electrode terminals at a much higher level than at the opposite polarity. Also recall that for rectification to occur in nanofluidic channels, there must be electrostatic asymmetry of some kind in the system, in order to produce these different conductivities.

Through experimentation performed by many groups, key factors have arisen that consistently correlate to significant ion current rectification being exhibited. First is that

at least one opening diameter of the nanochannel is comparable to the Debye length, so that the EDL overlap somewhere in the channel. Second, that there is an excess (net non-zero) surface charge embedded in the nanochannel walls. Lastly, that there is asymmetry between the two entrances of the nanochannel in the interactions the ions have with the charged channel walls [45]. These asymmetrical electrostatic interactions can be induced by asymmetrical EDL overlap or by asymmetrical surface charge.

Nanochannels embedded with positive or negative surface charge rectify ion current in opposite directions [45]. So, the surface charge polarity determines the direction of ion current rectification, serving as strong evidence that it is the electrostatic interactions that are the cause of this diode-like effect. Experiments also indicate that the type of solid material forming the membrane between the reservoirs, as well as the specific chemistry of the fixed wall charge, are independent of ionic rectification ability. The conclusion is that electrostatic asymmetry at the two openings is ultimately responsible for rectification [45].

6.6.1: General ICR Trends and Connections to Quantitative Relationships

As we mentioned, the root of ion current rectification (ICR) is the different conductivity profiles across the channel when opposite voltage polarities are applied. To support this claim, let us recall our discussion of the quantitative models that are useful for predicting nanofluidics behavior. For this research, we are focusing on the most basic, fundamental relationships to explain ICR. Therefore, we will neglect fluid dynamics here,

as electrostatic interactions are sufficient to qualitatively model ICR in the systems we are studying. We will explain current rectification in a general nanofluidic diode by using the PNP model to compare forward bias to reverse bias modes.

The PNP equations are given by equations 5.44 (the Poisson equation) and 5.45 (the Nernst-Planck equation), repeated here for convenience:

$$\nabla^2 \Phi = -\frac{1}{\varepsilon_0 \varepsilon_r} \sum_{i=1}^{N} q_e z_i n_i$$

$$\mathbf{J}_i = -D_i(\nabla n_i + \frac{q_e z_i n_i}{k_B T} \nabla \Phi).$$

The PNP model also showed a way to express ion current conductivity, given by equation 5.47-5.48:

$$\sigma_i = D_i \frac{q_e^2 z_i n_i}{k_B T} = \frac{q_e^2 z_i n_i}{6\pi \eta r_i}.$$

We can see that conductivity scales directly with concentration, so the conductivity (σ_i) of an ion species (i) is greater in areas where that species exists in higher concentrations, (n_i). Concentration is easier to change than the other parameters that affect conductivity, such as ion radius (r_i) or viscosity (η), so logically, concentration is the parameter which is manipulated to switch a nanofluidic diode on or off. In forward bias, the channel should have a high ion concentration so that conductivity is high and ion current is strong as a result, and in reverse bias the channel should have low ion concentration so that conductivity is low, repressing ion current. We can also see this connection between higher concentration and greater ion flux through the second term in the Nernst-Planck equation.

This is the function that asymmetric electrostatic interactions carry out, because on the side of the channel with stronger electrostatic forces, counter-ions will accumulate. Accumulation means ion concentration increases and counter-ion conductivity increases, promoting greater counter-ion flux. In forward bias, the counter-ions enter the channel at the opening with greater flux, so the channel is flooded with counter-ions, increasing overall concentration, conductivity, and flux. In contrast, reverse bias sees the counter-ions exit the channel on the opening with greater flux, so the channel is depleted of counter-ions, and overall concentration, conductivity, and flux decreases.

There are numerous ways to create asymmetrical electrostatic interactions across a nanofluidic channel to induce ICR. However, three types consistently appear the most in research publications, standing out as the most effective methods to fabricate functional nanofluidic diodes. These three asymmetries are in: fixed wall charge, bulk ion concentration, and channel diameter, as discussed in chapter 4. Interpretations of rectification, which are theoretical trends based on experimental and computational results, are depicted in figure 6.2 to help visualize the concentration trends and resulting ion current fluxes. Let us now examine figure 6.2 to clarify its features. There are three columns of diagrams, one for each of the three main types of nanofluidic diodes. The top diagram of each column is a simple depiction of that column's type of diode. They are length-wise cross-sectional diagrams of the systems, exactly the same setup as figures 4.2, 4.3, and 4.4. But unlike those previous figures, the top diagrams in figure 6.2 are more vague in how they indicate the presence of the reservoirs on either side, as well as the voltage ap-

plied to the electrodes in each. They are similar in that they are not to scale, however, since both representations enlarge the nanochannel vertically to show the channel more clearly.

Below the system diagrams in each column, there are ion concentration graphs corresponding to equilibrium state (labeled 1a, 2a, and 3a), forward bias (labeled 1b, 2b, and 3b), and reverse bias (labeled 1c, 2c, and 3c), with the upwards vertical direction being the axis of increasing ion concentration, n. The concentration profiles of K^+ ions are represented with a solid red line, while those of Cl^- are drawn with a dotted blue line. In the two reservoirs on either side of the nanochannel, electroneutrality applies, so the concentrations of the two ion species are equivalent in the reservoirs, and are represented by solid black lines.

The concentration graphs for the equilibrium state also label the regions of the graph that correspond to the nanochannel and the two reservoirs (baths), labeled n_L and n_R for the concentrations in the left bath and right bath, respectively. The comparisons between n_L and n_R are indicated just below the system diagrams, with $n_L = n_R$ indicating that the reservoirs contain equal ion concentrations, and $n_L > n_R$ indicating that the left reservoir contains a higher concentration than the right reservoir. The concentration graphs for the states of forward bias and reverse bias also label general regions inside the nanochannel where ion concentration is in accumulation and depletion.

Lastly, there are flux diagrams for forward bias and reverse bias states, presented below the concentration graphs to which they correspond. The boundaries between solid

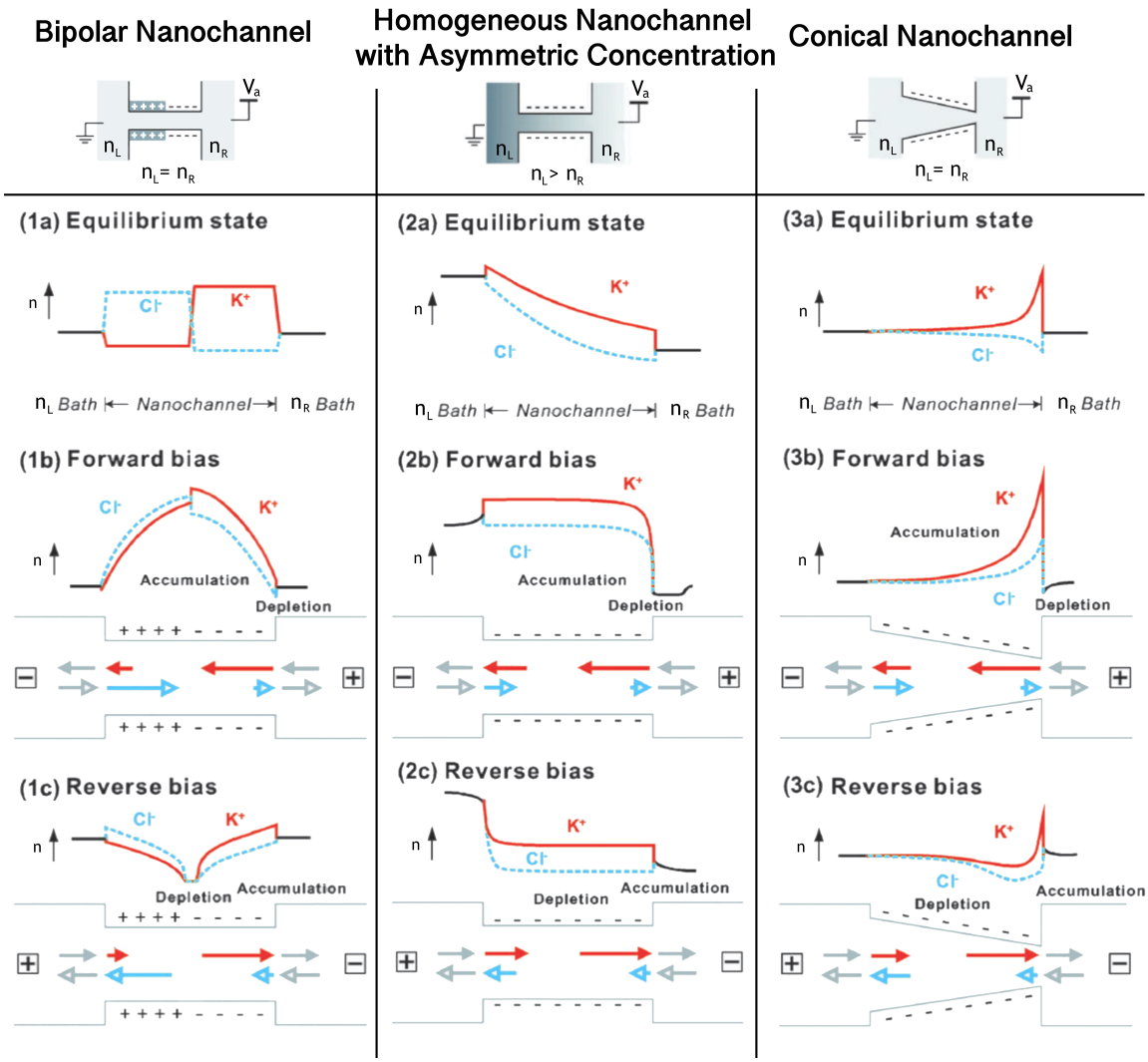

Figure 6.2: Interpretation of ionic rectification in different types of nanofluidic devices based on the analysis of asymmetric ion currents building up right after the external electric fields are applied. The solid red/dashed blue lines represent the cation/anion concentration profiles in nanochannels, respectively. Areas of noteworthy ion accumulation and ion depletion are indicated by labels. Channel flux diagrams are presented below the concentration graphs for the forward and reverse bias modes. The solid red/empty blue arrows symbolize cation/anion fluxes respectively. For each ion species, if the inward current is greater than outward current, ions will accumulate in the channel when the system reaches the steady state. On the contrary, if there is more outward current than inward current, ion depletion takes place in the channel. Adapted from [26].

and liquid are outlined with gray lines, and the arrows indicate ion fluxes, with the length of the arrow indicating the relative value of the flux – longer arrows correspond to greater fluxes. Solid red arrows denote K^+ ion flux in the nanochannel, while empty blue arrows indicate Cl^- ion flux in the nanochannel. Gray solid and open arrows in the reservoirs indicate the presence (but not necessarily magnitude) of K^+ and Cl^- ion flux, respectively, between the reservoirs and the nanochannel. The applied voltage polarity to each reservoir's electrode is indicated by a boxed symbol + or –.

We will carefully analyze the behavior of each of these nanofluidic diode types, using the example systems from chapter 4 and which are depicted in figure 6.2. By doing so, we will fulfill our main objective of this theoretical research project, which is to build a stable, fundamentals-based understanding of ion current rectification in nanofluidic channels.

6.6.2: Asymmetry in Surface Charge

The first case we will delve into is asymmetrical surface charge density in the nanochannel's walls. These nanochannels are structurally symmetric, located between reservoirs of identical electrolyte solution and bulk ion concentration, with the only asymmetry existing in the surface charge distribution. The system is known as a "nanofluidic bipolar diode" or a "bipolar nanochannel" when the surface charge densities at the two halves of a channel possess the same magnitude but opposite signs [55]. We present figure 6.3 as an example system with this type of asymmetry, showing the EDL

which form in equilibrium (when applied voltage is zero). The EDL in the positive portion of the channel are enriched with negative ions and appear as a blue "cloud" to symbolize the accumulated anions. In the negative portion of the channel, the EDL are enriched with positive ions and appear as a red "cloud" to symbolize the accumulated cations.

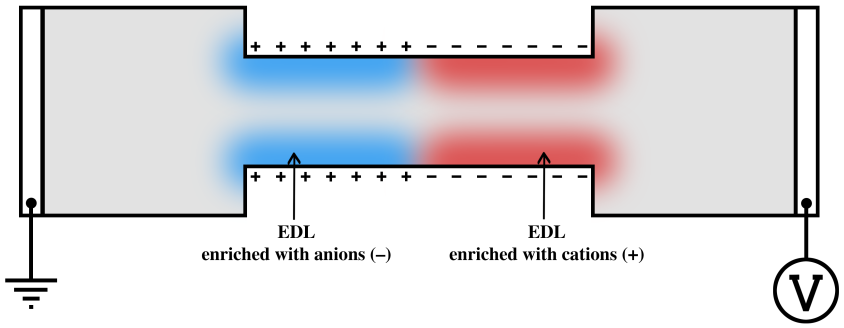

Figure 6.3: Qualitative representation of EDL formed in bipolar nanofluidic channel with zero applied potential (equilibrium).

The rectifying effect is a natural consequence of the changes that occur in the cation and anion concentrations when the system is given an applied voltage bias. Referring to the system in figure 6.3 and the first column of figure 6.2 to facilitate our discussion, we will approach the theory qualitatively from the molecular perspective. We will explain that rectification occurs due to ion enrichment and ion depletion at the central junction, where the surface charge densities of opposite polarities meet [55].

6.6.2a: Off Mode

The "off" mode of any nanofluidic diode, in general, occurs when the entrance resistance (inverse of conductance) is higher than the exit resistance for both ion species [1]. In a system with asymmetrical fixed wall charge, the off-mode requires the electrode with the positive applied potential to face the positively charged side of the nanochannel, and the electrode with the negative applied potential to face the negatively charged side.

The system in figure 6.3 is in the off mode when a negative voltage is applied to the right electrode with respect to the left electrode, meaning the applied electric field points from the left to the right. Figure 6.2, panel 1c represents the bipolar nanochannel under reverse bias, the off mode, illustrating the behavior of this system.

Under these conditions, cations exit the channel on the right, and since the negative wall charge forms EDL enriched with cations, there is a high conductivity provided for them as they leave. Cations try to enter the channel on the left, but the positive wall charge repels them, resulting in a high resistance (low conductance) at the entrance. The exact same reasoning applies (just in the opposite direction) for anions, with higher resistance at their entrance to the channel compared to their exit. So as a result of the applied bias, both cations and anions are depleted from the central junction of the nanochannel [38], and the channel as a whole. Ion depletion lowers conductivity, so the off mode, enabled when "reverse bias" voltage is applied, is characterized by low conductance and low ion current.

6.6.2b On Mode

The system switches to its "on" mode when the entrance resistance is lower than the exit resistance for both ion species [1]. As the inverse of the off mode, the on mode has its electrode with the positive applied potential facing the negatively charged side of the nanochannel, and the electrode with the negative applied potential facing the positively charged side.

In figure 6.3, a positive voltage applied to the right electrode with respect to the left puts the system into the "on" mode. Figure 6.2, panel 1b represents the bipolar nanochannel under forward bias, illustrating the behavior we will now be describing.

Now, the cations are pulled by the applied voltage into the channel on the side of lower resistance (the right side), where negative fixed charge enriches the channel with cations and provides a conductive region for them. The left side is their exit, and is the side of higher resistance. However, with cations able to rush in at the entrance and accumulate at the junction, they reach a concentration much higher than the bulk in the reservoirs. Drift current (appearing as the first term of the Nernst-Planck equation) dominates and allows cations to exit the channel smoothly, resulting in a steady ion current flow [13, 38, 44]. Just as before, the same logic applies to anions, in reverse. So, in the on mode, a "forward bias" applied voltage causes the cations and anions to move toward the central junction, toward each other, and diffuse the remaining half to exit the channel, setting up a path of high conduction for ion current.

6.6.2c Fluid Flow

The velocity of the fluid in the bipolar nanofluidic diode is mainly induced by excess charge under the effect of the electric field, known as the body force, as well as fluid pressure. The fluid flow within a nanochannel is extremely difficult to measure experimentally, so the best way to gain insight is through simulations, usually through molecular dynamics simulations or numerically solving the PNP-NS equations with appropriate boundary conditions. Fluid flow is of interest to researchers and engineers studying nanofluidic diodes because it is the source of electroosmosis. The momentum of solution molecules can be transferred to ions suspended in the solution, thus providing a source of ion flow known as electroosmosis.

Kunwar Pal Singh and Manoj Kumar numerically modeled a nanofluidic bipolar diode, and among their findings, they presented profiles of the fluid flow in the system, included here as figure 6.4 [44]. Their results indicate that in both forward bias and reverse bias, the fluid velocity along the center of the nanochannel and the fluid velocity close to the walls flow in opposite directions, resulting in nonuniform fluid flow.

In reverse bias, fluid enters the nanochannel close to the walls and exits through the center of the channel. In forward bias, fluid enters the nanochannel through the center and exits close to the walls. These simulation results are presented in figure 6.4, with fluid flow magnitude and direction indicated by arrow size and direction.

Singh and Kumar repeated the simulation to solve for the PNP and the PNP-NS systems of equations, to exclude and include electroosmotic flow, respectively. Interest-

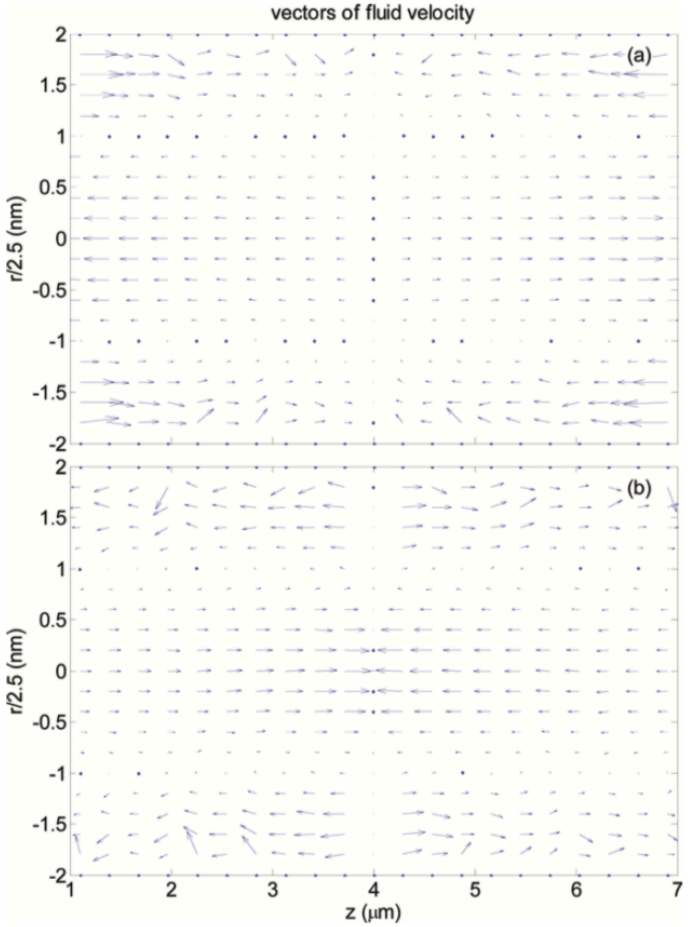

Figure 6.4: Vectors of fluid velocity in a bipolar nanochannel for (a) forward bias at V_a = +2.4 V and (b) reverse bias at V_a = –2.4 V for surface charge density σ_0 = 10 mC/m^2, bulk electrolyte concentration n_∞ = 100.0 mM, and a nanochannel diameter of 10 nm [44].
These plots depict a two-dimensional length-wise cross-section of the bipolar nanochannel, which considers the nanochannel walls to be horizontal and positioned at the top and the bottom of each graph, and the fluid occupying the space between them.
In this diagram, 'z' is the coordinate system along the length of the channel, and the vertical axis represents the width/diameter coordinates.

ingly, for the nanofluidic bipolar diode, they found negligible difference between the calculations. Further analysis led them to conclude that the oppositely-charged zones contribute electroosmotic flow that cancels out at the junction close to the walls [44]. We can conclude from these results that the electroosmotic components of ion current can be neglected because they cancel out. It can be inferred, however, that this same fluid flow cancellation is not present in the other types of nanofluidic diodes (asymmetrical ion concentrations and asymmetrical channel diameter), so it may not be valid to neglect electroosmosis in non-bipolar nanofluidic diodes.

6.6.3: *Asymmetry in Ion Concentration*

The second we are studying is asymmetry in ion concentration. This system has a structurally symmetric nanochannel and uniform surface charge density in the channel walls, but the bulk concentrations in the two reservoirs are not equal. We depict such a system in figure 6.5, showing the concentration gradient with a dark gray to light gray color gradient denoting the higher and lower ion concentrations, respectively. The EDL is shown as a red "cloud" to indicate positive ion enrichment, and has a nonuniform thickness from the walls.

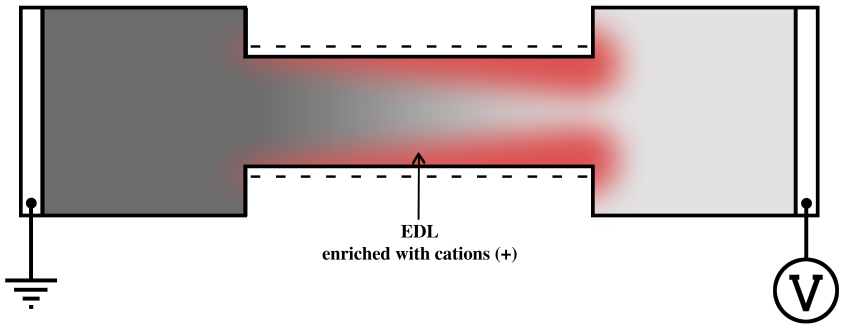

Figure 6.5: Asymmetry in ion concentration. The left reservoir holds a high ion concentration, while the right holds a low ion concentration. The shade gradient across the channel corresponds to the resulting concentration gradient between the two reservoirs.

As with all nanofluidic diodes, the rectifying effect is attributed to disparate ion concentration profiles that arise from opposite applied biases [11]. The asymmetrical electrostatic impact that gives rise to such disparate concentrations comes from asymmetrical EDL [26, 56]. On the low concentration side (right side in figure 6.5), the EDL are thick, represented by the red cloud, illustrating the accumulated positive counter-ions and

extending further into the center of the channel, while on the high concentration side (left side in figure 6.5), EDL are thin, represented by thinner red clouds. As the Debye-Hückel approximation (equation 5.14) indicates: larger screening lengths, which correspond to thicker EDL, result in farther-reaching electric potentials, meaning that $\Phi(x)$ extends farther in x. So the unipolar region of electrolyte solution extends farther out from the walls for thicker EDL compared to thinner EDL.

To view this from the molecular-level perspective of the system in figure 6.5, we know that the EDL will be dominated by positive ions, as they are attracted to the negative surface charge. The right channel opening will have thicker EDL than the left opening, meaning that cations will experience higher conductivity on the right than on the left.

6.6.3a: *Off Mode*

The diode is off in figure 6.5 when the voltage applied to the right reservoir electrode is negative with respect to the left reservoir. Figure 6.2, panel 2c represents this nanochannel under reverse bias, illustrating the following behavior description.

Under these circumstances, cations will flow from the left reservoir to the right, and will experience lower conductivity as they enter the channel as compared to when they exit. Their concentration will therefore be depleted within the channel as it is easier for them to flow out than to flow in. Anions experience similar conductivity asymmetry in the opposite direction, as they flow from the right reservoir towards the left. The right entrance to the nanochannel has a repulsive effect, from the far-reaching electrostatic ef-

fects of the negative surface charge in the lower electrolyte concentration. The exit on the left opening is more conductive, as the higher electrolyte concentration screens out the field from the negative fixed charge much closer to the surface. Just like the cations, the anions will be depleted from the channel as they exit much easier than as they enter, and overall, ion current is suppressed.

6.6.3b *On Mode*

The diode turns on when the positive potential is applied to electrode in the reservoir containing lower ion concentration. Figure 6.2, panel 2b represents this nanochannel under forward bias, illustrating the behavior we are describing. Now, cations flow from the right to the left, experiencing high conductivity at the entrance, where EDL occupy most of the cross-sectional area, and lower conductivity at the exit, where EDL only exist closer to the walls. Cation concentration is enriched in the channel as a result. Anions flow from left to right, and their entrance has a higher conductivity than their exit. In the left opening, the EDL screen out the negative wall charge close to the wall. But on the right, the electric field from the negative charge reaches farther into the center of the channel, lowering anion conductivity. Anion concentration is therefore also enriched in the channel compared to the bulk values. With enrichment of both ion species in the channel, ion transport is enhanced.

Theoretically, EDL overlap may not be necessary to produce the asymmetric electrostatic effect needed to rectify current. However, ICR is most pronounced, and most

clearly measured, when one side of the channel has overlap in its EDL [26]. When the channel becomes unipolar throughout the whole cross-sectional area (when EDL overlap), cations experience enhanced conductivity and anions are repelled by the un-screened fixed negative wall charge.

6.6.4: Asymmetry in Channel Diameter

The final case we will consider in-depth is that of asymmetrical channel geometry. This system features uniform fixed wall charge and uniform ion concentration reservoirs, but the diameter of one opening is larger than the other, with a smooth transition between, forming a conical nanochannel. We illustrate a system that serves as an example of an asymmetrical geometry in figure 6.6, with its left opening being a larger diameter, which decreases at a constant rate moving towards the right opening. Once again, the EDL are enriched with cations and represented as red clouds, but now with a constant thickness from the wall.

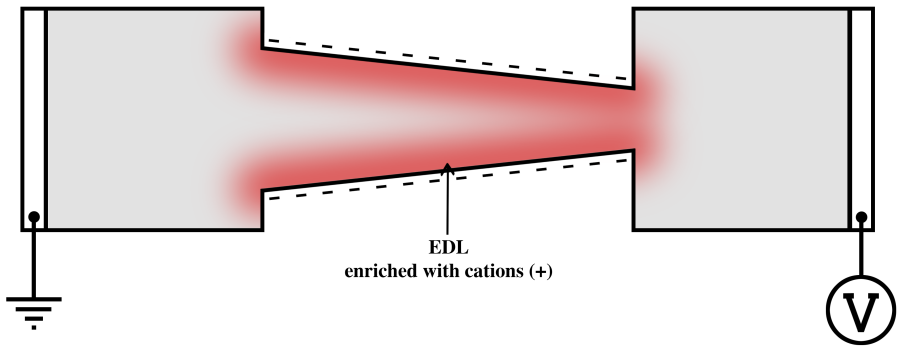

Figure 6.6: Asymmetry in geometry. The channel diameter is at a minimum on the right opening, and at a maximum on the left opening, with a smooth slope along the channel between them. The result is a conical nanochannel.

Interestingly, conical nanochannel diodes and asymmetric ion concentration diodes (the previous type of asymmetry) share the same physical basis for ICR [26]. Both of these systems feature more EDL cross-section occupation at one end than the other, with EDL overlap on the smaller end of the channel producing the best ICR. Unlike the previous case, this system maintains a consistent EDL thickness (screening length from the charged wall) across the entire length of the channel. The EDL overlap is produced by a smaller physical distance between the walls (i.e. a smaller diameter) at one end compared to the other.

In the "off" state, reverse bias, a zone of ion depletion is observable at the small end of the conical nanochannel, forming an electric potential well [56]. The potential well disappears when applied voltage is inverted from reverse bias to forward bias, lending further proof that the disparate induced ion concentration profiles between the biases are the cause of ICR. The molecular-level description that follows will be brief due to its similarity to the previous case.

6.6.4a: Off Mode

The conical diode is reverse biased when the applied voltage on the side of the smaller channel opening is negative (in figure 6.6, when negative voltage is applied to the right side with respect to the left). Figure 6.2, panel 3c represents the conical nanochannel under reverse bias, illustrating the behavior of this mode of operation. Cations will flow from left to right, but their concentration will be depleted in the channel because the left

opening has lower cation conductivity than the right opening. Negative fixed wall charge impacts more of the cross-sectional area of the channel at the right channel opening, resulting in attractive forces enhancing cation flow.

Anions will flow right to left, and their concentration in the channel will also be depleted because they enter the right side of the channel, where repulsive forces from the fixed wall charge are stronger. Both ion species being depleted from the channel restricts the ion current, so the system is in its off mode.

6.6.4b: On Mode

When the applied potential to the electrode facing the smaller channel opening is positive, the diode is forward biased. Figure 6.2, panel 3c represents the conical nanochannel under forward bias, illustrating the behavior of this mode of operation. Cation and anion flows are reversed, so they both enter the channel at their respective higher conductivity openings, and exit at lower conductivities for their species. Both ion species concentrations are enriched in the channel compared to the reservoirs, which gives them an extra diffusive flow component to help transport them across the side of the channel with lower conductance, which greatly increases ion current. Therefore, this applied bias results in the system's on mode.

6.6.5: Optimal Characteristics for Current Rectification

Measuring current-voltage relationships in different variations of the nanofluidic bipolar diode have helped researchers design systems that maximize ICR. Here, we will briefly review how combinations of asymmetries and/or the manipulation of properties such as fixed charge density, channel diameter, and bulk electrolyte concentration affect ICR in nanofluidic bipolar diodes.

6.6.5a: Combining Asymmetries

Often, fabricated nanofluidic diodes are designed to incorporate more than one of the three cases of asymmetry we have discussed. By combining multiple sources of asymmetrical electrostatic impact, the rectification factor can be enhanced. The most common combination of asymmetry types into one nanofluidic diode is that of asymmetrical fixed charge and asymmetrical geometry [15, 55]. Bipolar nanochannels also induce the largest rectification factors, so asymmetric charge is very commonly used in designing highly-rectifying nanofluidic diodes [44].

6.6.5b: Effects of Manipulating Characteristics

Variation in fixed charge density, channel diameter and bulk electrolyte concentration affects ICR properties in nanofluidic diodes. Researchers have manipulated these characteristics to learn what improves the rectification ability, so that nanofluidic diodes can be designed to suit a desired need.

Although the systems depicted in our examples have fixed wall charge along the entire channel, there are other possible configurations. A system with the same nanochannel length, but a shorter zone of fixed charge, cannot electrostatically hold as many ions in the channel compared to a longer charged zone. Therefore, the ion current decreases as the length of the charged zone inside the nanochannel decreases [55].

Affixing charge to the walls around the openings of the nanochannel (the walls facing the reservoirs, perpendicular to the inner channel walls) is another possible modification, which creates an extension of EDL surrounding the nanochannel openings. For the bipolar nanofluidic diode, this means extending the charged zones of each polarity around their respective openings. A combination of inside and outside charge asymmetry has been shown to further increase the current rectification factor [57]. The additional EDL at the openings serves to strengthen the selectivity filters for ions' entrance and exit to the nanochannel, thus improving the asymmetric conductivity strength.

The density of the fixed wall charge also has an impact, as symmetrically increasing the densities in a bipolar nanofluidic diode increases ICR [44, 57]. Higher charge density embedded in the walls produces a higher electric field, which requires more counter-ions to compensate. Increasing the counter-ion enrichment increases the conductivity for that ion species [57]. The electric field decreases as a result of higher ion concentration, but the concentration (and conductivity) increase dominates the diminished field, so the overall effect is an increase in ion current for applied forward bias. The recti-

fication factor increases dramatically with surface charge density because of the simultaneous increase in forward current and decrease in reverse current [44].

The diameter of the nanochannel is important, as we know from our understanding of EDL. An increase in the ratio of channel diameter to Debye length decreases ICR because the solution in the channel becomes less unipolar as the EDL becomes thinner. The counter-ion concentration decreases as diameter increases because there is less excess charge required to maintain electroneutrality, so the counter-ion conductivity in the channel drops. Interestingly, Singh and Kumar found through their simulations that for any given ratio of channel diameter to Debye length, the ICR increases with an increase in channel diameter [44]. They determined the reason to be a relatively higher increase in the forward current density compared to the increase in the reverse current density as diameter increased. This shows that it is the ratio between diameter and EDL thickness that is most important in ICR, since maintaining the same ratio while increasing the diameter gives the benefits of having more ions in the channel without compromising the conductivity asymmetry.

Lastly, the electrolyte concentration affects the system by manipulating the Debye length which characterizes EDL thickness. Ion current rectification decreases as electrolyte concentration increases [44], which may be surprising if we did not consider the importance of EDL. As ion concentrations increase in the electrolyte solution, clearly, a higher number of ions can flow across the nanochannel connecting the reservoirs due to the applied electric field. The ion current in forward bias therefore increases, so why does

ICR decrease? With higher concentration comes more efficient screening of the wall's fixed charge. Counter-ions accumulate close to the walls in higher concentrations when the electrolyte concentration is higher, screening out the fixed charge density's field over a shorter distance (EDL is thinner). The unipolar character of the solution is decreased, increasing reverse bias ion current more rapidly than forward bias current increases. This results in rapidly diminishing ICR with increasing electrolyte concentration [44].

An apt conclusion to this section is discussing the core similarities shared by all nanofluidic diode systems. All nanochannels that exhibit ion current rectification do so with areas of ion depletion and ion enrichment, especially at the entrances to the channel. The creation of these regions at the mouths of the channel under the applied potential is referred to as polarization concentration, and they are the reason the current-voltage curves deviate from linear, ohmic behavior [1]. In all nanofluidic diodes, ion depletion and accumulation regions can be explained by a combination of different flow components, including electrophoresis, electroosmosis, diffusiophoresis and diffusioosmosis [15, 18]. We sufficiently and thoroughly analyzed the most important effects in three types of nanofluidic diodes under forward bias and reverse bias, enabling us to explain the phenomenon of ion current rectification.

6.7: Semiconductor Diode Analogy

All of our discussion and analysis of nanofluidic diodes begs the question: how do they compare to PN-junction semiconductor diodes? In this section, we will explore simi-

larities and differences between the two, with the purpose of coming to a more complete understanding of nanofluidic diodes' capabilities, strengths and weaknesses.

6.7.1: Similarities in Equations and Materials

To start, let us look at the quantitative expressions that describe behavior within a nanofluidic diode. The Poisson-Nernst-Planck equations, which are very useful for modeling nanofluidics and microfluidics, are formulated on the basis of describing charged particle diffusion and migration in a self-consistent electric field [26]. Since electrons and holes can be thought of as charged particles, the Nernst-Planck equations can be adapted for semiconductors to describe their charge carrier behavior. Both diodes' charge carriers flow by a combination of drift and diffusion mechanisms, so electric potential and concentration profiles are very important to the function of both devices. The Debye-Hückel theory accurately describes the screening effects that take place in both nanofluidics and semiconductors, since both types of charge carriers (ions and electrons) can dampen an electric field from other particles. Because of this, the Debye length appears in many quantitative relationships in both types of materials.

To compare the material composition of the devices, we will take a look at how fixed wall charge density induces ion environments that are similar to N-type and P-type semiconductors. N-type semiconductors have been doped with donor atoms, providing extra electrons in the lattice. P-type semiconductors have "missing" electrons, known as holes, and have been doped with acceptor atoms [52]. Electrons serve as the negative

charge carriers in the semiconductor material, while holes can move as valence band electrons shift, acting as mobile positive charge carriers. So, in N-type semiconductors, electrons are the majority charge carriers and in P-type semiconductors, holes are the majority charge carrier.

N-type semiconductors are analogous to nanochannels with positive fixed wall charge. This is because the EDL that is induced is populated with negative counter-ions, so that anions are the majority charge carrier. P-type semiconductors are analogous to nanochannels with negative fixed wall charge, since their EDL is enriched with positive counter-ions, so that cations serve as the majority charge carrier [26]. This suggests comparing the EEE to semiconductor diodes' areas of charge carrier depletion and enrichment, because the parallel is very clear. In a nanofluidic diode, the fixed wall charge induces dramatic co-ion depletion and counter-ion accumulation. At the junction between regions of positive and negative charge carriers in a bipolar nanofluidic diode, diffusion across the interface creates a region of depletion very similar to the depletion region in a PN-junction diode. In both types of devices, the induced regions of accumulation and depletion are critical to the desired current rectification behavior.

6.7.2: Built-in Potential Analogy

PN-junction semiconductor diodes are built by connecting a P-type semiconductor region with an N-type semiconductor region. The interface where the doping concentration switches from P-type to N-type is known as the "metallurgical junction" and the

abrupt switch is referred to as a step junction. Electrons in the electron-enriched N-type region will immediately diffuse into the electron-depleted P-type region (and holes diffuse from P-type to N-type). The charge displacement gives rise to a built-in potential called the junction potential [52].

In nanofluidic bipolar diodes, a junction is formed by connecting oppositely-charged nanochannels, resulting in EDL of opposite charge polarity to form next to each other. Some positive ions in the negatively-charged nanochannel will diffuse across the junction towards the negative EDL, while some negative ions in the positively-charged nanochannel will diffuse in the opposite direction towards the positive EDL. The diffusion depletes the junction of both ion species, leaving behind the fixed wall charge junction. The electric field generated by the exposed surface charges reaches a balance with the ion concentration difference, and the resulting electric potential set up across the junction is analogous to the built-in potential in a semiconductor system [12, 26].

For nanofluidic systems, this potential is known as a Donnan potential, and shares the same physics as the semiconductor's built-in potential. The Donnan potential suppresses the diffusion of mobile ions across the depleted junction until the system reaches equilibrium [26]. This is essentially identical to how the built-in potential suppresses diffusion of electrons and holes across the space-charge region in a PN-junction diode. The applied potential in forward bias has to overcome the built-in potential before the diode switches to its on-mode.

6.7.3: Breakdown Potential Analogy

A "breakdown regime" has been observed to occur in nanofluidic bipolar diodes when the applied reverse bias potential becomes sufficiently strong [13]. The breakdown regime is defined to occur when the current in reverse bias continues to increase in magnitude with an increase in applied potential. It is surmised to be the result of water splitting, where the applied electric field is strong enough to begin breaking apart water molecules into their ionic components [13].

The analogous breakdown regime in semiconductor devices occurs in PN-junction diodes, where reverse bias current suddenly increases from its saturated value at strong enough reverse-bias potentials. Current rapidly increases in magnitude due to avalanche multiplication (impact ionization) of electron-hole pairs induced by the high applied field magnitude [13].

6.7.4: Key Differences

As we have seen, PN-junction semiconductor diodes and nanofluidic bipolar diodes share many similarities, including comparable material structure, built-in potential, and breakdown regimes at large enough reverse bias potential. Despite these analogous parallels, there are plenty of differences that separate semiconductor and nanofluidic devices.

One of the most pronounced differences is in the charge carriers, because electrons and holes can recombine, while cations and anions cannot. For semiconductor

diodes in forward bias, the depletion width is reduced at the junction, and electrons and holes are able to diffuse more easily across the junction, increasing overall current. While they are transported by means of drift and diffusion, some holes and electrons will recombine, and this recombination is important to consider in modeling. Also, the concentrations of electrons and holes are restricted by the concentrations of doped donors and acceptors, respectively [38]. In contrast, nanofluidic diodes use positive and negative ions as charge carriers, and they cannot recombine near the junction. Instead, they accumulate at the junction in forward bias, leading to concentrations that are much higher than the bulk ion concentrations [38]. This difference manifests itself in the continuity equation for current flux, as it features a recombination term in semiconductor physics that does not exist in nanofluidic physics.

Even more striking is the difference between carrier mobilities. Ions flowing in a solution have far smaller mobilities than electrons and holes in semiconductor crystals, at a factor of around 10^6-10^7 times smaller [26]. As a result, it takes a much longer time for ions to be transported from one reservoir to the other. In fact, permeation of ions through a nanochannel connecting electron solutions occurs on a time scale of microseconds to milliseconds, while atomic motion that transports electrons and holes has time scales in the femtoseconds range [41].

The majority-minority charge carrier concentrations also have some different sources affecting their fluctuations. In most semiconductors, the doping level is high enough, and the dopants are considered completely ionized at room temperature, so the

assumption can be made that there are equal fixed charge and majority carrier populations, while the minority carrier concentrations are orders of magnitude smaller. In nanofluidics, the counter-ion concentration inside charged nanochannels is determined by the surface charge density on its walls as well as other factors such as channel geometry and the bulk ion concentrations. The latter two factors are unique to nanofluidics as they do not apply to semiconductor charge concentration profiles. To achieve the high counter-ion to co-ion concentration ratio in the nanochannel, surface charge density must be high, the channel diameter should be small, and the bulk ion concentrations should be low [26].

The current-potential curves also differ between semiconductor and nanofluidic diodes. Semiconductor diodes exhibit an exponential current increase in forward bias. Nanofluidic diodes with non-overlapping EDL show more of a quadratic increase in current with respect to potential in forward bias [38]. This difference can be attributed to the more ohmic behavior of the electrolyte solution outside of the EDL, which dampens the rectifying effect. When EDL overlap, the EEE occurs in the whole cross-section, and ICR increases.

Despite sharing some functional similarities, these numerous incongruences between nanofluidic diodes and semiconductor diodes distinguish them as fundamentally different devices. Many of the differences, especially the massive disparity in charge mobility, strongly diminish the utility of nanofluidic diodes as traditional current switches for purely electronic applications. However, consider the fact that current is carried through ions instead of electrons in nanofluidic diodes, and then the connections to chem-

istry and biology encourage our research endeavor. By developing the theory, we hope to advance the pursuit of harnessing ion flow for biochemical-electrical integration and new medical technologies, as discussed in chapter 3.

CHAPTER 7

Modeling Ion Current Rectification

Originally, the goal of this research was to perform our own simulations of the PNP equations through use of a commercial software package such as COMSOL. This goal evolved over time, and gradually changed as we gathered more information about nanofluidics and the complexity of modeling nanofluidic diodes. Ultimately, our primary interest shifted to forming a comprehensive foundation for future simulation research, achieved through the interpretation and organization of a fundamentals-based theory. We wanted to create a resource that conveys topics relevant to the engineering and physics of nanofluidic diodes, so that the reader can form an intuitive understanding of these devices.

This has been the purpose of the preceding chapters – to develop an understanding of ion current rectification in nanofluidic diodes – which we did by building a strong theory from fundamental physics concepts. Most of our descriptions have been logical in nature, supplemented with the most commonly-used and well-evidenced quantitative relationships.

These mathematical models serve as representations of physical reality, and were developed to analyze and calculate quantities predicted for a system's real-world behavior [58]. However, though the mathematical models themselves can show relationships between parameters that affect behavior, it is their solutions that give the most insight. The complexity of nanofluidics, even at the fundamental level, means that

numerical simulations are crucial for calculating solutions to the models. So in this chapter, we will review some of the many methods that yield predictions for nanofluidics behavior, including classical molecular dynamics (MD) and the finite difference method (FDM). Then we will use a simplified, fundamental physics-based set of equations to conduct our own analysis of one of the nanofluidic diode types – a homogeneous nanochannel with asymmetric ion concentration. Our simulation goal is to illustrate the theoretical understanding we have developed about the source of ion current rectification.

7.1: Classical Molecular Dynamics (MD)

Let us begin with a method of simulation which has been used to provide evidence for parts of the theory we have developed: molecular dynamics, or MD. In classical MD, the dynamics of ions, the solution, proteins, etc. are described in atomic detail [8]. Numerically integrating equations of motion as functions of time allows a state-by-state prediction of behavior for each individual particle involved in the system [20]. Although massively computationally exhaustive and demanding in time to simulate each consecutive state, the results are among the most accurate and insightful possible due to the method's meticulous consideration of individual molecules [8]. MD is therefore ideal for simulating flow, and for finding transport properties such as the ion transport behavior we wish to analyze in nanofluidic diodes, but it suffers immensely from limitations in computational power and simulation time, so the size of the system that can be modeled is very restricted [8].

One example of a MD simulation is presented by Liakopoulos, Sofos, and Karakasidis [32], where they investigated liquid flow in nanochannels with varying hydrophobic/hydrophilic interactions. They used their MD simulation results to estimate the effect that the wettability of the channel walls, as well as the effect their roughness (surface unevenness) had on fluid flow. They concluded that the friction factor decreases as the channel walls become more hydrophobic (lower wettability), and the rougher a channel wall is, the greater the frictional impact on flow [32]. The results agree with the logical relationships between these characteristics, as described in section 6.5. Similar investigative goals involving fluid flow at nanochannel walls, such as the slip length investigation conducted by Xinran Geng et. al. [53], rely on molecular dynamics to illuminate the complex behavior, especially because of how difficult it is to experimentally measure in such close proximity to the walls [20, 53].

For the purpose of analyzing transport mechanisms through a nanofluidic diode, the number of molecules that need to be simulated is too staggeringly large for practical applications of molecular dynamics, so methods that rely on approximations to simplify calculation are preferred to simulate meaningful behavior [8]. Mean-field approximations, such as the PNP model we discussed in section 5.10, are the most widely-used alternative because they are reliable, efficient, and accurate. MD and PNP models disagree by less than a 10% margin unless the nanochannel has a fixed surface charge density magnitude more than about 19×10^{-2} C/m^2 in its walls, and a radius on the order of 1 nm [22]. The nanofluidic diodes we want to analyze have typical wall charge

densities on the order of 1×10^{-2} C/m^2 or less, and radii around 10 nm, so the PNP models are well-suited to model many fabricated nanofluidic diodes.

7.2: Methods to Solve the PNP Equations

In mean-field approximation models, or continuum theory, ion species are represented by macroscopic ion concentration profiles instead of microscopic discrete particles [8]. The Poisson-Nernst-Planck equations are one such continuum-based model, and though their system of equations is complex, it uses more manageable computational processes to obtain results. Analytical attempts at solving PNP equations do exist, but their coupled, nonlinear nature usually makes numerical simulation more attractive for general use [58].

In this section, our goal is not to provide a full tutorial on how to implement these numerical simulation methods, but rather to introduce the reader to them for the purpose of familiarization. As a result, these methods will be described on a conceptual level instead of a mathematical one, as general comprehension is our emphasis. Another benefit of this brief review is to help conceptualize what kind of process the PNP model (or any continuum-based model, including the PNP-NS model) must be put through before meaningful results are achieved.

7.2.1: Gummel Iteration Method

To begin, we will consider a method that is most applicable to a one-dimensional simplification of the targeted system, and is easier to implement than the later methods. It is known as Gummel's method, or the Gummel iteration method, and is used to solve a nonlinear discrete system, such as the drift-diffusion and continuity equations in semiconductor physics as well as nanofluidics [4].

For the PNP model, the Gummel iteration begins with a starting prediction of the electric potential and ion concentration profiles obtained from initial conditions and the geometry of the system. The "guess" of the electric potential profile is substituted into the steady-state Nernst-Planck equations (equation 5.49, one for each ion species), and solved for the concentration profiles of each ion species throughout the system [8, 42]. Next, these concentration profiles are substituted into the Poisson equation, which is solved to obtain a new version of the electric potential profile. The predictions of the ion concentration and electric potential profiles are updated using the new, calculated profiles, usually through a relaxation method. To find the prediction to be used for the next iteration using a relaxation method, a parameter w with a value chosen between 0 and 2 is multiplied by the new prediction, which is then added to the old prediction multiplied by a factor of $(1 - w)$. Updating the profiles by relaxation instead of simply switching to the new predictions often improves the convergence of the system, as it ensures smoother steps in the iteration process for narrowing in on an accurate solution that satisfies all of the equations [42].

Essentially, when solving a system that follows Boltzmann statistics and drift-diffusion equations, the Gummel method alternates between solving linear differential equations for the electric potential and for the charge carrier densities [4]. Each iteration refines the predictions, until the change between one prediction and the next is smaller than some set threshold, at which point the model has converged on a solution.

7.2.2: Finite Difference Method (FDM)

As previously stated, the Gummel iteration method is most suited to one-dimensional systems, and is not as practical to attempt for domains of greater dimensions. Other methods are better adapted to discretize two-dimensional and three-dimensional spatial coordinate systems for approximating differential equations. One of the oldest and most commonly used methods of numerical approximation is the finite difference method (FDM) [58]. In essence, the finite difference method is a direct conversion of the mathematical model's equations from continuous to discrete form, converting the entire problem into a system of linear equations that are solvable by matrix inversion [47].

A simple way of understanding FDM is by reviewing the discretization expansion of first-order and second-order differential terms, and visualizing how values at each point are calculated relative to the values at their closest neighboring points. To apply FDM, you must first define a uniform grid of spatial points, known as a mesh, with each point holding a sampled value of the continuous function (i.e. discretizing the function). In two dimensions, each sample is only dependent on its own value and the values of its

four nearest neighbors. Since the computational evaluation of each sample involves values at five total grid points, the relationship structure is known as the 5-point star "computational molecule", which can also be thought of as a numerical stencil [47].

We visualize these concepts through figure 7.1, with the left image depicting mesh points for the FDM grid and the right image depicting the computational molecule for the 5-point star. Indices i and j are integers which are intended to serve as matrix indices to keep track of positional relationships between points. Shorthand notation is used for the left image in figure 7.1 so that $\Phi(i, j) = \Phi(x_i, y_j)$. For this example, the continuous function being approximated is electric potential, Φ, in the two-dimensional xy-plane, with i denoting the horizontal (x-direction) index and j denoting the vertical (y-direction) index.

Now, we have a framework for approximating the derivative operators in the PNP equations (or any other continuum-based equations), using finite differences. The most

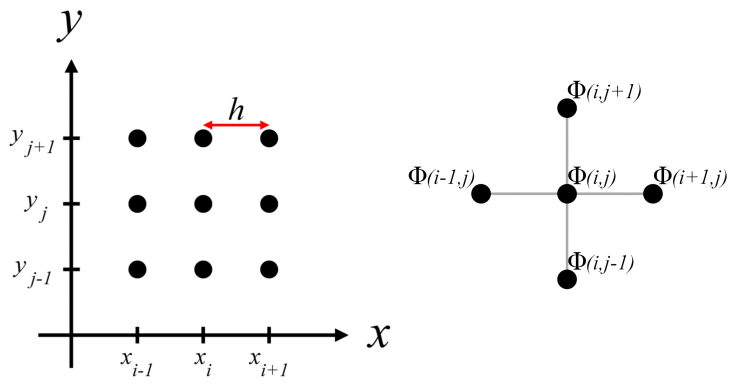

Figure 7.1: (Left) FDM grid, formed by discretizing the spatial domain into mesh points separated in the x and y directions by a uniform physical distance h. Coordinates are labeled using indices i and j to be used as matrix indices [47]. (Right) Computational molecule for the 5-point star, used to relate samples of a continuous parameter (here, electric potential, Φ) to each other for the purpose of approximating the differential profile (calculating the slope in each direction). Adapted from [47].

straightforward representations of first-order and second-order derivatives in finite difference form are as follows:

$$\frac{\partial}{\partial x}\Phi(i,j) \approx \frac{-\Phi(i,j)+\Phi(i+1,j)}{h} \tag{7.1}$$

$$\frac{\partial^2}{\partial x^2}\Phi(i,j) \approx \frac{\Phi(i-1,j)-2\Phi(i,j)+\Phi(i+1,j)}{h^2}. \tag{7.2}$$

Equation 7.1 is known as a two-point forward difference, and equation 7.2 is known as a three-point central difference. Similar expressions apply for the partial derivatives with respect to *y*.

Each differential operator in the PNP model's equations is translated into finite difference form, then re-arranged so the value at each point is expressed as a function of the values of its neighboring points (and boundary conditions, where applicable). Since each sample of the parameter (such as electric potential) is linearly dependent on the other samples in the five-point star, we can represent the solution over the whole system (all (*i,j*)) as a matrix-vector equation of the form $\mathbf{Ax} = \mathbf{b}$. Here, $\mathbf{x}$ is a vector containing all of the samples in the domain, and $\mathbf{A}$ is comprised of the linear relationships between the parameter samples [47].

Boundary conditions must also be discretized accurately so that mass, velocity, charge, etc. are conserved; constraints are critical for the accuracy of the long-term behavior of the solutions [43]. So, $\mathbf{b}$ is a vector that holds all of the discretized boundary condition information, such as fixed charge density. At last, the system's numerical solution using a finite-difference method is able to be obtained by solving $\mathbf{x} = \mathbf{A}^{-1}\mathbf{b}$ [47].

These concepts can be extended into a third dimension, which complicates the linear system, but follows the same principles. In three dimensions, the computation molecule needs two additional mesh points in the third dimension, and this stencil is known as the seven-point star [59].

7.2.3: Other Numerical Methods

Although it may seem complicated, the finite-difference method is fundamentally just a simplified form of another more complicated method known as the finite-element method (FEM). While FDM utilizes a fixed, rectangular mesh to discretize its domain, FEM requires a flexible, triangular mesh [47]. Clearly, the computational complexity is formidable, so most research groups wishing to use these methods primarily do so via a commercial software package, such as COMSOL, which can handle all of the computational tasks automatically in the background.

One last approximating method of solving continuum models such as the PNP equations that we will briefly mention is the finite volume method (FVM). As indicated by its name, FVM discretizes the domain into finite volumes. By explicitly considering the fluxes of each parameter through each finite volume, this method efficiently conserves mass [60]. We will not discuss this method in detail, but it is useful to think of FVM as a version of FDM that uses volume chunks instead of one-dimensional point samples.

Now that we have reviewed some of the most common methods for numerically simulating models such as the PNP equations, we have a better understanding of the general procedures they follow. Although in this research, we will not directly simulate nanofluidic diodes using the PNP model, we will take inspiration from the spatial domain discretization into matrix form utilized by FDM.

7.3: Modeling Electric Potential Profiles in a Nanofluidic Diode

The goal of forming an intuitive comprehension of nanofluidic diodes has served as a guiding compass for this research, and we will now depart from foundation-building and the review of existing simulation methods, in order to begin simulating a visual model of the fundamental theory. In this section, we will apply quantitative electrostatic and ion conductivity theory to see if we are able to demonstrate its mechanisms needed for ion rectification. If a simplified model can support the theory that has been solidified through experimentation and complex simulations by many other research groups, then we have credibly identified a fundamental basis for ion rectification in the system being modeled.

7.3.1: Motivation for Analyzing Electric Potential Profile: ICR Causal Chain

The approach we take in our fundamental physics-based modeling stems from our analysis of the causal chain that produces ion current rectification. In section 6.6, we explained how rectification is attributed to the ion accumulation and depletion regions

within the nanochannel under an externally applied voltage. The full flowchart of cause and effect can be summarized as follows:

1. For each ion species, asymmetrical electrostatic impact is stronger at one end of the nanochannel than the other due to asymmetry in the system structure/setup.
2. Each ion species forms regions of accumulation and depletion due to the nonuniform electrostatic impact, resulting in one nanochannel opening having higher concentration of that species than the other.
3. Conductivity is directly dependent on concentration, and ion current flux (under the same applied electric potential gradient) is greater in areas of higher concentration, so one opening will allow ions to flow through easier than the other opening.
4. Forward bias: When an ion species enters the nanochannel opening with higher conductivity and exits the opening with lower conductivity, the ion flux into the nanochannel is greater than the flux out of the nanochannel, resulting in channel-wide ion accumulation, further increasing conductivity and ion current flux.
5. Reverse bias: When an ion species enters the channel at the opening with lower conductivity and exits at the opening with higher conductivity, ion flux is greater out of the nanochannel than into the nanochannel, causing channel-wide ion depletion, consequentially lowering ion conductivity and repressing ion current flux.

For the simulation portion of this research, we aim to model the asymmetrical electrostatic impact, as it is the root cause of ion rectification in nanofluidic diodes. The subsequent causal chain relies on this electrostatic asymmetry in order to exist; it is

therefore prudent to model the system's electrostatic profile to verify if ion rectification is possible.

7.3.2: System to be Modeled and Equations to be Used

The electric field in a system requires vector quantities to model it, and this adds complexity to the simulation due to the necessity of vector addition. Therefore, we chose to represent the electrostatic profile using the scalar quantities of electric potential, so that the various electrostatic contributions are easily combined by scalar addition. In this investigation, we chose to model the electrostatic profile of a nanochannel with uniform charge and geometry that connects reservoirs of asymmetric ion concentration, which can be visualized in figure 4.3, repeated below.

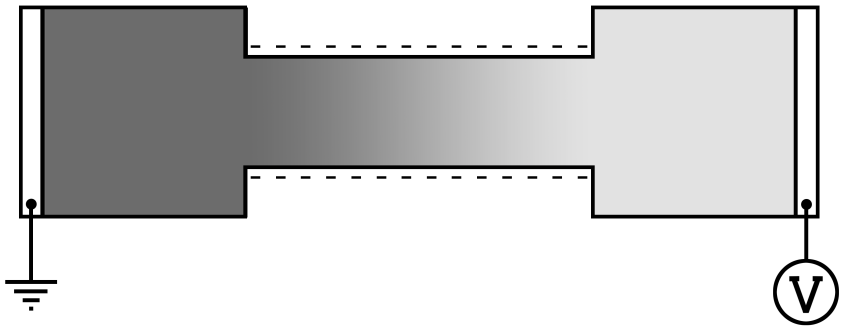

Figure 4.3: (repeated from chapter 4) Asymmetry in ion concentration. The left reservoir holds a high ion concentration, while the right holds a low ion concentration. The shade gradient across the channel corresponds to the resulting concentration gradient between the two reservoirs.

The equations we use are derived from the Guoy-Chapman model of EDL in nanofluidics, which we discussed in detail in section 5.4, and are given by equations 5.14, 5.15, and 5.16, repeated below for convenience:

$$\Phi(x) = \Phi_s e^{-\kappa x} \tag{5.14}$$

$$\lambda_D = \kappa^{-1} = \sqrt{\frac{\varepsilon k_B T}{2q^2 n_\infty}} \tag{5.15}$$

$$\sigma_{\mathbf{s}} = \sqrt{8\varepsilon n_\infty k_B T}\sinh\left(\frac{q\Phi_{\mathbf{s}}}{2k_B T}\right). \tag{5.16}$$

Recall that equation 5.14 is the Debye-Hückel approximation of the Poisson-Boltzmann equation, and it describes the electric potential at a perpendicular distance x from the charged surface (nanochannel wall). The potential demonstrates an exponential decay as x increases that is characterized by κ. The inverse of κ is known as the Debye screening length, and is related to system properties through equation 5.15. Finally, equation 5.16 – the Grahame equation – can be used to find the surface potential, Φ_s, if the surface charge density is known. Solving the Grahame equation, equation 5.16, for Φ_s, we obtain

$$\Phi_{\mathbf{s}} = \frac{2k_B T}{q}\sinh^{-1}\left(\frac{\sigma_{\mathbf{s}}}{\sqrt{8\varepsilon n_\infty k_B T}}\right). \tag{7.1}$$

The simulation we will present uses equations 5.14, 5.15, and 7.1 to model the electric potential profile in the system depicted in figure 4.3. A true nanofluidic diode is three-dimensional, but simulating in two dimensions instead of three is far more efficient, yet still valid, since the system is assumed to be radially symmetric around the central axis of the nanochannel. Therefore, we will model a two-dimensional length-wise cross-section of the system to simplify our procedure.

7.3.3: Description of the Simulation Algorithm

The software we use to code the simulation program is MATLAB R2019a. This section is focused on explaining the logical steps carried out by the simulation, using the language of the written code. The complete MATLAB code can be found in the Appendix.

Since we want to perform a numerical simulation that calculates values of electric potential throughout the system, we must discretize the system's domain. We will do so by creating a two-dimensional matrix that contains the spatial coordinates at each sampling point on the computational grid (mesh). Initializing the mesh requires creating constants for the length and width of the nanochannel, as well as the length of the reservoirs.

We present a visualization of the computational domain in figure 7.2, including the coordinate system. The origin of the *xy*-plane is located at the top left corner of the channel in the diagram, the positive *y*-direction is horizontal to the right (parallel to the length of the channel), and the positive *x*-direction is vertical downward (parallel to the width of the channel).

In addition to the spatial dimensions of the system, we must choose the number of points we wish to sample in the *x* and *y* directions to form a matrix. To maintain consistency between our diagrams and our MATLAB program, we consider the number of rows in the matrix to be in the *x*-direction, and the number of columns to be in the *y*-direction. We call these parameters Nx and Ny, respectively. Using the "linspace"

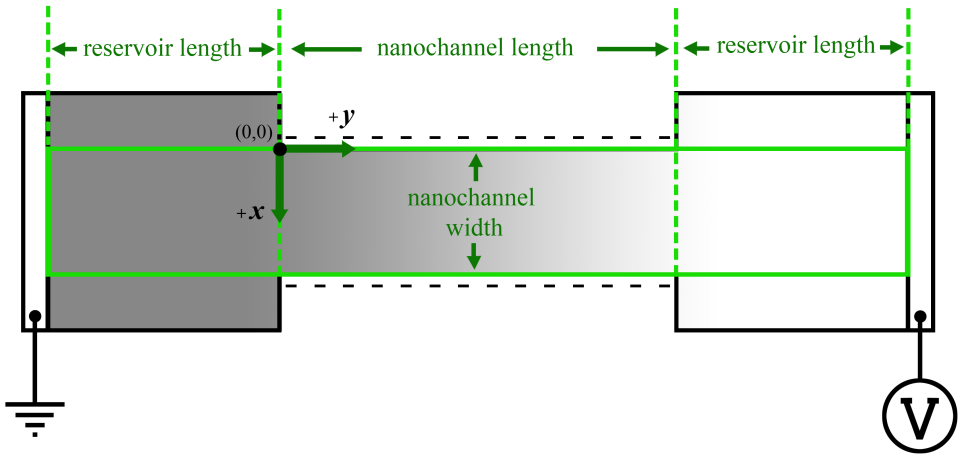

Figure 7.2: Diagram of the computational domain for simulating the electric potential, which is overlaid on the nanofluidic diode of asymmetrical ion concentration, as depicted in figure 4.3. The computational boundaries are outlined in solid green lines, with dotted green lines denoting the regions of the system.

MATLAB function, we create a vector, y_vec, that contains an Ny amount of evenly-spaced numbers between 0 and the length of the nanochannel, and another vector x_vec, that contains an Nx amount of evenly-spaced numbers between 0 and the width/diameter of the nanochannel. To account for the reservoirs, we similarly create vectors ry_vec and rx_vec, the former containing an Nry amount of evenly-spaced numbers between 0 and the reservoir length, and the latter being equivalent to x_vec. To place the reservoirs appropriately in the coordinate plane, we use a "for loop" that takes two copies of ry_vec and creates ry_vec_left and ry_vec_right. The for loop subtracts the reservoir length from every element in ry_vec_left, and adds the channel length to every element in ry_vec_right, so the *y*-coordinates of the left and right reservoirs are accurately described. Once this is done, we create yfull_vec, which concatenates ry_vec_left, y_vec, and

ry_vec_right to describe the full range of *y*-values in the mesh. This completes the spatial initialization.

Next, we create the electric potential profiles that are contributed to only by the applied potential difference. We create three versions, using the suffix "_e" for equilibrium, "_f" for forward bias, and "_r" for reverse bias. The left reservoir voltage is always grounded at Vl = 0. The following explanation will apply for forward bias, but the exact same procedure is used for equilibrium and reverse bias, with the only difference being that Vr = 0 for equilibrium, Vr = 1 for forward bias, and Vr = -1 for reverse bias.

To represent the potential gradient across the channel due to the applied bias, we use the linspace function to assign an Ny amount of evenly-spaced voltage values across the length of the nanochannel, from Vl to Vr, and the resulting vector is named Vay. To complete a two-dimensional matrix profile, we run a for loop that enters Vay as the columns in a Nx-by-Ny matrix named Va_f (_f for forward bias). A similar process is used to create a uniform electric potential profile in each reservoir: Vrl_f for the left reservoir, and Vrr_f for the right reservoir.

An approximate ion concentration profile must also be created to describe how the bulk ion concentration (n_∞ – the number concentration of ions existing absent the effects of the fixed wall charge) changes along the nanochannel connecting the reservoirs. The left reservoir contains a concentration cl, while the right contains cr, and a simplifying assumption we used when plotting the Debye length in figure 5.2 is that the concentration profile has a constant slope, changing uniformly from one concentration to

the other [11, 50]. The coding procedure is identical to how we initialized the electric potential gradient – first creating a vector Cy using linspace to assign a concentration value to every mesh point in the *y*-direction (from cl to cr with Ny entries), then running a for loop to create the two-dimensional matrix, C, that has Nx identical rows, each containing the vector Cy. The left and right reservoirs are given uniform concentration profiles as matrices Crl and Crr (both are Nx-by-Nry in dimension) with all entries containing cl and cr, respectively.

All initializations are complete, and the next step is the calculations. We assign all of the constants in equation 5.15 (the Debye length equation) with appropriate values. Then we perform the calculation of equation 5.15, using element-wise operations, on the vector Cy to create a vector named 'debye'. 'Debye' is a vector with Ny entries that contains the Debye screening length at each *y*-coordinate along the *y*-direction of the nanochannel, and is not uniform due to the ion concentration gradient along the channel.

The last calculations before plotting utilize equations 5.14 and 7.1 (the Deby-Hückel approximation, and the conductivity equation, respectively). The fixed wall charge density is defined as a constant, and since it is uniform for the system to be modeled, we create a vector Qy with Ny equivalent entries of that value of charge density. Performing element-wise operations, we create a vector Vs (also with Ny elements) that uses equation 7.1 to calculate the surface potential at every *y*-coordinate along the nanochannel. It is an element-wise calculation so that it can use the pre-defined

values of wall charge density and bulk ion concentration at each coordinate in the *y*-direction.

Finally, in a for loop, we apply the Debye-Hückel theorem (equation 5.14) to calculate the electric potential profile in the *x*-direction, Vq1, due to the horizontal charged nanochannel wall at $x = 0$. This for loop iterates through each *y* index (Ny total), substituting in the surface potential at each index from the Vs vector, and using element-wise operations to substitute each *x*-coordinate of x_vec to create column vectors that exhibit the potential decay at each *y*-coordinate. Since the electric potential profile induced by the bottom wall is just a mirrored version of the profile induced by the top wall, we use the "flip" function to create Vq2, which is identical to Vq1 but has all of its column vectors inverted.

The final step before plotting is to create the full electric potential profiles. Using two nested "for loops", we iterate through every (*x*,*y*) coordinate pair and add the scalar quantities of electric potential at each point. We create three Nx-by-Ny matrices: 1) Vtot_e that adds the potential contributions from Vq1, Vq2 (electric potential due to the fixed wall charges), and Va_e (electric potential due to the equilibrium applied bias); 2) Vtot_f that adds Vq1, Vq2, and Va_f (electric potential due to the forward applied bias); and 3) Vtot_r that adds Vq1, Vq2, and Va_r (electric potential due to the reverse applied bias). Vfull_e, Vfull_f, and Vfull_r are defined to concatenate Vrl_e, Vtot_e, and Vrr_e, Vrl_f, Vtot_f, and Vrr_f, and Vrl_r, Vtot_r, and Vrr_r, respectively. To create the graphs that plot these electric potential profiles, we use the meshgrid and mesh functions, in

order to plot Vfull_e, Vfull_f, and Vfull_r as surfaces in *x*-*y* space (with appropriate coordinates using yfull_vec and x_vec for the full system including reservoirs).

7.3.4: Results and Discussion

The MATLAB program we created maps out an approximation of the electric potential throughout the nanofluidic diode. It does so by calculating the surface potential (via equation 7.1, the Grahame equation) and the Debye length (via equation 5.15), which both change as a function of ion concentration along the length of the channel, in the *y*-direction. Then, through the Debye-Hückel approximation (equation 5.14), the electric potential profile in the *x*-direction is determined for each *y*-coordinate.

There are several approaches we could take to analyzing the results, such as changing the parameters to see how it affects the outcome, but for this research, we will mainly focus on the predicted behavior and how it depicts the theory we have developed.

The parameters we use are: a channel length of 10 μm, a channel width/diameter of 20 nm, a reservoir length of 1 μm, a left reservoir concentration of 10 mM (~6.022 $\times 10^{24}$ ions/m^3 of each ion species), a right reservoir concentration of 0.1 mM (~6.022 $\times 10^{22}$ ions/m^3 of each ion species), the left electrode fixed at 0 V (grounded), the right electrode given a forward/reverse bias applied voltage of +1/–1 V, and a uniform wall charge density of -5×10^{-2} C/m^2. The electrolyte is KCl in aqueous solution. The number of grid points in the *x*-direction is 200 (Nx = 200), along the channel length in the *y*-

direction it is 1000 (Ny = 1000), and each reservoir length has 100 grid points in the *y*-direction (Nry = 100).

We will now present the results of our electric potential profile simulation, for which we performed calculations using the Debye length equation (equation 5.15), the surface potential equation (equation 7.1), and the Debye-Hückel approximation (equation 5.14), to model electric potential at evenly-spaced grid points throughout the nanochannel. Running the simulation produces one figure containing three surface plots, and we present several perspectives of them in figures 7.3, 7.4, 7.5, 7.6, and 7.7.

The coloration of the surfaces indicate the "height" of the plotted surface (its values in the *z*-direction, which represents electric potential); in this case, yellower hues correspond to higher electric potentials (greater *z*-axis coordinates), while bluer hues correspond to lower electric potentials (lower *z*-axis coordinates). The *x*-axis and *y*-axis correspond to the width/diameter and length of the channel, respectively, and are labeled in nanometers and micrometers, respectively.

7.3

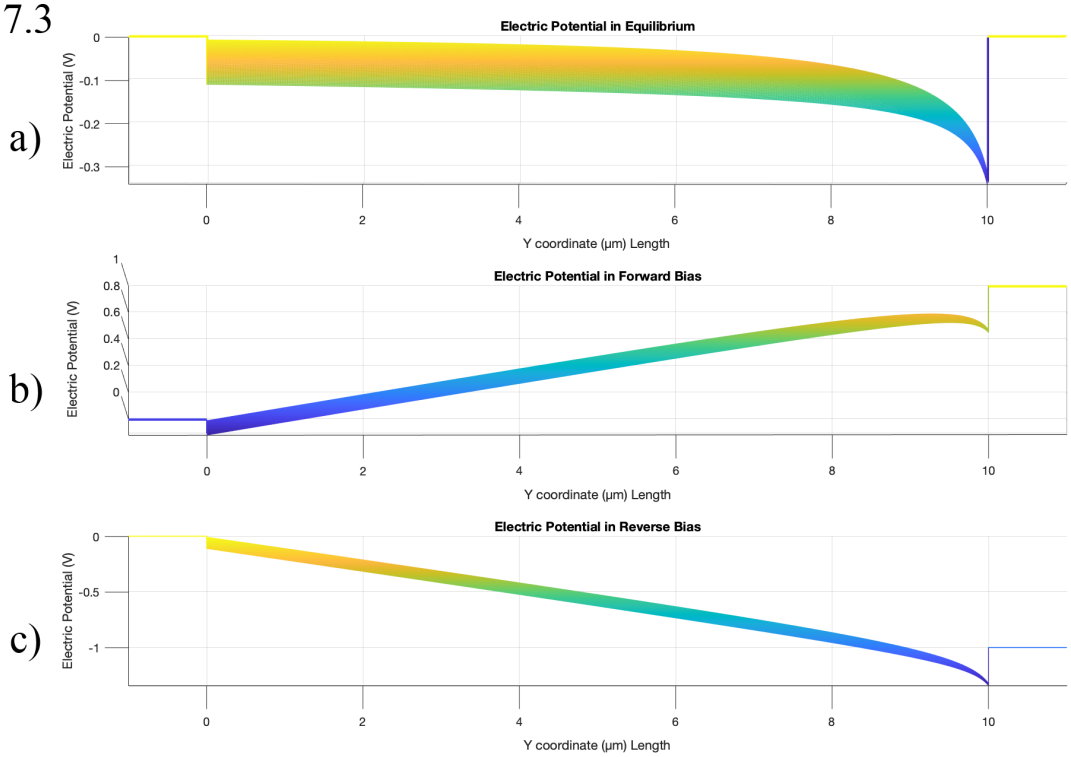

Figure 7.3: Simulation results of electric potential in a homogeneous nanochannel between reservoirs of different ion concentration, viewing the full *y*-axis, which is along the length of the nanochannel. The electric potential profile is shown in (a) equilibrium; (b) forward bias; (c) reverse bias.

7.4

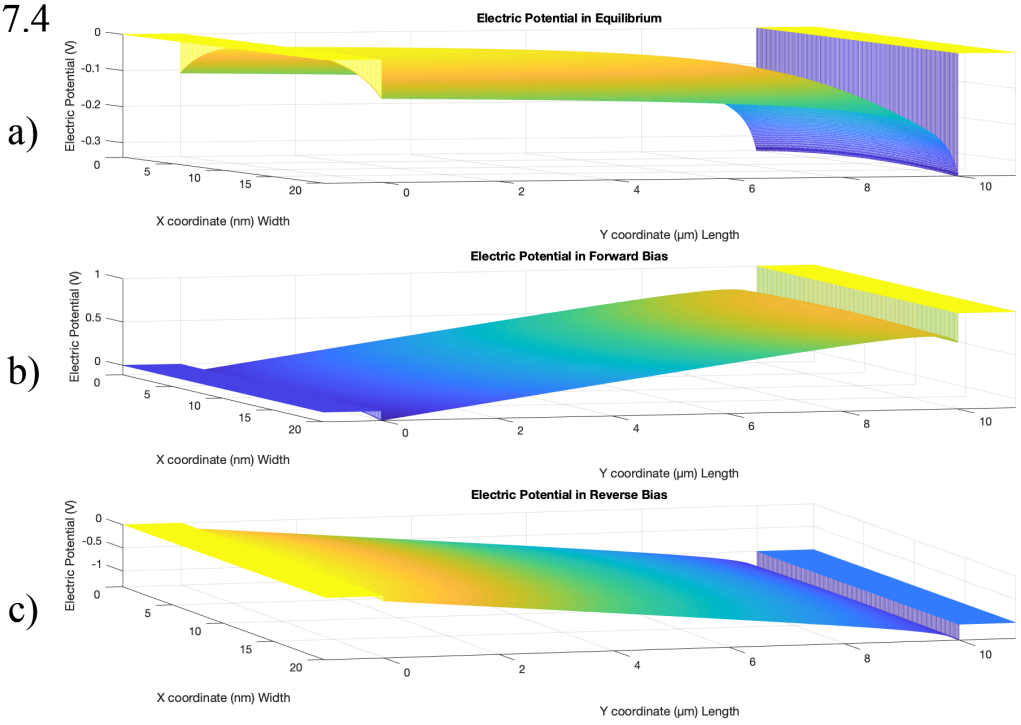

Figure 7.4: Simulation results of electric potential in a homogeneous nanochannel between reservoirs of different ion concentration, viewed from a skewed angle. (a) Equilibrium; (b) forward bias; (c) reverse bias.

7.5

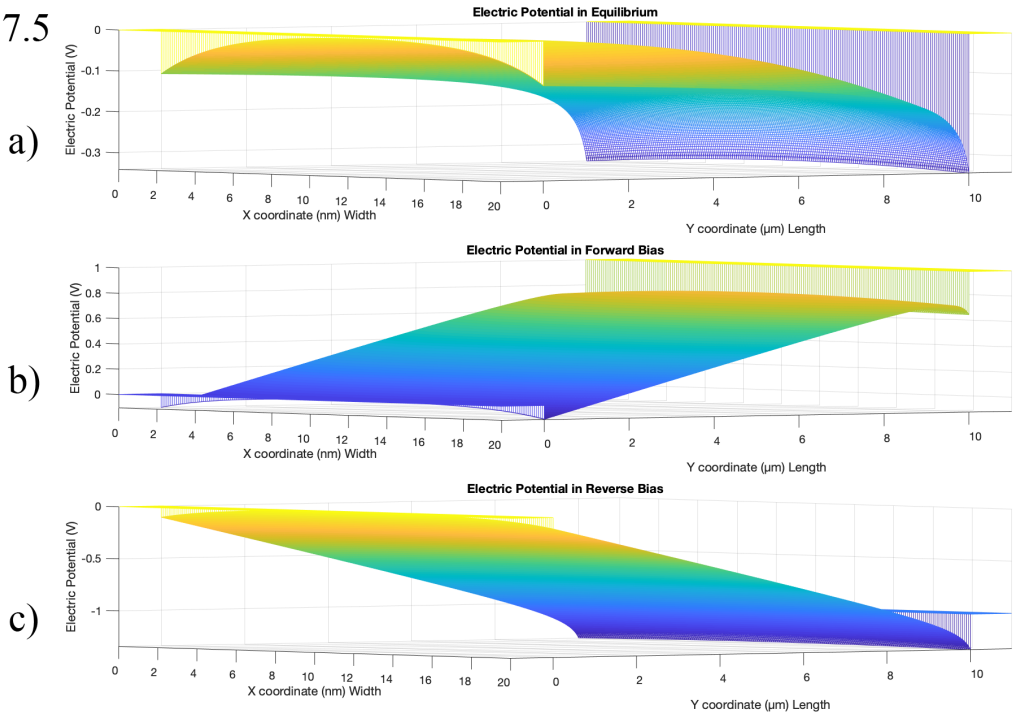

Figure 7.5: Simulation results of electric potential in a homogeneous nanochannel between reservoirs of different ion concentration, with a clear perspective of the *x*-axis (width/diameter of channel). (a) Equilibrium; (b) forward bias; (c) reverse bias.

7.6

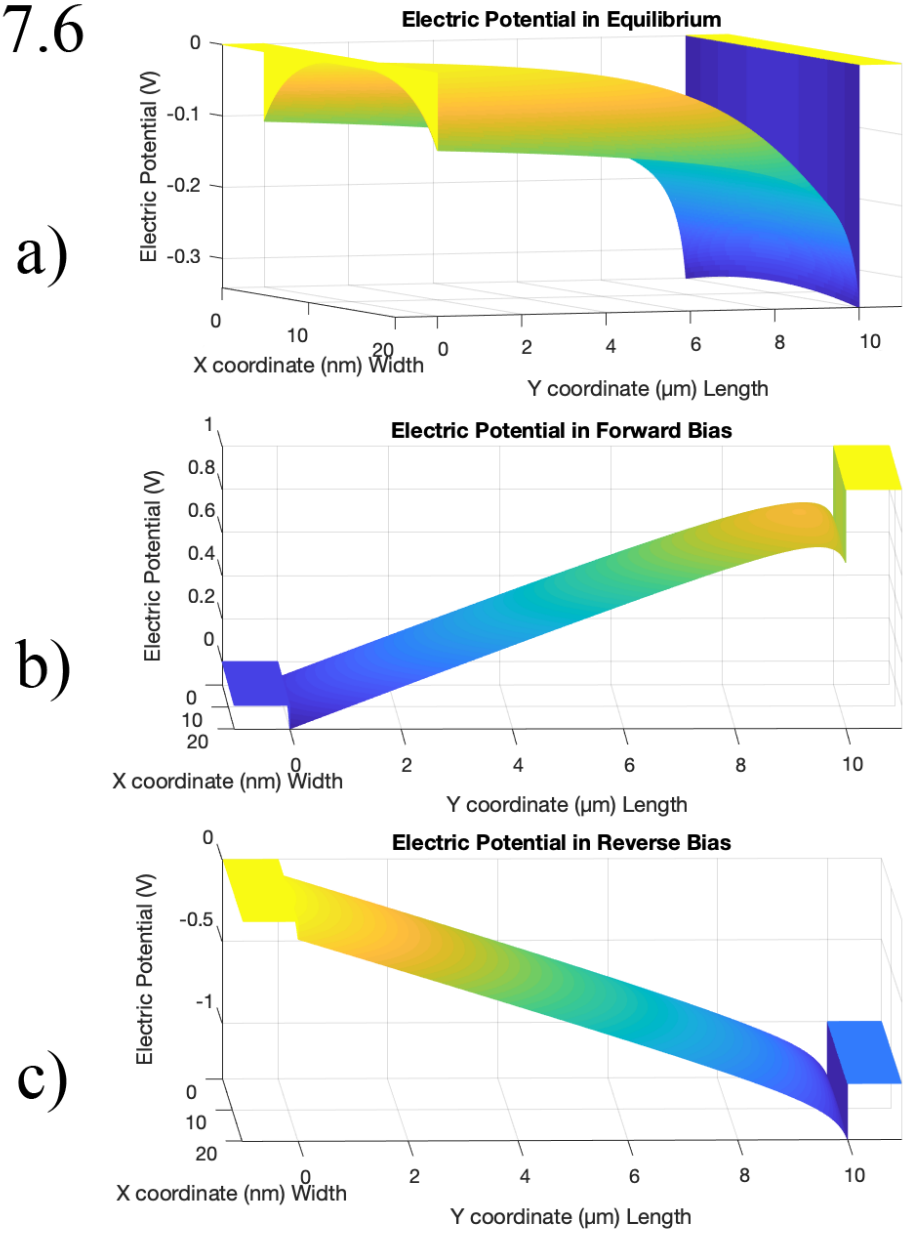

Figure 7.6: Simulation results of electric potential in a homogeneous nanochannel between reservoirs of different ion concentration, viewed at angles and compressed axes which best show the potential trough at y = 10 μm. (a) Equilibrium; (b) forward bias; (c) reverse bias.

7.7

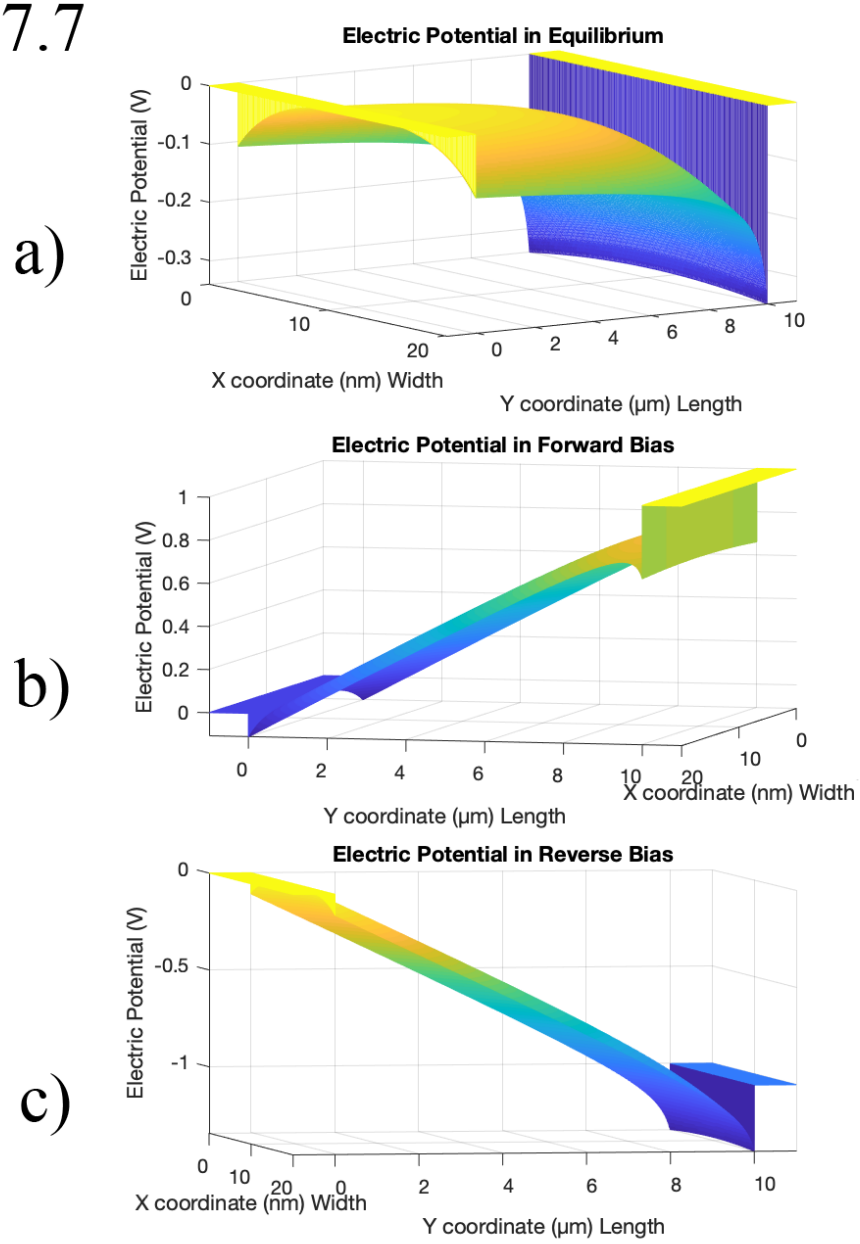

Figure 7.7: Simulation results of electric potential in a homogeneous nanochannel between reservoirs of different ion concentration, viewed at angles and compressed axes which best show the curvature along the walls at $x = 0$ nm and $x = 20$ nm. (a) Equilibrium; (b) forward bias; (c) reverse bias.

We present our results using figures 7.3, 7.4, 7.5, 7.6 and 7.7 to show various perspectives of the calculated electric potential profile. In each of these figures, we present the electric potential due to the uniform fixed charge and the applied voltage in the (a) equilibrium, (b) forward bias, and (c) reverse bias states of an asymmetric ion concentration type of nanofluidic diode.

Figure 7.3 depicts a length-wise view, where the reservoir of higher concentration corresponds to the left, and the reservoir of lower concentration is on the right. Figure 7.4 and figure 7.5 depict angled views, both with the reservoir of high concentration angled closer and the angle of low concentration reservoir angled farther away from the perspective. Figures 7.6 and 7.7 have compressed axes compared to figures 7.3-7.5, but they are able to better illustrate certain features of the electric potential profile. Figure 7.6 most clearly depicts the region around y = 10 nm, which is of interest to our following analysis. Figure 7.7 most clearly depicts the downward curvature of the electric potential at x = 0 nm and x = 20 nm, which are the locations of the charged channel walls.

7.3.4a: Analysis

These surface plots of electric potential throughout the nanofluidic diode can give us valuable insight. The forces experienced by cations and anions are due to their charges interacting with the electric field in the system, which we recall is related to the electric potential expressed by equation 5.4, repeated below:

$$\mathbf{E} = -\nabla\Phi. \qquad \textbf{(5.4)}$$

For the behavior analysis, we will also use equations 5.46 and 5.48, repeated below, which describe current density and conductivity, respectively. We will not be performing explicit calculations with them, but they will facilitate our discussion of the simulation results because they show the relationships between parameters.

$$\mathbf{J} = -\sigma \nabla \Phi \tag{5.46}$$

$$\sigma_i = \frac{q_e^2 z_i n_i}{6\pi \eta r_i}. \tag{5.48}$$

Equation 5.46 allows us to interpret cation or anion current flux, **J**, under the influence of a nonuniform electric potential. The negative sign before the gradient of the electric potential in equation 5.4 and equation 5.46 tells us that cations will be "pulled" down the slope of the surfaces depicted in figures 7.3-7.7 in a similar way a ball would roll down a hill, while anions will be pulled up the slope.

In plot (a) of each figure, where applied voltage is zero on both sides of the channel and the system is in equilibrium, we observe that the electric potential exhibits a strong "dip" near the opening of the channel at y = 10 μm, facing the reservoir of low ion concentration, which is on the right side. Figure 7.6 most clearly depicts this characteristic. This aligns with our understanding of the Debye length, since the screening length is longer in solutions of lower ion concentration. A longer screening length means that the electric potential induced by the wall charge decays at a slower exponential rate. So, our results illustrate our theory since the electric potential is lower (due to negative wall charge) over a longer distance where the ion concentration is lower.

The "dip" forms a "trench" or "trough" at $y = 10$ μm when either forward or reverse bias is applied (plots (b) and (c), respectively, in each figure). This is because the electric potential is larger in the reservoir of low ion concentration ($y > 10$ μm) than it is just inside the nanochannel opening (at $y = 10$ μm), where contributions from the fixed wall charge decrease the total electric potential the most significantly. This phenomenon is most clearly seen in (b) and (c) of figure 7.6,

The "trench" is more pronounced when comparing it to the opposite channel opening at $y = 0$. The electric potential in the reservoir containing higher ion concentration ($y < 0$) and in the closest opening of the channel (at $y = 0$) do not show as much of a difference in magnitude, which can most clearly be seen in figure 7.3. In fact, at the center of the channel's width (at $x = 10$ nm), the electric potential profile appears to have only a minuscule change. Examining figure 7.3, the top of the plotted surface, where the electric potential is highest, is nearly smooth in transition across the $y = 0$ axis. Comparing this to figure 7.5, we notice that the maximum value of electric potential is at the center of the channel's width, at $x = 10$ nm. This is because the electric potential contributed by the negative wall charge is screened out very rapidly (due to a smaller Debye length), and the center of the channel feels very little influence from the wall charge as a result. The symmetry in the system is the cause of the centralized maximum, with lower potential at the charged walls, where $x = 0$ nm and $x = 20$ nm.

This leads us to discuss the EDL that form in the system, particularly along $x = 0$ nm and $x = 20$ nm. These axes are the locations of the interface with the solid, charged

walls of the nanochannel, and the solid substrate that forms the confinements of the fluid extends beyond $x < 0$ nm and $x > 20$ nm. Because the fixed wall charge is negative, the EDL will be enriched with cations. So, if we picture the surfaces from our simulation as physical solid surfaces, we can imagine cations as small marbles, which will move down the gradients of the surface. Cations will cluster close to the walls of the nanochannel (at $x = 0$ and $x = 20$ nm), as well as at the right opening of the nanochannel (at $y = 10$ μm). The clearest depiction of the electric potential curvature near the walls is in figure 7.7a, but all of the figures show the curvature to varying degrees. Visualizing where the cations in the system would accumulate allows us to picture the EDL that form in the nanochannel, which assists our conceptual understanding of ion behavior.

The most important conclusion from considering cation accumulation is the way it impacts ion current conductivity. From equation 5.48, we know that higher concentrations of an ion species causes an increase in the conductivity for that species, so cation conductivity is increased at the right opening of the nanochannel. From equation 5.46, we know that the resulting ion current flux is greater when the conductivity is higher.

Analyzing the cases of forward bias and reverse bias, we can see that in forward bias, cations accumulate at the opening of the channel that they enter (which is at $y = 10$ μm; see 7.6b for a good perspective of the accumulation trench at the higher potential, where cations enter), resulting in a greater cation flux entering the channel compared to exiting. Conversely, in reverse bias, cations accumulate at the opening of the channel that

they exit from (at $y = 0$ μm, see 7.6c for a good perspective of the accumulation trench at the lower potential, where cations exit), so the cation flux out of the channel is greater than the cation flux into the channel.

Extrapolating forward in time, we can logically make the connection that applying a forward bias increases the overall accumulation of cations in the channel, while applying a reverse bias depletes cations from the channel. Although this is not directly visually apparent in figures 7.3-7.7, and requires conceptualizing the causal chain we discussed in section 7.3.1, we were able to connect the visible trends of electric potential to ion concentration. We then used our conductivity equation (equation 5.48) to interpret this accumulation as higher ion current conductance, which brings us to the final conclusion through the ion current flux equation (equation 5.46) that applying forward bias results in higher ion current than applying reverse bias in this type of nanofluidic diode.

7.3.4b: Simplifications and Weaknesses

In our effort to create a fundamental model that explains ICR, we have made several significant simplifications that are important to acknowledge. We have already mentioned the simplifying assumption of the uniform slope of the concentration gradient along the nanochannel, but we should also interpret its implications for our simulation results.

In a study of the exclusion-enrichment effect (EEE) in a negatively charged nanoslit (a wide rectangular nanochannel with a short height) between reservoirs of different ion concentration, Plecis, Schoch and Renaud interpret the concentration profile as a linear transition between the two concentration baths, but only for noninteracting diffusing species [50]. In the presence of a negative wall charge, the counter-ion concentration gradient has larger values and a steeper slope, while the co-ion concentration gradient has lower values and a less steep slope, compared to the linear transition between reservoirs. This is in accordance with and follows logically from the EEE.

Because we use the simple linear transition as our ion concentration gradient, we effectively neglect the EEE in our system setup. Therefore, the best interpretation of the system we modeled is if an uncharged nanochannel connecting reservoirs of different ion concentration is suddenly given a uniform fixed wall charge. Figures 7.3, 7.4 and 7.5 thus describe the electrostatic profile that forms at the instant the nanochannel walls are embedded with a uniform negative charge density, before ion fluxes from the potential gradient change the concentration profiles.

Another simplification that impacts our simulation's accuracy is the assumptions we make about the electric potential around the two openings of the nanochannel. To give perspective to the electrostatic profile in the nanochannel, we included the reservoirs as featuring uniform electric potentials equal to the voltage applied to the electrode in that reservoir. In reality, the negative fixed wall charge in the openings of the nanochannel

will induce some fringing effects that extend into the reservoir close to the opening. In a similar sense, the edge of the surface charge density is not accounted for within the nanochannel close to the openings. The Grahame equation best describes the electric potential decay perpendicular to the surface when the surface charge density extends to infinity in both directions. If we conceptually consider the finite end of the wall charge density, we can interpret from our understanding of electric fields that the electric potential would not have the sharp discontinuity seen in figures 7.3, 7.4 and 7.5. We can conclude that a model which accounts for the electrostatic impact of fringing effects would exhibit a smoother and less severe transition in electric potential between reservoir and channel. In other words, discontinuities at the two interfaces between channel and reservoir would be smoother, less angular, and less deep, most notably for the "trench" at $y = 10$ μm.

7.4.3c: Conclusions of Simulation Effectiveness

Through the analysis and interpretations of our simulation results, we can conclude that there is strong agreement between our developed nanofluidic ICR theory and the behavior suggested by our models of electric potential profiles. Our results also agree qualitatively with PNP-based simulations of a similar nanofluidic diode presented by Cheng and Guo [11]. Both the PNP model and our simplified model based on the Guoy-Chapman theory predict that in equilibrium, the nanochannel opening facing the reservoir of lower ion concentration has a larger dip in electric potential than the opening

facing the reservoir of greater ion concentration. Both models indicate asymmetrical EDL overlap and asymmetrical electrostatic impact, which are necessary characteristics for ICR. Therefore, we conclude that our model and simulation demonstrate the source of ion current rectification in a homogeneous nanochannel connecting reservoirs of asymmetric ion concentration.

CHAPTER 8

Conclusions, Reflections, and Future Works

8.1: Conclusions

In this research, we developed a cohesive theory that describes how ion current rectification (ICR) is exhibited by nanofluidic diodes. Three main types of nanofluidic diodes were focused on, which are formed by: asymmetry in fixed wall charge, asymmetry in ion concentration, and asymmetry in channel diameter. Our main goal was to clarify the research field's inconsistencies and complexities by creating a comprehensive review of nanofluidic diodes from an electrical engineering standpoint. Our secondary goal was to use this theory to simulate the electric potential profile in a nanofluidic diode of asymmetrical ion concentration, the interpretation of which helped to visualize the asymmetrical electrostatic impact necessary for ICR.

Through fundamental electrostatic physics relationships, we defined and explained major sources of ion movement, with the primary sources being that of electrostatic forces and diffusion. This supported our discussion of more complex models and concepts, such as electric double layers (EDL) and the Poisson-Nernst-Planck (PNP) equations. We discussed how electrophoresis usually has the most influential effect on total ion current in nanofluidic diodes, while electroosmotic and diffusive contributions are normally much smaller. This led to the molecular-level approach that we took to analyze ion transport in the different types of nanofluidic diodes. We concluded that asymmetric electrostatic impact is the foundational requirement for ion current rectification to occur,

and extrapolating ion flow trends from electrokinetics by using the second term in the Nernst-Planck equation is sufficient to explain ion current rectification.

As a visualization of some of the key theoretical findings, we wrote a MATLAB program that numerically calculates the electric potential at evenly-spaced grid points across a two-dimensional representation of a nanofluidic diode of asymmetrical ion concentration. We first calculate the Debye length from the varying ion concentration values along the length of the channel, then we use the Grahame equation to relate a given surface charge density to its surface potential. Substituting the surface potential and the Debye length into the Poisson-Boltzmann equation, we can numerically estimate the electric potential profile along points perpendicular to the channel walls at each point along the length of the system. The scalar contributions of electric potential from both sides of the channel are added, and any externally applied electric potential can be added as well to complete the profile.

The electric potential simulation we developed produces three-dimensional surface plots of electric potential throughout a nanofluidic diode of asymmetrical ion concentration when the device is in equilibrium, forward bias, and reverse bias. Through the result of our numerical simulations, we observed that the electric potential forms a "trench" at the nanochannel opening at the opening of the nanochannel on the side of lower ion concentration. The location of the trench was the same regardless of the externally applied voltage. Analyzing the ion flow trends using our developed electrokinetic theory, we determined that the trench will accumulate counter-ions and become a region

of high conductivity for ion current, since counter-ions are the majority charge carriers in nanofluidic diodes.

This region of higher ion current conductivity remains at the same nanochannel opening regardless of voltage polarity, but the direction of ion flow reverses when applied voltage polarity switches. Forward bias causes higher cation current into the channel than out of, increasing conductivity throughout the channel and promoting high ion current. Reverse bias causes higher cation current out of the channel than into the channel, decreasing conductivity and repressing ion current. This demonstrates the requirements for ion current rectification in the nanofluidic system, showing that the causal chain constructs itself given a systemic electrostatic asymmetry.

The causal chain is as follows:

1. For each ion species, asymmetrical electrostatic impact is stronger at one end of the nanochannel than the other due to asymmetry in the system structure/setup.
2. Each ion species forms regions of accumulation and depletion due to the non-uniform electrostatic impact, resulting in one nanochannel opening having higher concentration of that species than the other.
3. Conductivity is directly dependent on concentration, and ion current flux (under the same applied electric potential gradient) is greater in areas of higher concentration, so one opening will allow ions to flow through easier than the other opening.

4. Forward bias: When an ion species enters the nanochannel opening with higher conductivity and exits the opening with lower conductivity, the ion flux into the nanochannel is greater than the flux out of the nanochannel, resulting in channel-wide ion accumulation, further increasing conductivity and ion current flux.
5. Reverse bias: When an ion species enters the channel at the opening with lower conductivity and exits at the opening with higher conductivity, ion flux is greater out of the nanochannel than into the nanochannel, causing channel-wide ion depletion, consequentially lowering ion conductivity and repressing ion current flux.

Since it is the culmination of our theoretical investigation into ion current rectification in nanofluidic diodes, this causal chain succinctly describes the necessary processes for nanofluidic diode function. In a sense, it is a main conclusion of this research, as all of the theory we developed and clarified gives foundational evidence to this ICR causal chain's veracity.

8.2: Reflections and Future Works

Through compiling knowledge of fundamental nanofluidics and researching nanofluidic diodes, it became clear that there are no limits to the possible routes of focus or the depth of any one topic in the field. As is common with any research subject, we found that what initially appeared to be straightforward concepts would expand once we delved into them. However, for a subject as multidisciplinary as nanofluidic diodes are, obtaining a comprehensive understanding of any one topic – such as the formation of

electric double layers – required diligent review and study of many different descriptions and perspectives to grasp the big picture. So inevitably, there is more work that could be done to build on the research we have presented in this thesis.

The most direct and natural next step would be to apply the theoretical modeling method introduced in section 7.3.3 to the two other types of nanofluidic diodes we analyzed: asymmetry in fixed wall charge and asymmetry in channel diameter. It would be very interesting to see the electric potential profiles as surface plots for those different systems, and be able to compare and contrast characteristics and trends between them.

A more distant step would be to fully numerically simulate the PNP equations or even the PNP-NS equations, as we originally conceived. As we have described, the PNP equations are limited to describing electrophoretic (drift) and diffusion components of ion transport, but the PNP-NS equations include fluid dynamics considerations such as fluid momentum (electroosmosis). This type of model simulation would need to be done via a commercial software package, such as COMSOL, which would handle the computational finite-element method or finite-difference method, so that the primary focus could be on manipulating parameters to see how the predicted transport properties are affected. However, correctly and meticulously setting up the correct equations and boundary conditions is vital. There would still be a significant learning curve for those who are inexperienced with the software or numerical simulations in general. However, an intuitive understanding of the systems under investigation is crucial for such simulations, especially for making simplifications, modifications, and forming interpretations of the results. So in any

case, the theory compiled in this research provides a very useful first step towards that goal.

Perhaps an option beyond the fundamental electric potential simulation but not as large of a reach in software complexity would be to perform a modified iterative algorithm (possibly similar to the Gummel iteration method) that adds more components of the PNP model to our model for electric potential. If the concentration profile could be updated using predictions from the electric potential that indicate how ions would move over time, there could be some interesting results that give insight into the mechanisms at work. The PNP model has been tested and validated to be qualitatively accurate by many research groups. Therefore, its proven accuracy in predicting ion transport characteristics in nanofluidic systems make it a logical choice to pursue further in any future work.

APPENDIX

MATLAB Code for Electric Potential Simulation

```
%Electric Potential In Nanofluidic Diode
%Author: Julia Proctor
%Completed June 2021
clear; clc; close all;

%% PARAMETERS

L = 10e-6; %channel length (m)
D = 20e-9; %channel diameter (m)
RL = 1e-6; %length and width of reservoirs (m)
cl = 10*10^-3*(1000*6.022e23); %high (10 mM) left reservoir ion concentration of each
species (ions/m^3)
cr = 0.1*10^-3*(1000*6.022e23); %low (0.1 mM) right reservoir ion concentration of
each species (ions/m^3)
Q = -5e-2; %fixed charge density on wall (C/m^2)
Vl = 0; %left electrode applied potential (V) --always grounded
Vr = 1; %right electrode applied potential (V) --applied potential

%% SPATIAL INITIALIZING
%Discretize area

%%Channel
%y (length-direction)
Ny = 1000; %Number of gridlines along y (1D)
y_vec = linspace(0, L, Ny); %y direction coordinates for channel

%x (width/diameter-direction)
Nx = 200; %Number of gridlines along x (1D)
x_vec = linspace(0, D, Nx); %x direction coordinates for channel

%%Reservoirs
%y (length-direction)
Nry = 100; %number of gridlines in reservoir along y (1D)
ry_vec = linspace(0, RL, Nry); %y direction coordinates for reservoir

%x (width/diameter-direction)
```

```
Nrx = Nx; %number of gridlines in reservoir along x (1D)
rx_vec = linspace(0, D, Nrx); %x direction coordinates for reservoir (same as channel)

%making 2 copies of the reservoir
ry_vec_left = ry_vec;  %left reservoir
ry_vec_right = ry_vec; %right reservoir
%calibrating y coordinates to allow joining of reservoir grids with channel grid
 for i = 1:Nry
    ry_vec_left(i) = ry_vec(i) - RL;
    ry_vec_right(i) = ry_vec(i) + L;
 end
%concatenating for full y-direction coordinates computational domain
yfull_vec = [ry_vec_left y_vec ry_vec_right];

%% POTENTIAL INITIALIZING

%Equilibrium (_e)
Vr = 0; %equilibrium; zero applied potential to right electrode
Vay = linspace(Vl,Vr,Ny); %length-wise (y) applied potential gradient
Va_e = zeros(Nx,Ny); %initializing potential matrix in channel
%electric potential in channel due to equilibrium applied voltage
for i = 1:Ny
    Va_e(:,i) = Vay(i);
end
%initializing potential matrix in reservoirs
Vrl_e = zeros(Nrx,Nry); %Vrl: voltage reservoir left
Vrr_e = zeros(Nrx,Nry); %Vrr: voltage reservoir right
%electric potential in reservoirs due to equilibrium applied voltage
for i = 1:Nry
    Vrl_e(:,i) = Vl;
    Vrr_e(:,i) = Vr;
end

%Forward bias (_f)
Vr = 1; %forward bias; positive applied potential to right electrode
Vay = linspace(Vl,Vr,Ny); %length-wise (y) applied potential gradient
Va_f = zeros(Nx,Ny); %initializing potential matrix in channel
%electric potential in channel due to forward bias applied voltage
for i = 1:Ny
    Va_f(:,i) = Vay(i);
```

```
end
%initializing potential matrix in reservoirs
Vrl_f = zeros(Nrx,Nry); %Vrl: voltage reservoir left
Vrr_f = zeros(Nrx,Nry); %Vrr: voltage reservoir right
%electric potential in reservoirs due to forward bias applied voltage
for i = 1:Nry
   Vrl_f(:,i) = Vl;
   Vrr_f(:,i) = Vr;
end

%Reverse bias (_r)
Vr = -1; %reverse bias; negative applied potential to right electrode
Vay = linspace(Vl,Vr,Ny); %length-wise (y) applied potential gradient
Va_r = zeros(Nx,Ny); %initializing potential matrix in channel
%electric potential in channel due to reverse bias applied voltage
for i = 1:Ny
   Va_r(:,i) = Vay(i);
end
%initializing potential matrix in reservoirs
Vrl_r = zeros(Nrx,Nry); %Vrl: voltage reservoir left
Vrr_r = zeros(Nrx,Nry); %Vrr: voltage reservoir right
%electric potential in reservoirs due to reverse bias applied voltage
for i = 1:Nry
   Vrl_r(:,i) = Vl;
   Vrr_r(:,i) = Vr;
end

%% CONCENTRATION INITIALIZING

Cy = linspace(cl, cr, Ny); %length-wise (initial) concentration gradient (1D)
C = zeros(Nx,Ny); %initializing 2D mesh of ion concentration profile
%concentration profile in channel
for i = 1:Ny
   C(:,i) = Cy(i);
end
%initializing concentration matrix in reservoirs
Crl = zeros(Nrx,Nry); %Crl: concentration reservoir left
Crr = zeros(Nrx,Nry); %Crr: concentration reservoir right
%concentration profile in reservoirs
for i = 1:Nry
```

```
   Crl(:,i)=cl;
   Crr(:,i)=cr;
end

%% Debye length

%parameters
er = 80.2; %relative permittivity (of water)
e0 = 8.854*10^-12; %vacuum permittivity constant
kb = 1.381*10^-23; %Boltzmann's constant
T = 293;  %temperature of system; room temperature in Kelvin
qe = 1.602*10^-19; %magnitude charge of electron in Coulombs
qk = 1*qe; %charge of K+ ions in Coulombs; z*qe = 1*qe
qcl = -1*qe; %charge of Cl- ions in Coulombs; z*qe = -1*qe

%Calculating Debye length profile along channel y direction
debye = sqrt((er*e0*kb*T)./((Cy.*qk^2)+(Cy.*qcl^2)));  %equation 5.15

%% Debye-Hückel approximation of Poisson-Boltzmann potential equation for diffuse
layer
%Guoy-Chapman EDL model

Qy = linspace(Q, Q, Ny); %uniform charge density in channel walls (y direction)
%Element-wise calculation of surface potential using Grahame equation
Vs = ((2*kb*T)/qe)*asinh(Qy./sqrt(8*er*e0.*Cy.*kb*T)); %equation 5.16

%Initializing electric potential profile in channel due to fixed wall charge
Vq1 = zeros(Nx,Ny); %potential due to charge in "top" channel wall
%Calculating electric potential proflile using Debye-Hückel equation
for i = 1:Ny
   Vq1(:,i)=Vs(i).*exp(-x_vec./debye(i)); %equation 5.14
end
Vq2 = flip(Vq1,1); %potential due to charge in "bottom" channel wall

%% Total electric potential profiles in channel
%due to charged channel walls and applied voltage

%Initializing total electric potential
Vtot_e = zeros(Nx, Ny); %equilibrium
Vtot_f = zeros(Nx, Ny); %forward bias
```

```
Vtot_r = zeros(Nx, Ny); %reverse bias
%Calculating total electric potential
for x = 1:Nx
  for y = 1:Ny
     Vtot_e(x,y)=Vq1(x,y)+Vq2(x,y)+Va_e(x,y); %equilibrium
     Vtot_f(x,y)=Vq1(x,y)+Vq2(x,y)+Va_f(x,y); %forward bias
     Vtot_r(x,y)=Vq1(x,y)+Vq2(x,y)+Va_r(x,y); %reverse bias
  end
end

%Concatenating Full Electric Potential Profiles
Vfull_e = [Vrl_e Vtot_e Vrr_e]; %equilibrium
Vfull_f = [Vrl_f Vtot_f Vrr_f]; %forward bias
Vfull_r = [Vrl_r Vtot_r Vrr_r]; %reverse bias

%% PLOTTING

figure() %Plotting all three modes (equilibrium, forward bias, reverse bias) in one figure
p1 = subplot(311);
[xx,yy] = meshgrid(yfull_vec,x_vec);
mesh(yy,xx,Vfull_e); %Electric Potential in equilibrium
title('Electric Potential in Equilibrium')
xlabel('X coordinate (m) Width')
ylabel('Y coordinate (m) Length')
zlabel('Electric Potential (V)')
ax = gca();
ax.XRuler.Exponent = -9;
ax.XRuler.TickLabelFormat = '%.f';
axis([0 D -RL L+RL -inf inf])

p2 = subplot(312);
[xx,yy] = meshgrid(yfull_vec,x_vec);
mesh(yy,xx,Vfull_f); %Electric Potential in forward bias
title('Electric Potential in Forward Bias')
xlabel('X coordinate (m) Width')
ylabel('Y coordinate (m) Length')
zlabel('Electric Potential (V)')
ax = gca();
ax.XRuler.Exponent = -9;
ax.XRuler.TickLabelFormat = '%.f';
```

```
axis([0 D -RL L+RL -inf inf])

p3 = subplot(313);
[xx,yy] = meshgrid(yfull_vec,x_vec);
mesh(yy,xx,Vfull_r); %Electric Potential in reverse bias
title('Electric Potential in Reverse Bias')
xlabel('X coordinate (m) Width')
ylabel('Y coordinate (m) Length')
zlabel('Electric Potential (V)')
ax = gca();
ax.XRuler.Exponent = -9;
ax.XRuler.TickLabelFormat = '%.f';
axis([0 D -RL L+RL -inf inf])
```

REFERENCES

[1] Mario Tagliazucchi and Igal Szleifer, “Transport mechanisms in nanopores and nanochannels: can we mimic nature?”, Materials Today, Volume 18, Issue 3, pp. 131-142, 2015.

[2] Aleksei Alsimentiev and Klaus Schulten, “Bacterial Toxin Alpha-Hemolysin”, Biophysical Journal, 88, pp. 3745-3761, 2005.

[3] Richard M. A. Manara, Susana Tomasio, and Syma Khalid, “The Nucleotide Capture Region of Alpha Hemolysin: Insights into Nanopore Design for DNA Sequencing from Molecular Dynamics Simulations”, Nanomaterials, 5, pp. 144-153, 2015.

[4] Patricio Farrell, Nella Rotundo, Duy Hai Doan, Markus Kantner, Jürgen Fuhrmann, and Thomas Koprucki, “Numerical Methods for Drift-Diffusion Models”, Weierstraß-Institut, 2016.

[5] Marc Thiriet, “Main Sets of Ion Channels and Pumps.” Signaling at the Cell Surface in the Circulatory and Ventilatory Systems. New York, NY: Springer New York, pp. 157–271, 2011.

[6] M. Pavlenok, I. M. Derrington, J. H. Gundlach, and M. Niederweis, “MspA Nanopores from Subunit Dimers”, PLoS ONE 7(6): e38726, 2012.

[7] Peng Jing, Farzin Haque, Anne P. Vonderheide, Carlo Montemagno, and Peixuan Guo, “Robust Properties of Membrane-Embedded Connector Channel of Bacterial Virus Phi29 DNA Packaging Motor”, Mol Biosyst. October; 6(10), pp. 1844–1852, 2010.

[8] Qiong Zheng and Guo-Wei Wei, “Poisson-Boltzmann-Nernst-Planck model”, The Journal of Chemical Physics, 2011.

[9] Xiao Tao, Jose L. Avalos, Jiayun Chen, and Roderick MacKinnon, “Crystal Structure of the Eukaryotic Strong Inward-Rectifier K+ Channel Kir2.2 at 3.1 Å Resolution”, Science, 326 (5960): 1668, 2009.

[10] Bob Eisenberg, “Ionic Channels in Biological Membranes: Electrostatic Analysis of a Natural Nanotube”, Contemporary Physics, 39(6), pp. 447-466, 1998.

[11] Li-Jing Cheng and L. Jay Guo, “Rectified Ion Transport through Concentration Gradient in Homogeneous Silica Nanochannels” Nano Letters, Vol. 7, Issue 10, pp. 3165-3171, 2007.

[12] Weihua Guan, Sylvia Xin Li, and Mark A Reed, “Voltage gated ion and molecule transport in engineered nanochannels: theory, fabrication and applications”, Nanotechnology, 25, 2014.

[13] Li-Jing Cheng and L. Jay Guo, “Ionic Current Rectification, Breakdown, and Switching in Heterogeneous Oxide Nanofluidic Devices”, American Chemical Society Nano, 3, pp. 575-584, 2009.

[14] Y.A. Perez Sirkin, M. Tagliazucchi, and I. Szleifer, “Transport in nanopores and nanochannels: some fundamental challenges and nature-inspired solutions”, Materials Today Advances, 5, 2020.

[15] Ivan Vlassiouk and Zuzanna S. Siwy, “Nanofluidic Diode”, Nano Letters, Vol. 4, Issue 1, pp. 137-142, 2004.

[16] Andrew C. Miklos, Conggang Li, Naima G. Sharaf, and Gary J. Pielak, “Volume Exclusion and Soft Interaction Effects on Protein Stability Under Crowded Conditions”, Biochemistry, 49, pp. 6984-6991, 2010.

[17] Emily E. Meyer, Kenneth J. Rosenberg, and Jacob Israelachvili. “Recent progress in understanding hydrophobic interactions”, PNAS vol. 103 no. 43, pp. 15739-15746, 2006.

[18] Shengjie Zhai and Hui Zhao, “The Influence of Concentration Polarization on DNA Translocation through a Nanopore”, Physical Review E, 2016.

[19] Eric Lee, “Theory of Electrophoresis and Diffusiophoresis of Highly Charged Colloidal Particles”, Interface Science and Technology, Section A, Chapter 5, 2018.

[20] Masoumeh Nazari, Ali Davoodabadi, Dezhao Huang, Tengfei Luo, and Hadi Ghasemi, “Transport Phenomena in Nano/Molecular Confinements”, ACS Nano, 14, pp. 16348-16391, 2020.

[21] Hirofumi Daiguji, Peidong Yang, Andrew J. Szeri, and Arun Majumdar, “Electrochemomechanical Energy Conversion in Nanofluidic Channels”, Nano Letters, Vol. 4, No. 12, pp. 2315-2321, 2004.

[22] Javier Cervera, Patricio Ramirez, Salvador Mafe, and Pieter Stroeve, “Asymmetric nanopore rectification for ion pumping, electrical power generation, and information processing applications”, Electrocimica Acta, 56, 2011.

[23] Vicente Gomez, Patricio Ramirez, Javier Cervera, Mubarak Ali, Saima Nasir, Wolfgang Ensinger, and Slavador Mafe, “Concatenated logic functions using nanofluidic diodes with all-electrical inputs and outputs”, Electrochemistry Communications, 88, 2018.

[24] Shaurya Prakash and Junghoon Yeom, “Nanofluidics and Microfluidics: Systems and Applications”, Elsevier Science & Technology Books, 2014.

[25] Raymond A. Serway and John W. Jewett, Jr., “Physics for Scientists and Engineers with Modern Physics”, Brooks/Cole CENGAGE Learning, Ninth Edition, 2014.

[26] Li-Jing Cheng and L. Jay Guo, “Nanofluidic diodes”, Chemical Society Reviews, 2009.

[27] Hirofumi Daiguji, Peidong Yang, Arun Majumdar, “Ion Transport in Nanofluidic Channels”, Nano Letters, Vol. 4, Issue 1, pp. 137-142, 2004.

[28] David J. Griffiths, “Introduction to Electrodynamics, Fourth Edition”, Cambridge University Press, 2017.

[29] Peter Wust, Benedikt Kortüm, Ulf Strauss, Jacek Nadobny, Sebastian Zschaeck, Marcus Beck, Ulrike Stein, and Pirus Ghadjar, “Non-thermal effects of radiofrequency electromagnetic fields”, Scientific Reports Nature, 2020.

[30] Mika M. Kohonen, Marilyn E. Karaman, and Richard M. Pashley, “Debye Length in Multivalent Electrolyte Solutions”, Langmuir, 16, pp. 5749-5753, 2000.

[31] Hiroyuki Ohshima, “Electrical Double Layer at Nanolayer Interface”, Elsevier, 2017.

[32] Antonios Liakopoulos, Filippos Sofos, and Theodoros E. Karakasidis, “Friction Factor in Nanochannel Flows”, Microfluidics and Nanofluidics, Vol. 20, Issue 1, 2016.

[33] E. Gongadze, S. Petersen, U. Beck, and U. van Rienen, “Classical Models of the Interface between an Electrode and an Electrolyte”, COMSOL Conference 2009 Milan, 2009.

[34] Hermann Nirschl and Bastian Schäfer, “Distinction between Electrostatic and Electroviscous Effects on the Permeability of Colloidal Packed Beds”, C.&E.T. Communications, 28, no. 8, 2005.

[35] Todd M. Squires and Martin Z. Bazant, “Breaking symmetries in induced-charge electro-osmosis and electrophoresis”, Journal of Fluid Mechanics, 329, 2005.

[36] Pijush K. Kundu, Ira M. Cohen, and David R. Dowling, “Fluid Mechanics, Fifth Edition”, Elsevier, 2012.

[37] Bastian E. Rapp, “Microfluidics: Modeling, Mechanics and Mathematics”, Elsevier, 2016.

[38] Hirofumi Daiguji, Yukiko Oka, and Katsuhiro Shirono, “Nanofluidic Diode and Bipolar Transistor”, Nano Letters, Vol. 5, Issue 11, pp. 2274-2280, 2005.

[39] Shizhi Qian, Sang W. Joo, Ye Ai, Marcos A. Cheney, and Wensheng Hou, “Effect of linear surface-charge non-uniformities on the electrokinetic ionic-current rectification in conical nanopores”, Journal of Colloid and Interface Science, volume 560, pp. 65-101. 2006.

[40] Aloke Paul, Tomi Laurila, Vesa Vuorinen, and Sergiy Divinski, “Thermodynamics, Diffusion and the Kirkendall Effect in Solids: Chapter 3 Fick’s Laws of Diffusion”, Springer, 2014.

[41] Z. Schuss and B. Nadler, “Derivation of Poisson and Nernst-Planck equations in a bath and channel from a molecular model”, Physical Review E, Vol. 64, 2001.

[42] Qiong Zheng, Duan Chen, and Guo-Wei Wei, “Second-order Poisson-Nernst-Planck solver for ion transport”, Journal of Computational Physics, 230, 2011.

[43] Allen Flavell, Michael Machen, Bob Eisenberg, Chun Liu, and Xiaofan Li, “A Conservative Finite Difference Scheme for Poisson-Nernst-Planck Equations”, Math.NA, 2013.

[44] Kunwar Pal Singh and Manoj Kumar, “Effect of Nanochannel Diameter and Debye Length on Ion Current Rectification in a Fluidic Bipolar Diode”, The Journal of Physical Chemistry C, 115, pp. 22917-22924, 2011.

[45] Zuzanna S. Siwy, “Ion-Current Rectification in Nanopores and Nanotubes with Broken Symmetry”, Advanced Functional Materials, 16, pp. 735-746, 2006.

[46] Rohit Karnik, Chuanhua Duan, Nenneth Castelino, Hirofumi Daiguji, and Arun Majumdar, “Rectification of Ionic Current in a Nanofluidic Diode”, Nano Letters, Vol. 7, Issue 3, pp. 547-551, 2007.

[47] James R. Nagel, “Solving the Generalized Poisson Equation Using the Finite-Difference Method (FDM)”, my.ece.utah.edu, 2012.

[48] J.J. López-García, J. Horno, and C. Grosse, “Transport Properties in Nanochannels: Ionic Size-, Permittivity-, and Viscosity-Related Effects”, The Journal of Physical Chemistry C, 124, pp. 10764-10775, 2020.

[49] Chenyu Wen, Shuangshuang Zeng, Shiyu Li, Zhen Zhang, and Shi-Li Zhang, “On Rectification of Ionic Current in Nanopores” Analytical Chemistry, 91 (22), pp. 14597-14604, 2019.

[50] Adrien Plecis, Reto B. Schoch, and Philippe Renaud, “Ionic Transport Phenomena in Nanofluidics: Experimental and Theoretical Study of the Exclusion-Enrichment Effect on a Chip”, Nano Letters, pp. 1147-1155, Vol. 5, No. 6, 2005.

[51] Jim Clark, “Atomic and Ionic Radius”, LibreTexts, https://chem.libretexts.org/@go/page/3616, 2021.

[52] Jean-Pierre Colinge and Cynthia A. Colinge, “Physics of Semiconductor Devices”, Kluwer Academic Publishers, 2002.

[53] Xinran Geng, Miao Yu, Wei Zhang, Qiwei Liu, Xiaopeng Yu, and Yang Lu, “Slip length and structure of liquid water flowing past atomistic smooth charged walls”, Sci Rep 9, 18957, 2019.

[54] Nikolai V. Priezjev, Anton A. Darhuber, and Sandra M. Troian, “Slip length in sheared liquid films subject to mixed boundary conditions”, Phys. Rev. E 71, 041608, 2005.

[55] Kunwar Pal Singh, “Ion current rectification influenced by length and location of surface charge in fluidic unipolar conical nanopores”, Sensors and Actuators B: Chemical, 230, 2016.

[56] Yue Zhou, Xuewei Liao, Jing Han, Tingting Chen, and Chen Wang, “Ionic current rectification in asymmetric nanofluidic devices”, Chinese Chemical Letters, 31, 2020.

[57] Chih-Yuan Lin, Jyh-Ping Hsu, and Li-Hsien Yeh, “Rectification of ionic current in nanopores functionalized with bipolar polyelectrolyte brushes”, Sensors and Actuators B: Chemical, 258, 2018.

[58] Grégoire Allaire, “Numerical Analysis and Optimization: An Introduction to Mathematical Modelling and Numerical Simulation”, Oxford University Press, Inc., 2007.

[59] Da Meng, Bin Zheng, Guang Lin, and Maria L. Sushko, “Numerical Solution of 3D Poisson-Nernst-Planck Equaions Coupled with Classical Density Functional Theory for Modeling Ion and Electron Transport in a Confined Environment”, Global Science, 2014.

[60] Akshay Subramaniam, Jerry Chen, Taejin Jang, Natalie R. Geise, Robert M. Kasse, Michael F. Toney, and Venkat R. Subramanian, “Analysis and Simulation of One-Dimensional Transport Models for Lithium Symmetric Cells”, Journal of the Electrochemical Society, 166, 2019.

[61] Ming-Jiang Huang, Lanju Mei, Li-Hsien Yeh, and Shizhi Qian, “pH-Regulated nanopore conductance with overlapped electric double layers”, Electrochemistry Communications, 55, 2015.

[62] Ye Ai, Mingkan Zhang, Sang W. Joo, Marcos A. Cheney, and Shizhi Qian, “Effects of Electroosmotic Flow on Ionic Current Rectification in Conical Nanopores”, The Journal of Physical Chemistry C, 114, pp. 3883-3890, 2010.

[63] Iat Wai Leong, Makusu Tsutsui, Sanae Murayama, Yuhui He, and Masateru Taniguchi, “Electroosmosis-Driven Nanofluidic Diodes”, The Journal of Physical Chemistry B, 124, pp. 7086-7092, 2020.

[64] Zhongpeng Zhu, Dianyu Wang, Ye Tian, and Lei Jiang, “Ion/Molecule Transportation in Nanopores and Nanochannels: From Critical Principles to Diverse Functions”, Journal of the American Chemical Society, 141, pp. 8658-8669, 2019.

[65] Qian Liu, Liping Wen, Kai Xiao, Heng Lu, Zhen Zhang, Ganhua Xie, Xiang-Yu Kong. Zhishan Bo, and Lei Jiang, “A Biomimetic Voltage-Gated Chloride Nanochannel”, Advanced Materials, 28, pp. 3181-3186, 2016.

[66] Ruigang Shen, Shi Shu, Ying Yang, and Benzhuo Lu, “A decoupling two-grid method for the time-dependent Poisson-Nernst-Planck equations”, Numerical Algorithms, 83, pp. 1613-1651, 2019.

[67] Tai-Chia Lin, “The Poisson-Nernst-Planck (PNP) system for ion transport”, 3rd OCAMI-TIMS Workshop in Osaka, Japan, 2011.

[68] Peter W. Bates, Yusheng Jia, Guojian Lin, Hong Lu and Mingji Zhang, “Individual flux study via steady-state Poisson-Nernst-Planck systems: Effects from boundary conditions”, LibreTexts, 2020.

[69] D. Constantin, Z. S. Siwy, “Poisson-Nernst-Planck Model of Ion Current Rectification Through a Nanofluidic Diode”, Phys. Rev. E, 76, No. 041202, 2007.

[70] L.P. Endresen, K. Hall, J. S. Høye and J. Myrheim, “A Theory for the Membrane Potential of Living Cells”, arXiv:physics/9811011, 1998.

[71] Farzin Haque, Jinghong Li, Hai-Chen Wu, Xing-Jie Liang, and Peixuan Guo, “Solid-state and biological nanopore for real-time and sequencing of DNA”, Nano Today, 8, pp. 55-74, 2013.

[72] Qi Chen and Zewen Liu, “Fabrication and Applications of Solid-State Nanopores”, Sensors, 19, 2019.

[73] Tomer Markovich, David Andelman, and Rudi Podgornik, “Charged Membranes: Poisson-Boltzmann theory, DLVO paradigm and beyond”, Handbook of Lipid Membranes: Molecular, Functional, and Materials aspects, CRC Press, 2016.